

## 7. Fields in Uniaxially Anisotropic Regions

### 7.1 INTRODUCTION

The present and following chapters deal with the effects of anisotropy in a medium. Under suitable restrictions, macroscopic electromagnetic properties of physical media—including solid-state crystals, magnetized ferrites, magnetoplasmas, and artificial dielectrics—may be described in terms of a dyadic permittivity  $\epsilon$  and (or) permeability  $\mu$ . Plane waves in such media have been studied for some time in connection with the propagation of visible light in crystals,<sup>1,2</sup> the propagation of radio waves in the ionosphere,<sup>3,4</sup> and the propagation of microwaves in ferrite-loaded waveguides.<sup>5</sup> More recently, problems of radiation from stationary or moving sources, and of diffraction by objects, in an anisotropic medium have gained in importance. To understand electromagnetic propagation in a medium whose characteristics are a function of the propagation direction, it is useful to consider first the simplest type of anisotropy—the uniaxial. In this case, the constitutive parameters may be described in an appropriate coordinate system by a diagonal dyadic with two identical (transverse) elements that differ from the remaining (longitudinal) element. Physical media representable in this manner include uniaxial crystals, and plasmas or ferrites in a strong external magnetic field. The formulation and solution of radiation and diffraction problems in uniaxial regions, and the physical interpretation of the results, constitutes the substance of the present chapter. Problems in such media may sometimes be reduced to equivalent ones in isotropic regions, thereby facilitating the analysis. In the more complicated case of gyrotropic media, characterized by non-diagonal  $\epsilon$  and (or)  $\mu$  dyadics, no such simplification is generally possible; gyrotropic effects are treated in Chapter 8.

As in the isotropic case, propagation in anisotropic media can be described in terms of guided waves or modes, but there are characteristic differences. To elucidate these differences, let us first consider unbounded homo-

geneous media. In an unbounded isotropic non-spatially-dispersive† medium, modes with transverse field dependence  $\exp [i(\mathbf{k}_t \cdot \mathbf{p} - \omega t)]$  propagate along the guiding direction  $z$  with wavenumbers  $\pm \kappa(\mathbf{k}_t, \omega)$ ; for given  $\mathbf{k}_t, \omega$ , there are two such mode types ( $E$  and  $H$ ), yielding four waves with the same isotropic wavenumbers  $\pm \kappa, \pm \kappa$  independently of the choice of guiding direction (see Sec. 1.4 and Sec. 7.2). In an unbounded anisotropic, non-spatially-dispersive medium, guided waves with the same transverse field dependence likewise exist; there are again four possible waves for each  $\mathbf{k}_t, \omega$ , but the wavenumbers along the guiding direction are not in general negatives of one another. However, for the special case of a uniaxial medium, wherein the guiding axis  $z$  is chosen along the uniaxial direction, the four waves for given  $\mathbf{k}_t, \omega$  separate into two types with wavenumbers  $\pm \kappa', \pm \kappa''$  ( $\kappa' \neq \kappa''$ ). Furthermore, the characteristic impedance properties of these wave types are similar to those for an isotropic medium and lead to similar uncoupled transmission line descriptions. Modes remain uncoupled even in the presence of uniaxially anisotropic, planar stratification, or boundaries along  $z$  provided that all regions have  $z$  as the uniaxial direction. However, mode coupling is introduced in general by boundaries or stratification oblique to the uniaxial direction.

To illustrate these remarks, we consider the dispersion equations relating the longitudinal and transverse wavenumbers  $\kappa$  and  $\mathbf{k}_t$  of a plane wave in a homogeneous anisotropic medium. If the electric field is taken as  $\mathbf{E}(\mathbf{r}) = \bar{\mathbf{E}} \exp(i\mathbf{k} \cdot \mathbf{r} - i\omega t)$ , with  $\bar{\mathbf{E}}$  denoting a constant amplitude and polarization, then on eliminating  $\mathbf{H}(\mathbf{r})$  from the source-free form of Eqs. (1.5.4la), one has

$$\left[ \mathbf{k} \times (\mathbf{k} \times \mathbf{1}) + \frac{\omega^2}{c^2} \epsilon' \right] \cdot \bar{\mathbf{E}} = 0, \quad \epsilon' = \frac{\epsilon}{\epsilon_0}, \quad c^2 = \frac{1}{\mu_0 \epsilon_0}, \quad (1)$$

in a medium with scalar permeability  $\mu_0$  and dyadic permittivity  $\epsilon$ . In a uniaxial medium,  $\epsilon$  has the form

$$\epsilon = \mathbf{1}_t \epsilon_t + \mathbf{z}_0 \mathbf{z}_0 \epsilon_z, \quad \mathbf{1}_t = \mathbf{1} - \mathbf{z}_0 \mathbf{z}_0. \quad (2)$$

The parameters  $\epsilon_t = \epsilon_0$  and  $\epsilon_z = \epsilon_0(1 - \omega_p^2/\omega^2)$  are representative of a cold plasma under the influence of an infinitely strong axial magnetic field [see Eqs. (1.5.20), with  $\omega_c = \infty$ ]. Substituting Eq. (2) into Eq. (1) and taking the dot product with  $\mathbf{z}_0, \mathbf{k}_t$ , and  $\mathbf{z}_0 \times \mathbf{k}_t$ , respectively, where  $\mathbf{k}_t = \mathbf{k} - \mathbf{z}_0 \kappa$ , one obtains the three equations:

$$\left( \frac{\omega^2}{c^2} \epsilon'_z - k_t^2 \right) \bar{E}_z + \kappa (\bar{\mathbf{E}}_t \cdot \mathbf{k}_t) = 0, \quad (3a)$$

$$k_t^2 \kappa \bar{E}_z + \left( \frac{\omega^2}{c^2} \epsilon'_t - \kappa^2 \right) (\bar{\mathbf{E}}_t \cdot \mathbf{k}_t) = 0, \quad (3b)$$

$$\left( \frac{\omega^2}{c^2} \epsilon'_t - k^2 \right) (\bar{\mathbf{E}}_t \cdot \mathbf{z}_0 \times \mathbf{k}_t) = 0. \quad (3c)$$

---

† In a non-spatially-dispersive medium, the dielectric constant and permeability are independent of the spatial derivative operator  $\nabla$ , or in a  $(\mathbf{k}, \omega)$  basis, of the wavevector  $\mathbf{k}$ .

When  $\tilde{E}_z = 0$ , Eqs. (3a) and (3b) yield  $\bar{\mathbf{E}}_t \cdot \mathbf{k}_t = 0$ , whence, from Eq. (3c), the only non-vanishing electric-field component is parallel to  $\mathbf{z}_0 \times \mathbf{k}_t$  provided that the plane-wave field obeys the dispersion equation

$$k^2 = k_t^2 \epsilon'_t, \quad k_0^2 = \frac{\omega^2}{c^2}. \quad (4)$$

Thus, the uniaxial medium can support plane waves with the electric field polarized perpendicular both to the  $z$  axis and to the wavevector  $\mathbf{k}$  along which the equiphasic surfaces advance ( $H$  modes with respect to  $z$ ); one notes from Eq. (4) that these waves are propagated as in an *isotropic* medium with effective permittivity  $\epsilon_t$ . The latter behavior follows from the transverse isotropy of the  $\epsilon$  dyadic in Eq. (2) and from the ineffectiveness of the longitudinal dependence of  $\epsilon$  for transverse-electric waves.

When  $\tilde{E}_z \neq 0$ ,  $\bar{\mathbf{E}}_t \cdot \mathbf{k}_t \neq 0$  but  $\bar{\mathbf{E}}_t \cdot (\mathbf{z}_0 \times \mathbf{k}_t) = 0$ , Eqs. (3a) and (3b) describe waves with electric-field polarization orthogonal to that discussed above provided that  $\kappa$  and  $k_t$  satisfy the dispersion equation

$$\kappa^2 + \frac{k_t^2}{\epsilon} = k_0^2 \epsilon'_t, \quad \epsilon = \frac{\epsilon_z}{\epsilon'_t}. \quad (5)$$

One may verify from the relation  $\mathbf{H} = (i\omega\mu)^{-1} \nabla \times \mathbf{E}$  that  $H_z = 0$ , whence these waves are  $E$  modes with respect to  $z$ . Since from Eq. (5),  $\kappa^2 + k_t^2 = k^2$  is not constant,  $E$ -mode waves display anisotropic behavior. The dependence of  $\kappa$  on  $\mathbf{k}_t$ , expressed in Eqs. (4) and (5),

$$\kappa \equiv \kappa' = \sqrt{k_0^2 \epsilon'_t - \left( \frac{k_t^2}{\epsilon} \right)} \quad \text{for } E \text{ modes}, \quad (6a)$$

$$\kappa \equiv \kappa'' = \sqrt{k_0^2 \epsilon'_t - k_t^2} \quad \text{for } H \text{ modes}, \quad (6b)$$

indicates that, in contrast with isotropic media,  $E$  and  $H$  modes in a uniaxially anisotropic region are propagated with different phase speeds unless  $k_t = 0$ .

Further insight into propagation characteristics in a uniaxial medium is gained from a study of the wavenumber surfaces traced out, for real  $\kappa$  and  $k_t$ , by the endpoints of the wavevector  $\mathbf{k}$  in Eqs. (4) and (5). If the medium is a plasma with  $\epsilon'_t = 1$ , the wavenumber surface for  $H$  modes is a sphere with radius  $k_0$  as in vacuum. For the  $E$  modes, two distinct situations arise, depending on whether in Eq. (5),  $\epsilon = 1 - (\omega_p^2/\omega^2)$  is positive or negative. As shown in Fig. 7.1.1, when  $\epsilon > 0$ , the endpoints of the vector  $\mathbf{k}$  lie on an ellipsoid, and when  $\epsilon < 0$  on a hyperboloid, of revolution about the  $z$  axis. As noted in Sec. 1.6, the direction of energy transport [i.e., the direction of the group velocity vector  $\mathbf{v}_g$ , or of the time-averaged Poynting vector  $\bar{\mathbf{S}} = \text{Re}(\mathbf{E} \times \mathbf{H}^*)$ ] in a plane wave with wavevector  $\mathbf{k}$ , coincides with that of the normal to the surface at the point  $\mathbf{k}$ ; to ascertain the directions of  $\mathbf{k}$ ,  $\mathbf{v}_g$  or  $\bar{\mathbf{S}}$  in the  $(\rho, z)$  coordinate space, the  $\rho$  and  $z$  axes are superposed on the  $k_t$  and  $\kappa$  axes, respectively. While  $\mathbf{k}$  and  $\mathbf{v}_g$  are parallel for  $H$  modes, propagating as in vacuum, their directions differ for the  $E$  modes; this situation is depicted in Fig. 7.1.1, where  $\bar{\theta}$  and  $\theta$  are the angles between the positive  $z$  axis and  $\mathbf{k}$  and

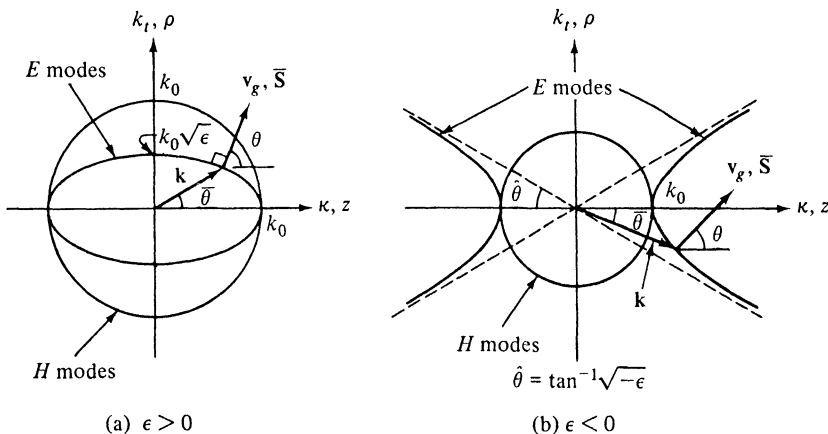


**FIG. 7.1.1** Wavenumber surfaces for a uniaxially anisotropic plasma.

$v_g$ , respectively. One observes that  $E$ -mode plane waves propagate in all space directions when  $\epsilon > 0$ , but when  $\epsilon < 0$  their group velocity (or ray) vectors are confined to the interior of the conical regions  $|\tan \theta| < \tan \theta_c = 1/\sqrt{|\epsilon|}$ . The limiting angle  $\theta_c$  is defined by the perpendicular to the asymptote for the wavenumber surface in Fig. 7.1.1(b), and since the asymptote makes an angle  $\hat{\theta} = \tan^{-1} \sqrt{|\epsilon|}$  with the  $z$  axis, the above expression for  $\theta_c$  follows. For ray directions  $\theta_c < \theta < \pi - \theta_c$ ,  $k$  is complex and the wave is exponentially damped. Thus, plane-wave propagation for  $\epsilon < 0$  is confined to certain angular domains in space, and if the medium is excited by a point source, it is to be expected that the energy is confined to regions supporting “real rays.” This conclusion is confirmed by the analysis in Sec. 7.3. For  $\epsilon > 0$  in Fig. 7.1.1(a), the  $\rho$  and  $z$  components of  $E$ -mode  $k$  and  $v_g$  vectors have the same algebraic sign, and hence describe a propagation mechanism similar to that in an isotropic medium. This is not true for the strongly anisotropic, open-branched  $E$ -mode surface in Fig. 7.1.1(b). Opposite signs of corresponding wavevector and group velocity components imply “backward” wave characteristics (i.e., oppositely directed phase and energy propagation).

Because of the simple form of the dispersion equation, the relation between the angles  $\theta$  and  $\bar{\theta}$  is determined readily. Since the slope of the  $k$  versus  $\bar{\theta}$  plot with respect to the  $\kappa$  axis is given by  $dk_i/d\kappa$ , the slope of the normal to the curve is  $-dk_i/d\kappa$ , which is evaluated from Eq. (5) as

$$\tan \theta = -\frac{dk}{d\kappa} = \frac{1}{\epsilon} \frac{k_t}{\kappa} = \frac{1}{\epsilon} \tan \bar{\theta}. \quad (7)$$

When  $\epsilon < 0$ ,  $\theta$  and  $\bar{\theta}$  are measured from opposite sides of the  $z$  axis as in Fig. 7.1.1(b).

One observes from Fig. 7.1.1 that because of the rotational symmetry of the wavenumber surfaces with respect to the  $z$  axis, the two values of  $\kappa'$  or  $\kappa''$

corresponding to given  $k_r, \omega$  are negatives of one another, with positive and negative  $\kappa$  distinguishing waves carrying energy along the  $+z$  and  $-z$  directions, respectively. As shown in Sec. 7.2, this feature permits the network representation of the propagation process in a manner similar to that employed for isotropic media, even in the presence of perfectly conducting waveguide boundaries parallel to  $z$  and of stratification along  $z$ . One finds that the  $H$ -mode portion of the field is the same as in an isotropic region while the  $E$ -mode portion can be deduced from the isotropic solution by a simple scaling of coordinates. These procedures are illustrated in Sec. 7.3, wherein are constructed explicit results for various sources in an unbounded uniaxially anisotropic region. In the discussion, emphasis is placed on the physical interpretation of field behavior, especially on the use of ray techniques and on the resolution of the "infinity catastrophe" for radiation from point sources in a medium with an open-branched wavenumber surface.

When, as is sometimes necessary, the  $(\rho, z)$  coordinate system is rotated with respect to the principal axes of the  $E$ -mode dispersion surfaces, the two solutions  $\kappa'_1(k_r, \omega)$  and  $\kappa'_2(k_r, \omega)$  are no longer related by  $\kappa'_1 = -\kappa'_2$  (see Fig. 7.5.2). This lack of reflection symmetry with respect to the new  $z$  direction precludes a network formulation of the field problem since a conventional transmission-line representation requires identical propagation constants for waves traveling in opposite directions. Rotated coordinates are introduced to describe planar boundaries or interfaces obliquely oriented with respect to the uniaxial direction. Such boundaries introduce coupling between  $E$  and  $H$  modes, and the associated field problem must be attacked by the more general techniques presented in Chapter 8 for arbitrary anisotropy. Simplifications occur for two-dimensional problems wherein the excitation is a magnetic line current perpendicular to the uniaxial direction but parallel to planar or cylindrical boundary surfaces; only  $E$  modes are required in this case. When the boundaries are perfectly conducting, or have a special surface impedance, coordinate scaling may be used to relate the uniaxial medium solutions to corresponding isotropic ones. As shown in Sec. 7.4, uniaxial media exhibit peculiarly anisotropic phenomena such as non-specular reflection of rays, producing distorted imaging of a line source field in a perfectly reflecting plane. Diffraction by a half-plane is an example exhibiting the influence of anisotropy on edge diffraction patterns.

When an oblique interface separates a uniaxial from an isotropic medium, coordinate scaling does not simplify the two-dimensional field problem in the manner noted above. It is then necessary to employ a representation in terms of non-reflection symmetric plane-wave modes  $\kappa'_1 \neq -\kappa'_2$ . Section 7.5 contains a formulation of this problem, and a detailed asymptotic evaluation of the radiation field that exhibits effects of anisotropy on reflected, refracted, and diffracted (lateral) wave constituents in both the uniaxial and isotropic medium. Although the media in the present chapter are uniaxial, an interpretation involving rays and wavenumber surfaces permits inferences to be drawn for more general anisotropy.

## 7.2 NETWORK FORMULATION OF FIELD PROBLEM

### 7.2a Derivation of the Transmission-Line Equations

Consider a uniform waveguide region (Fig. 7.2.1) bounded (if at all) by a perfectly conducting surface whose generators are parallel to the  $z$ -axis of a cylindrical coordinate system. The medium filling the region is characterized

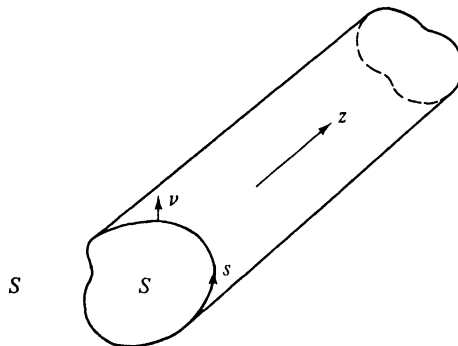


FIG. 7.2.1 Optic axis and waveguide boundaries.

by a permittivity dyadic  $\epsilon = \epsilon(z)$  and a permeability dyadic  $\mu = \mu(z)$  (i.e., the medium properties may vary along the  $z$  direction; if the region is comprised of homogeneous layers, the  $z$  axis is oriented perpendicular to the layer interfaces). The dyadics are assumed to have the special form appropriate to uniaxial anisotropy,<sup>1,2</sup> with the “optic axis” parallel to  $z$ :

$$\alpha(z) = \mathbf{1}_t \alpha_t(z) + \mathbf{z}_0 \mathbf{z}_0 \alpha_z(z), \quad (1)$$

where  $\mathbf{1}_t$  is the unit dyadic in the transverse (to  $z$ ) vector space,  $\mathbf{z}_0$  is a unit vector along the positive  $z$  axis, and  $\alpha$  represents either  $\epsilon$  or  $\mu$ .

Upon following the same procedure as for the isotropic problem in Sec. 2.2a, one may reduce the Maxwell field equations [with an  $\exp(-i\omega t)$  dependence],

$$\nabla \times \mathbf{E}(\mathbf{r}) = i\omega \mu(z) \cdot \mathbf{H}(\mathbf{r}) - \mathbf{M}(\mathbf{r}), \quad (2a)$$

$$\nabla \times \mathbf{H}(\mathbf{r}) = -i\omega \epsilon(z) \cdot \mathbf{E}(\mathbf{r}) + \mathbf{J}(\mathbf{r}), \quad (2b)$$

to their equivalent form for the transverse (to  $z$ ) components  $\mathbf{E}_t$  and  $\mathbf{H}_t$ ,

$$-\frac{\partial \mathbf{E}_t}{\partial z} = -i\omega \mu_t \left[ \mathbf{1}_t + \frac{\nabla_t \nabla_t}{k_1^2} \right] \cdot (\mathbf{H}_t \times \mathbf{z}_0) + \mathbf{M}_{te} \times \mathbf{z}_0, \quad k_1^2 = \omega^2 \mu_t \epsilon_z, \quad (3a)$$

$$-\frac{\partial \mathbf{H}_t}{\partial z} = -i\omega \epsilon_t \left[ \mathbf{1}_t + \frac{\nabla_t \nabla_t}{k_2^2} \right] \cdot (\mathbf{z}_0 \times \mathbf{E}_t) + \mathbf{z}_0 \times \mathbf{J}_{te}, \quad k_2^2 = \omega^2 \mu_z \epsilon_t. \quad (3b)$$

In these equations,  $\mathbf{E}$ ,  $\mathbf{H}$ ,  $\mathbf{J}$ , and  $\mathbf{M}$  denote the vector electric field, magnetic field, applied electric current density, and applied magnetic current density, respectively. The equivalent transverse source currents  $\mathbf{M}_{te}$  and  $\mathbf{J}_{te}$  are given by

$$\mathbf{M}_{te} = \mathbf{M}_t + \frac{\nabla_t \times \mathbf{z}_0 J_z}{i\omega\epsilon_z}, \quad \mathbf{J}_{te} = \mathbf{J}_t - \frac{\nabla_t \times \mathbf{z}_0 M_z}{i\omega\mu_z}, \quad (3c)$$

where the subscripts  $t$  and  $z$  distinguish transverse and longitudinal components. From a knowledge of  $\mathbf{E}_t$  and  $\mathbf{H}_t$ , one determines  $E_z$  and  $H_z$  via the relations

$$E_z = \frac{1}{-i\omega\epsilon_z} [\nabla_t \cdot (\mathbf{H}_t \times \mathbf{z}_0) - J_z], \quad H_z = \frac{1}{-i\omega\mu_z} [\nabla_t \cdot (\mathbf{z}_0 \times \mathbf{E}_t) - M_z]. \quad (4)$$

On the perfectly conducting transverse boundaries  $s$  of the region, the tangential components of the total electric field are required to vanish, whence, if  $J_z$  is assumed to vanish on  $s$ ,

$$\mathbf{v} \times \mathbf{E}_t = 0 = \nabla_t \cdot (\mathbf{H}_t \times \mathbf{z}_0) \quad \text{on } s, \quad (5)$$

where  $\mathbf{v}$  is a unit vector normal to  $s$ . If the region is unbounded in the transverse domain, a radiation condition is imposed at infinity. The boundary conditions at the  $z$  termini of the region are left unspecified for the moment.

As in Chapter 2, to satisfy Eqs. (3)–(5), one seeks a representation for  $\mathbf{E}_t$  and  $\mathbf{H}_t$  in terms of solutions of the source-free field equations in the given region. By virtue of the symmetry of the region with respect to the  $z$  coordinate, the transverse part of a source-free electric and magnetic field solution can be expressed in the form  $V_i(z) \mathbf{e}_i(\mathbf{p})$  and  $I_i(z) \mathbf{h}_i(\mathbf{p})$ , respectively, where  $\mathbf{e}_i$  and  $\mathbf{h}_i$  are transverse vector functions of the transverse vector coordinate  $\mathbf{p}$  only. In view of the homogeneity of the configuration in the cross-sectional domain and the simple form of Eqs. (3a) and (3b), the transverse eigenvalue problem (characterized by the operator  $\nabla_t, \nabla_t'$ ) is the same as for the corresponding isotropic case, whence the set of eigenfunctions can be similarly decomposed into  $E$  and  $H$  modes relative to the  $z$  direction (see Sec. 8.2 for formulation of the eigenvalue problem). Hence [see Eqs. (2.2.8)]

$$\mathbf{E}_t(\mathbf{r}) = \sum_i V'_i(z) \mathbf{e}'_i(\mathbf{p}) + \sum_i V''_i(z) \mathbf{e}''_i(\mathbf{p}), \quad (6a)$$

$$\mathbf{H}_t(\mathbf{r}) = \sum_i I'_i(z) \mathbf{h}'_i(\mathbf{p}) + \sum_i I''_i(z) \mathbf{h}''_i(\mathbf{p}), \quad \mathbf{h}_i = \mathbf{z}_0 \times \mathbf{e}_i, \quad (6b)$$

$$\mathbf{J}_{te}(\mathbf{r}) = \sum_i i'_i(z) \mathbf{e}'_i(\mathbf{p}) + \sum_i i''_i(z) \mathbf{e}''_i(\mathbf{p}), \quad (6c)$$

$$\mathbf{M}_{te}(\mathbf{r}) = \sum_i v'_i(z) \mathbf{h}'_i(\mathbf{p}) + \sum_i v''_i(z) \mathbf{h}''_i(\mathbf{p}), \quad (6d)$$

where the single and double primes denote  $E$ -mode and  $H$ -mode quantities, respectively. The vector-mode functions  $\mathbf{e}'_i, \mathbf{e}''_i, \mathbf{h}'_i, \mathbf{h}''_i$ , identical with those for isotropic waveguide regions, satisfy Eqs. (2.2.10) and the orthogonality conditions (2.2.11b). The source “voltages”  $v_i$  and “currents”  $i_i$  being known, it is desired to find the modal “voltages”  $V_i$  and “currents”  $I_i$ .

Substitution of Eqs. (6a–6d) into Eqs. (3a) and (3b) yields via Eqs. (2.2.10) the transmission line equations for the modal amplitudes  $V_i$  and  $I_i$  (note:  $\nabla_t \cdot \mathbf{e}''_i = \nabla_t \cdot \mathbf{h}'_i = 0$  in  $S$ ):

$$-\frac{dV_i(z)}{dz} = -i\kappa_i(z)Z_i(z)I_i(z) + v_i(z), \quad (7a)$$

$$-\frac{dI_i(z)}{dz} = -i\kappa_i(z)Y_i(z)V_i(z) + i_i(z), \quad Y_i(z) = \frac{1}{Z_i(z)}, \quad (7b)$$

where, for the  $E$  modes, the propagation constant  $\kappa_i$  and the characteristic impedance  $Z_i$  are defined as

$$Z'_i(z) = \frac{1}{Y'_i(z)} = \frac{\kappa'_i(z)}{\omega\epsilon_t(z)}, \quad \kappa'_i(z) = \sqrt{\frac{\epsilon_t(z)}{\epsilon_z(z)}} \sqrt{k_1^2(z) - k_{ti}^2}, \quad (8a)$$

while, for the  $H$  modes,

$$Z''_i(z) = \frac{1}{Y''_i(z)} = \frac{\omega\mu_t(z)}{\kappa''_i(z)}, \quad \kappa''_i(z) = \sqrt{\frac{\mu_t(z)}{\mu_z(z)}} \sqrt{k_2^2(z) - k_{ti}^2}. \quad (8b)$$

It should be noted that the characteristic impedances for the uniaxial and isotropic cases are different, and more importantly, the propagation wavenumbers  $\kappa'_i \neq \kappa''_i$  are anisotropic (see Sec. 7.1). The voltage and current source terms  $v_i$  and  $i_i$  are given in terms of the specified applied sources  $\mathbf{J}$  and  $\mathbf{M}$  as [see Eqs. (2.2.14)]

$$v_i = \int_S \mathbf{M}_{te} \cdot \mathbf{h}_i^* dS = \int_S \mathbf{M} \cdot \mathbf{h}_i^* dS + Z_i^* \int_S \mathbf{J} \cdot \mathbf{e}_{zi}^* dS, \quad (9a)$$

$$i_i = \int_S \mathbf{J}_{te} \cdot \mathbf{e}_i^* dS = \int_S \mathbf{J} \cdot \mathbf{e}_i^* dS + Y_i^* \int_S \mathbf{M} \cdot \mathbf{h}_{zi}^* dS, \quad (9b)$$

where

$$Y''_i \mathbf{h}_{zi}'' = z_0 \frac{\nabla_t \cdot \mathbf{h}_{zi}''}{-i\omega\mu_z}, \quad \mathbf{h}_{zi}'' \equiv 0, \quad (9c)$$

$$Z'_i \mathbf{e}_{zi}' = z_0 \frac{\nabla_t \cdot \mathbf{e}_{zi}'}{-i\omega\epsilon_z}, \quad \mathbf{e}_{zi}'' \equiv 0. \quad (9d)$$

From a network viewpoint,  $V_i$  and  $I_i$  are the voltage and current on a source-excited transmission line, and their solution can be inferred by network techniques.

If  $\epsilon$  and  $\mu$  are discontinuous at  $z = z_1$ , the required continuity of  $\mathbf{E}_t$  and  $\mathbf{H}_t$  in Eqs. (6a) and (6b) implies the continuity of  $V_i$  and  $I_i$ , in view of the invariability along  $z$  of the transverse vector-mode functions. Hence, the modal network representation for this discontinuous case comprises a simple junction of the two transmission lines representative of the regions  $z < z_1$  and  $z > z_1$ , respectively.

The real power carried in the  $i$ th mode along the positive  $z$  direction is given by

$$\bar{S}_{zi} = \operatorname{Re} \int_S (V_i \mathbf{e}_i) \times (I_i \mathbf{h}_i)^* \cdot \mathbf{z}_0 dS = \operatorname{Re}(V_i I_i^*), \quad (10a)$$

where all quantities are root mean square and use has been made of the orthogonality condition (2.2.11b). If the region is homogeneous, lossless, extends

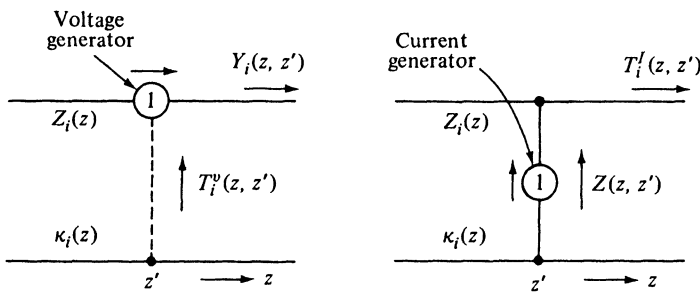


FIG. 7.2.2 Network problems for the determination of the modal Green's functions.

to  $z = \infty$ , and if all sources are contained in the space  $z < z_0$ , each modal field in  $z > z_0$  comprises a traveling wave  $\propto \exp(i\kappa_i z)$  which propagates without reflection toward  $z = \infty$ . In this case, the transmission-line equations, or the network representation in Fig. 7.2.2, yield  $I_i = Y_i V_i$ , whence

$$\tilde{S}_{zi} = Y_i |V_i|^2, \quad z > z_0, \quad \kappa_i \text{ real.} \quad (10b)$$

Equation (10b) is relevant only for the propagating modes ( $\kappa_i$  real) since  $\tilde{S}_{zi} = 0$  when  $\kappa_i$  is imaginary. In view of the assumption that all sources are confined in  $z < z_0$ , power must be carried toward  $z = \infty$  and  $\tilde{S}_{zi}$  must be positive. This *radiation condition* implies that

$$Y_i > 0 \quad \text{when } \kappa_i \text{ is real and positive,} \quad (10c)$$

and serves to specify the multivalued propagation constants  $\kappa'_i$  and  $\kappa''_i$  (similar conclusions are reached for waves carrying power to  $z = -\infty$ ). Thus, for a propagating mode,

$$\kappa'_i \gtrless 0 \text{ if } \epsilon_i \gtrless 0 \quad \text{and} \quad \kappa''_i \gtrless 0 \text{ if } \mu_i \gtrless 0. \quad (10d)$$

Negative values of  $\epsilon_i$  or  $\mu_i$  may still admit propagating modes. If  $(\epsilon_i/\epsilon_z)$  and  $k_i^2$  are both negative,  $\kappa'_i$  is real for all values of  $k'_{ii}$  and there is no *E*-mode cutoff; dual considerations apply to *H* modes. It should be noted that in contrast to wave propagation in isotropic media, it is possible to have a phase variation  $\exp(-i|\kappa_i|z)$  (i.e., phase progressing in the  $-z$  direction) associated with power flow in the  $+z$  direction. This observation emphasizes the importance of phrasing the radiation condition in anisotropic media in terms of outward power flow rather than in terms of "outgoing waves". The latter condition, implying phase propagation away from the source region, is equivalent to the (energy) radiation condition in isotropic, but not in anisotropic, media. In this connection, it may be noted that because of the mode orthogonality properties (2.2.11b), the total real power  $\tilde{S}_z$ , in a lossless medium is given by  $\tilde{S}_z = \sum_i \tilde{S}_{zi}$ , with only the propagating modes included. If each of the  $\tilde{S}_{zi}$  satisfies the radiation condition, so does the total power  $\tilde{S}_z$ . If  $\kappa_i$  is imaginary (non-propagating wave), the requirement of boundedness at infinity, in conjunction with the

assumed dependence  $\exp(i\kappa_i z)$ , implies that  $\text{Im } \kappa_i > 0$ , thereby specifying the multivalued functions in Eqs. (8) for all values of the transverse wavenumbers  $k_{ii}$ .

If the inhomogeneous medium is thought to be comprised of a series of thin homogeneous layers, the above conditions must be satisfied for each constituent traveling wave carrying power in the positive  $z$  direction and are therefore still applicable.

### 7.2b Formulation in Terms of Potential Functions

Instead of evaluating the electromagnetic fields via Eqs. (6a) and (6b) and (4), it is frequently convenient to deal with scalar potential functions from which the vector fields are derived by differentiation. The desired formulation is achieved upon noting as in Eqs. (2.3.1) that the vector-mode functions can be derived from scalar-mode functions  $\Phi_i$  and  $\psi_i$ , or, more conveniently, from the scalar potential functions  $I'(\mathbf{r})$  and  $V''(\mathbf{r})$  of Eqs. (2.3.4). After proceeding as in Sec. 2.3, one derives the analogue of Eqs. (2.3.38):<sup>6</sup>

$$\mathbf{E}(\mathbf{r}) = \frac{1}{-i\omega\epsilon_i(z)} \mathbf{Q}_\epsilon I'(\mathbf{r}) - \mathbf{L}_1 V''(\mathbf{r}), \quad (11a)$$

$$\mathbf{H}(\mathbf{r}) = \mathbf{L}_1 I'(\mathbf{r}) - \frac{1}{i\omega\mu_i(z)} \mathbf{Q}_\mu V''(\mathbf{r}), \quad (11b)$$

where  $\mathbf{L}_1$  and  $\mathbf{Q}_\alpha$  are the vector differential operators

$$\begin{aligned} \mathbf{Q}_\alpha &= \nabla_t \frac{\partial}{\partial z} - \mathbf{z}_0 \frac{\alpha_t(z)}{\alpha_z(z)} \nabla_t^2 = \nabla \times \nabla \times \mathbf{z}_0 - \left[ \frac{\alpha_t(z)}{\alpha_z(z)} - 1 \right] \nabla_t^2 \mathbf{z}_0 \\ \mathbf{L}_1 &= \nabla \times \mathbf{z}_0 \equiv -\mathbf{z}_0 \times \nabla_t. \end{aligned} \quad (11c)$$

In Eq. (11c),  $\alpha$  stands for either  $\epsilon$  or  $\mu$ . Equations (11a) and (11b) are valid at any *source-free* point  $z$  [i.e., any point at which  $v_i(z) = i_i(z) = 0$ ]. One verifies that the *E*-mode potential function  $I'(\mathbf{r})$  satisfies at any source-free point  $z$  the wave equation [see Eqs. (2.3.44)]:

$$\left[ \frac{\epsilon_t(z)}{\epsilon_i(z)} \mathcal{D}_\epsilon^2 + \nabla_t^2 + k_1^2(z) \right] I'(\mathbf{r}) = 0, \quad k_1^2(z) = \omega^2 \mu_i(z) \epsilon_i(z), \quad (12a)$$

$$\mathcal{D}_\epsilon^2 \equiv \epsilon_i(z) \frac{\partial}{\partial z} \frac{1}{\epsilon_i(z)} \frac{\partial}{\partial z}, \quad (12b)$$

while, for the *H*-mode potential function  $V''(\mathbf{r})$ ,

$$\left[ \frac{\mu_z(z)}{\mu_i(z)} \mathcal{D}_\mu^2 + \nabla_t^2 + k_2^2(z) \right] V''(\mathbf{r}) = 0, \quad k_2^2(z) = \omega^2 \mu_i(z) \epsilon_i(z). \quad (12c)$$

One notes from Eqs. (2.3.36a) and (2.3.37a) that on the perfectly conducting transverse boundaries  $s$  of the region,  $I'$  and  $V''$  satisfy the boundary conditions

$$I'(\mathbf{r}) = 0, \quad \frac{\partial V''(\mathbf{r})}{\partial \nu} = 0 \quad \text{on } s. \quad (12d)$$

### 7.2c The Dyadic Green's Functions

#### General case

For waveguide regions filled with the uniaxially anisotropic medium specified in Eq. (1), the dyadic Green's functions are derived by following the steps leading to Eqs. (2.3.40). Let  $Y_i(z, z')$  and  $T''_i(z, z')$  denote the current and voltage, respectively, observed at  $z$  due to excitation at  $z'$  by a unit strength voltage generator  $v_i(z') \equiv -1$ , and let  $Z''_i(z, z')$  and  $T'_i(z, z')$  denote the voltage and current, respectively, observed at  $z$  due to excitation at  $z'$  by a unit-strength current generator  $i_i(z') \equiv -1$  (see Fig. 7.2.2). Then the  $E$ -mode current  $I'_i(z, z')$  and  $H$ -mode voltage  $V''_i(z, z')$  due to the simultaneous presence of  $v_i(z')$  and  $i_i(z')$  are given by Eqs. (2.3.19) and (2.3.20) provided that  $\epsilon$  and  $\mu$  are replaced by  $\epsilon_i(z')$  and  $\mu_i(z')$ , respectively, and that  $j \rightarrow -i$  to account for the time dependence  $\exp(-i\omega t)$  in the present discussion. Instead of Eq. (2.3.39), one now obtains

$$I'(\mathbf{r}, \mathbf{r}') = -\mathbf{L}'_i \mathcal{S}'_d(\mathbf{r}, \mathbf{r}') \cdot \mathbf{M}^\circ - \frac{1}{i\omega\epsilon_i(z')} \mathbf{Q}'_\epsilon \mathcal{S}'_d(\mathbf{r}, \mathbf{r}') \cdot \mathbf{J}^\circ, \quad (13a)$$

$$V''(\mathbf{r}, \mathbf{r}') = \mathbf{L}'_i \mathcal{S}''_d(\mathbf{r}, \mathbf{r}') \cdot \mathbf{J}^\circ - \frac{1}{i\omega\mu_i(z')} \mathbf{Q}'_\mu \mathcal{S}''_d(\mathbf{r}, \mathbf{r}') \cdot \mathbf{M}^\circ, \quad (13b)$$

where the scalar functions  $\mathcal{S}'_d$  and  $\mathcal{S}''_d$  have the modal representations

$$\mathcal{S}'_d(\mathbf{r}, \mathbf{r}') = \sum_i \frac{1}{k_{ii}^2} Y_i(z, z') \Phi_i(\mathbf{p}) \Phi_i^*(\mathbf{p}'), \quad (13c)$$

$$\mathcal{S}''_d(\mathbf{r}, \mathbf{r}') = \sum_i \frac{1}{k_{ii}^2} Z''_i(z, z') \psi_i(\mathbf{p}) \psi_i^*(\mathbf{p}'). \quad (13d)$$

The prime on the operators  $\mathbf{L}'_i$  and  $\mathbf{Q}'_\alpha$  [see Eq. (11c)] denotes that all variables are replaced by their primed values. In deriving Eqs. (13a) and (13b) it is assumed that differentiation and summation operations can be freely interchanged, leading to the appearance of the factor  $1/k_{ii}^2$  in the summands of  $\mathcal{S}'_d$  and  $\mathcal{S}''_d$ . In this connection, the remarks made in connection with Eq. (2.3.24) are pertinent.

The dyadic Green's functions defined in Eqs. (2.3.26) are then found to be given

$$\mathcal{Z}(\mathbf{r}, \mathbf{r}') = -\frac{\mathbf{Q}_\epsilon}{i\omega\epsilon_i(z)} \frac{\mathbf{Q}'_\epsilon}{i\omega\epsilon_i(z')} \mathcal{S}'_d(\mathbf{r}, \mathbf{r}') + \mathbf{L}_i \mathbf{L}'_i \mathcal{S}''_d(\mathbf{r}, \mathbf{r}'), \quad (14a)$$

$$\mathcal{Y}(\mathbf{r}, \mathbf{r}') = \mathbf{L}_i \mathbf{L}'_i \mathcal{S}'_d(\mathbf{r}, \mathbf{r}') - \frac{\mathbf{Q}_\mu}{i\omega\mu_i(z)} \frac{\mathbf{Q}'_\mu}{i\omega\mu_i(z')} \mathcal{S}''_d(\mathbf{r}, \mathbf{r}'), \quad (14b)$$

$$\mathcal{T}_e(\mathbf{r}, \mathbf{r}') = -\frac{\mathbf{Q}_\epsilon}{i\omega\epsilon_i(z)} \mathbf{L}'_i \mathcal{S}'_d(\mathbf{r}, \mathbf{r}') - \mathbf{L}_i \frac{\mathbf{Q}'_\mu}{i\omega\mu_i(z')} \mathcal{S}''_d(\mathbf{r}, \mathbf{r}'), \quad (14c)$$

$$\mathcal{T}_m(\mathbf{r}, \mathbf{r}') = \mathbf{L}_i \frac{\mathbf{Q}'_\epsilon}{i\omega\epsilon_i(z')} \mathcal{S}'_d(\mathbf{r}, \mathbf{r}') + \frac{\mathbf{Q}_\mu}{i\omega\mu_i(z)} \mathbf{L}'_i \mathcal{S}''_d(\mathbf{r}, \mathbf{r}'). \quad (14d)$$

$\mathcal{S}'_d(\mathbf{r}, \mathbf{r}') = \mathcal{S}'_d(\mathbf{r}', \mathbf{r})$  and  $\mathcal{S}''_d(\mathbf{r}, \mathbf{r}') = \mathcal{S}''_d(\mathbf{r}', \mathbf{r})$ , so the dyadic Green's functions

satisfy the usual reciprocity conditions (2.3.28); this is a consequence of the symmetrical tensors  $\epsilon = \tilde{\epsilon}$  and  $\mu = \tilde{\mu}$ , which characterize the medium [see Eq. (1) and Sec. 1.5b]. The modal Green's functions  $Y'_i(z, z')$  and  $Z''_i(z, z')$  satisfy via Eqs. (7a) and (7b) the second-order differential equations

$$[D_\epsilon^2 + \kappa_i'^2(z)] Y'_i(z, z') = i\omega\epsilon_i(z')\delta(z - z'), \quad (15a)$$

$$[D_\mu^2 + \kappa_i''^2(z)] Z''_i(z, z') = i\omega\mu_i(z')\delta(z - z'), \quad (15b)$$

where the differential operator  $D_\alpha^2$  is defined in Eq. (12b), with the partial derivatives replaced by total derivatives. Hence, one verifies from Eqs. (13c), (13d), and (2.3.43) that

$$\nabla_t^{1/2} \mathcal{S}'_d(\mathbf{r}, \mathbf{r}') = i\omega\epsilon_z(z')G'(\mathbf{r}, \mathbf{r}'), \quad \nabla_t^{1/2} \mathcal{S}''_d(\mathbf{r}, \mathbf{r}') = i\omega\mu_z(z')G''(\mathbf{r}, \mathbf{r}'), \quad (16)$$

where  $G'$  and  $G''$  are scalar three-dimensional Green's functions that solve the inhomogeneous wave equation

$$\left[ \frac{\epsilon_z(z)}{\epsilon_i(z)} \mathcal{D}_\epsilon^2 + \nabla_t^2 + k_1^2(z) \right] G'(\mathbf{r}, \mathbf{r}') = -\delta(\mathbf{r} - \mathbf{r}'), \quad k_1^2 = \omega^2\mu_z\epsilon_z, \quad (17a)$$

$$\left[ \frac{\mu_z(z)}{\mu_i(z)} \mathcal{D}_\mu^2 + \nabla_t^2 + k_2^2(z) \right] G''(\mathbf{r}, \mathbf{r}') = -\delta(\mathbf{r} - \mathbf{r}'), \quad k_2^2 = \omega^2\mu_z\epsilon_z. \quad (17b)$$

From the modal representations [see Eqs. (13c), (13d), and (16)]

$$G'(\mathbf{r}, \mathbf{r}') = \frac{-1}{i\omega\epsilon_z(z')} \sum_i Y'_i(z, z') \Phi_i(\mathbf{p})\Phi_i^*(\mathbf{p}'), \quad (18a)$$

$$G''(\mathbf{r}, \mathbf{r}') = \frac{-1}{i\omega\mu_z(z')} \sum_i Z''_i(z, z') \psi_i(\mathbf{p})\psi_i^*(\mathbf{p}'). \quad (18b)$$

one recognizes that  $G'$  and  $G''$  satisfy on the transverse boundaries  $s$  of the region the boundary conditions

$$G' = 0, \quad \partial G''/\partial v = 0 \quad \text{on } s. \quad (19)$$

Concerning the boundary conditions in the  $z$  domain, a radiation condition is imposed on  $Y'_i(z, z')$  and  $Z''_i(z, z')$  if the region extends to infinity along  $z$ . If two media characterized by  $\epsilon_i(z)$ ,  $\mu_i(z)$  and  $\epsilon_2(z)$ ,  $\mu_2(z)$ , respectively, are joined at the plane  $z = z_1$ , the required continuity of  $\mathbf{E}_t$  and  $\mathbf{H}_t$  implies that of the modal voltages and currents. Since  $Y'_i(z, z')$  represents a current, and  $(1/\kappa'_i)Y'_i(d/dz)Y'_i(z, z') = (1/\omega\epsilon_i)(d/dz)Y'_i(z, z')$  represents a voltage,<sup>†</sup> one notes from Eq. (18a) that, for  $z_1 \neq z'$ ,

$$G' \text{ and } \frac{1}{\epsilon_i(z)} \frac{\partial G'}{\partial z} \quad \text{are continuous at } z = z_1, \quad (20a)$$

while, from dual considerations,

$$G'' \text{ and } \frac{1}{\mu_i(z)} \frac{\partial G''}{\partial z} \quad \text{are continuous at } z = z_1. \quad (20b)$$

---

<sup>†</sup>We recall the meaning of  $Y'_i(z)$  and  $Y'_i(z, z')$ , which denote, respectively, the modal characteristic admittance and the current response to unit voltage excitation.

If the region is terminated at  $z = z_2$  in a surface with constant impedance  $\mathcal{Z}$ , i.e.,  $\mathbf{E}_t = \mathcal{Z}\mathbf{H}_t \times \mathbf{z}_0$  at  $z = z_2$ , one has, from Eqs. (6a) and (6b),  $V_i(z_2) = \mathcal{Z}I_i(z_2)$ , whence from Eqs. (18a), (18b), (7a) and (7b),

$$\begin{aligned}\frac{\partial G'}{\partial z} &= i\omega\epsilon_t(z)\mathcal{Z}G', \\ \frac{\partial G''}{\partial z} &= \frac{i\omega\mu_t(z)}{\mathcal{Z}}G'',\end{aligned}\quad \text{at } z = z_2. \quad (20c)$$

For the above-stated boundary conditions,  $G'$  and  $G''$  in the waveguide region are uniquely determined by Eqs. (17), (19), and (20); Eqs. (18) constitute their solution in terms of a  $z$ -transmission modal representation. These remarks apply also to  $\mathcal{S}'_d$  and  $\mathcal{S}''_d$ . It is noted that the  $E$  and  $H$  modes are not coupled by these boundary conditions.

### *Longitudinal sources*

If the current elements  $\mathbf{J}^\circ$  and  $\mathbf{M}^\circ$  in Eqs. (2.3.26) are longitudinal, i.e.,  $\mathbf{J}^\circ = \mathbf{z}_0 J^\circ$ ,  $\mathbf{M}^\circ = \mathbf{z}_0 M^\circ$ , substantial simplification results in Eqs. (14) since  $\mathbf{z}_0 \cdot \mathbf{L}'_1 = 0$  and  $\mathbf{z}_0 \cdot \mathbf{Q}'_z = -[\alpha_t(z')/\alpha_z(z')] \nabla'^2$ . Hence, in view of Eq. (16),

$$\mathbf{E}(\mathbf{r}, \mathbf{r}') = -\frac{J^\circ}{i\omega\epsilon_t(z)} \mathbf{Q}_\epsilon G'(\mathbf{r}, \mathbf{r}') - M^\circ \mathbf{L}_1 G''(\mathbf{r}, \mathbf{r}'), \quad (21a)$$

$$\mathbf{H}(\mathbf{r}, \mathbf{r}') = J^\circ \mathbf{L}_1 G'(\mathbf{r}, \mathbf{r}') - \frac{M^\circ}{i\omega\mu_t(z)} \mathbf{Q}_\mu G''(\mathbf{r}, \mathbf{r}'). \quad (21b)$$

### *Piecewise constant media*

If  $\epsilon_t$ ,  $\epsilon_z$ ,  $\mu_t$ , and  $\mu_z$  are constant, then  $\mathcal{D}_\alpha^2 \rightarrow \partial^2/\partial z^2$ . Upon introducing the change of variable

$$\zeta = \sqrt{\frac{\epsilon_t}{\epsilon_z}} z, \quad (22)$$

one may write the expression inside the brackets in Eq. (17a) as  $\nabla_\zeta^2 + k_1^2$ , where  $\nabla_\zeta^2 = \nabla_z^2 + \partial^2/\partial\zeta^2$ . If  $(\epsilon_t/\epsilon_z)$  is positive real,  $\zeta$  can be interpreted as a real coordinate, whence the modified Eq. (17a) represents a Green's function problem in a homogeneous isotropic  $(\rho, \zeta)$  space characterized by a wavenumber  $k_1 = \omega\sqrt{\mu_t\epsilon_z}$ .<sup>6,7</sup> Consider the isotropic Green's function defined by the equation

$$(\nabla_\zeta^2 + k_1^2)G'_\zeta(\rho, \zeta; \rho', \zeta') = -\delta(\rho - \rho')\delta(\zeta - \zeta'); \quad (23)$$

then the anisotropic Green's function  $G'$  is given in terms of  $G'_\zeta$  as [note:  $\delta(ax) = (1/|a|)\delta(x)$ ]

$$G'(\rho, z; \rho', z') = \sqrt{\frac{\epsilon_t}{\epsilon_z}} G'_\zeta \left( \rho, \sqrt{\frac{\epsilon_t}{\epsilon_z}} z; \rho', \sqrt{\frac{\epsilon_t}{\epsilon_z}} z' \right). \quad (24)$$

The boundary conditions on  $G'_\zeta$  are inferred from those on  $G'$  in Eqs. (19) and (20). If  $\epsilon_t/\epsilon_z$  is not positive real, one may still derive  $G'$  from the isotropic Green's function  $G'_\zeta$  if the resulting function can be continued analytically into the appropriate domain of complex  $\epsilon_t/\epsilon_z$ .

Dual considerations apply to  $G''$  in Eq. (17b).

***Isotropic media***

For isotropic media with  $\epsilon_r(z) = \epsilon_z(z) \equiv \epsilon(z)$ ,  $\mu_r(z) = \mu_z(z) \equiv \mu(z)$ , the operator  $\mathbf{Q}_z$  in Eq. (11c) reduces to  $\nabla \times \nabla \times \mathbf{z}_0$ , and the results become identical with those in Sec. 2.3d.

**7.3 SOURCES IN UNBOUNDED MEDIA**

The results in Sec. 7.2 are now applied to radiation problems in an unbounded homogeneous medium characterized by a uniaxially anisotropic permittivity  $\epsilon$  and a scalar permeability  $\mu_0$ :

$$\boldsymbol{\epsilon} = \epsilon_0(\mathbf{1}_t + \mathbf{z}_0\mathbf{z}_0\epsilon) \rightarrow \epsilon_0 \begin{pmatrix} 1 & 0 & 0 \\ 0 & 1 & 0 \\ 0 & 0 & \epsilon \end{pmatrix}, \quad \boldsymbol{\mu} = \mathbf{1}\mu_0, \quad (1)$$

where  $\mathbf{1}$  and  $\mathbf{1}_t = \mathbf{1} - \mathbf{z}_0\mathbf{z}_0$  are the unit dyadic and the dyadic in the domain transverse to the optic ( $z$ ) axis, respectively;  $\mathbf{z}_0$  is a unit vector along  $z$ , and  $\epsilon_0$  and  $\mu_0$  are the constitutive parameters in vacuum. Because  $H$ -mode fields in this medium behave as in vacuum and  $E$ -mode fields can be derived from vacuum solutions by coordinate scaling (see Sec. 7.2), the results for fields and potentials in the uniaxial medium can be written down directly from corresponding isotropic solutions in Sec. 5.4. The discussion in this section is therefore concerned with the interpretation of such scaled solutions, with emphasis on features of the radiation process typical of an anisotropic environment. In this connection, rays and wavenumber surfaces are utilized for relating the uniaxial results to radiation characteristics observed in more general anisotropic media.

When  $\epsilon > 0$ , the wavenumber surface is ellipsoidal but resembles the spherical surface for isotropic media. The propagation mechanism in this case may be regarded as undergoing a continuous distortion in the transition from an isotropic to an anisotropic regime. This is not true for  $\epsilon < 0$ , when the wavenumber surface is open-branched and thus admits propagating wave solutions for arbitrarily large transverse and longitudinal wavenumbers. The partial differential equations descriptive of wave behavior along the open branches are hyperbolic, thus permitting the existence of field discontinuities and singularities on “characteristic cones” (shadow boundaries) similar to those encountered in time-dependent, impulse-excited fields in an isotropic medium. For *point*-and *line*-source excitation, the singularities on the shadow boundaries are so strong as to render the total radiated power infinite, an anomaly referred to in the literature as the “infinity catastrophe.” While the infinity indicates the inadequacy of the equivalent dielectric description of a cold, lossless plasma as in Eq. (1), it is of interest to explore the cause of the infinity and methods for its removal. This is done in detail in Secs. 7.3a and 7.3e.

The presentation begins in Sec. 7.3a with radiation from a time-harmonic current element oriented along the optic axis. After a discussion of the closed-

form solution, obtained by coordinate scaling of the vacuum fields, attention is given to a modal (integral) representation that must be employed under more general conditions, when results cannot be expressed in closed form. Analytic properties of the integrand, arising especially from saddle points and singularities, are related to features observed in the closed-form expressions, thereby providing further insight into the radiation mechanism. Sections 7.3b, 7.3c, and 7.3e deal with other time-harmonic source configurations and Sec. 7.3d explores the radiation properties of a uniformly moving point charge.

### 7.3a Dipoles Oriented Along the Optic Axis

*Time-harmonic electric source current density*

$$\mathbf{\hat{J}}(\mathbf{r}, t) = Il\delta(\mathbf{r})e^{-i\omega t}\mathbf{z}_0. \quad (2)$$

The electromagnetic fields in the uniaxial medium described by Eq. (1) can be derived from the scalar *E*-mode Green's function  $G'_f(\mathbf{r}, \mathbf{r}')$  defined by [see Eq. (7.2.17a)]

$$\left[ \epsilon \left( \frac{\partial^2}{\partial z^2} + k_0^2 \right) + \nabla_i^2 \right] G'_f(\mathbf{r}, \mathbf{r}') = -\delta(\mathbf{r} - \mathbf{r}'), \quad (3a)$$

subject to an energy radiation condition at  $\infty$ . The solution is given by

$$G'_f(\mathbf{r}, \mathbf{r}') = \frac{e^{ik_0N(\theta)|\mathbf{r}-\mathbf{r}'|}}{4\pi N(\theta)|\mathbf{r}-\mathbf{r}'|}, \quad (3b)$$

where

$$k_0 = \omega\sqrt{\mu_0\epsilon_0} \quad \text{and} \quad N(\theta) = \sqrt{\cos^2\theta + \epsilon\sin^2\theta}, \quad (3c)$$

with  $N(\theta)$  denoting the ray refractive index. Field components are derived via Eqs. (7.2.21) and yield for  $r' = 0$ , in spherical coordinates,<sup>6</sup>

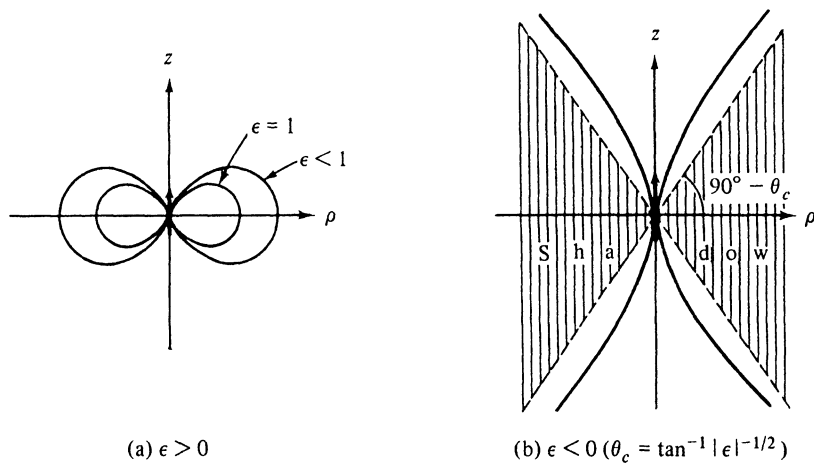
$$E_r = \sqrt{\frac{\mu_0}{\epsilon_0}} \frac{Ik_0 l \cos\theta e^{ik_0 r N(\theta)}}{2\pi k_0 r^2 N^2(\theta)} \left( 1 + \frac{i}{k_0 r N(\theta)} \right), \quad (4a)$$

$$E_\theta = \sqrt{\frac{\mu_0}{\epsilon_0}} \frac{-iIk_0 l \epsilon \sin\theta e^{ik_0 r N(\theta)}}{4\pi r N^3(\theta)} \times \left[ 1 + \left( 1 + 2\frac{\epsilon-1}{\epsilon} \cos^2\theta \right) \left( \frac{i}{k_0 r N(\theta)} - \frac{1}{k_0^2 r^2 N^2(\theta)} \right) \right] \quad (4b)$$

$$H_\phi = \frac{-iIk_0 l \epsilon \sin\theta e^{ik_0 r N(\theta)}}{4\pi r N^2(\theta)} \left( 1 + \frac{i}{k_0 r N(\theta)} \right), \quad (4c)$$

$$H_r = H_\theta = E_\phi = 0, \quad (4d)$$

where  $I$  is the current in the element and  $l$  is an infinitesimal length. For arbitrary  $\mathbf{r}'$ , one replaces  $r$  by  $|\mathbf{r} - \mathbf{r}'|$ . The coordinate system, with  $\rho = r \sin\theta$ ,  $z - z' = r \cos\theta$ , is the same as for the dipole in an isotropic medium (Fig. 5.4.1). Provided that one chooses  $\text{Im } N(\theta) \geq 0$ , the results are valid for  $0 \leq \arg \epsilon \leq \pi$  (i.e., for the dissipative case  $\text{Im } \epsilon > 0$  and also for the “hyperbolic” case  $\epsilon < 0$ ,  $\text{Im } \epsilon = 0$ ). The radiated power density  $\bar{S}$  in a lossless

FIG. 7.3.1 Pattern functions:  $A(\theta) = \sin^2 \theta / N^s(\theta)$ .

medium is given via Eqs. (4) by

$$\bar{S}_r = \begin{cases} \operatorname{Re}(E_\theta H_\phi^*) = \sqrt{\frac{\mu_0}{\epsilon_0}} \frac{\epsilon^2 |Ik_0 l|^2 \sin^2 \theta}{(4\pi)^2 r^2 N^s(\theta)}, & N \text{ real} \\ 0, & N \text{ imaginary} \end{cases} \quad (5a)$$

$$\bar{S}_\theta = \bar{S}_\phi = 0, \quad N \text{ real or imaginary} \quad (5c)$$

Typical shapes of the radiation pattern function  $A(\theta) = \sin^2 \theta / N^s(\theta)$  are shown in Fig. 7.3.1. The total radiated power is

$$P = 2\pi r^2 \int \bar{S}_r \sin \theta d\theta = \begin{cases} \text{finite}, & \epsilon > 0, \\ \infty, & \epsilon < 0. \end{cases} \quad (6a)$$

$$(6b)$$

### Discussion

The solution in Eq. (3b) is derived by a direct application of the coordinate scaling in Eq. (7.2.22) to the isotropic free-space Green's function in Eq. (5.4.2b) when  $\arg \epsilon = 0$ , with subsequent analytic continuation into the range  $0 < \arg \epsilon \leq \pi$  [see also Eq. (9) et seq.]. When  $\epsilon = 1$ , Eqs. (4) reduce properly to the vacuum fields in Eqs. (5.4.3).

The simple closed-form solutions in Eqs. (4) and (5) reveal interesting features that are characteristic of radiation phenomena in anisotropic regions. When  $\epsilon > 0$ , the effect of anisotropy is primarily to distort, but not to alter fundamentally, the equiphase surfaces, radiation patterns, etc., encountered in an isotropic environment, whereas negative real values of  $\epsilon$  yield novel and anomalous characteristics. This may be anticipated from the partial differential equation (3a), which is elliptic when  $\epsilon > 0$  but hyperbolic when  $\epsilon < 0$ , with the consequent appearance of (characteristic) surfaces of singularity in the latter instance. Thus, it is no longer sufficient to define the far zone as  $k_0 r \gg 1$  as

in the isotropic case but instead one must have  $k_0 r N(\theta) \gg 1$ . When  $\epsilon > 0$ , a far zone exists at sufficiently great distance from the source, and the corresponding radiation field, given by Eqs. (4) with the bracketed expressions equated to unity, varies like  $1/r$  and is transverse to  $r$ . This is not true when  $\epsilon < 0$ , since  $N(\theta)$  then possesses a zero on the cone  $\theta_c = \tan^{-1}(|\epsilon|^{-1/2})$ , on which all the field components have singularities regardless of the value of  $r$ . To make matters worse, the corresponding radiated power density in Eq. (5a) behaves near  $\theta_c$  like  $(\theta_c - \theta)^{-5/2}$ , which singularity is non-integrable near  $\theta_c$  and leads to the result in Eq. (6b). Phrased in terms of the radiation resistance  $R = P/I^2$ , one concludes that  $R = \infty$  when  $\epsilon < 0$ , a behavior found to be exhibited also by dipoles in a more general gyrotropic medium with open-branched refractive index surfaces (hyperbolic regime; see Sec. 8.3). It must be kept in mind, however, that the infinities disappear when a loss mechanism is included ( $\epsilon$  complex), and that the entire description of a plasma medium by the simple tensor in Eq. (1), with  $\epsilon = [1 - (\omega_p^2/\omega^2)]$ , is valid only in the small signal approximation, which is clearly violated near  $\theta_c$ . It is worth noting that even within the framework of the present idealized model, the field singularities for  $\epsilon < 0$  disappear if the source is distributed and hence characterized by a more regular spatial function than the delta function  $\delta(\mathbf{r} - \mathbf{r}')$  descriptive of the Hertzian dipole element.<sup>8,9</sup> This aspect is considered further in Sec. 7.3e.

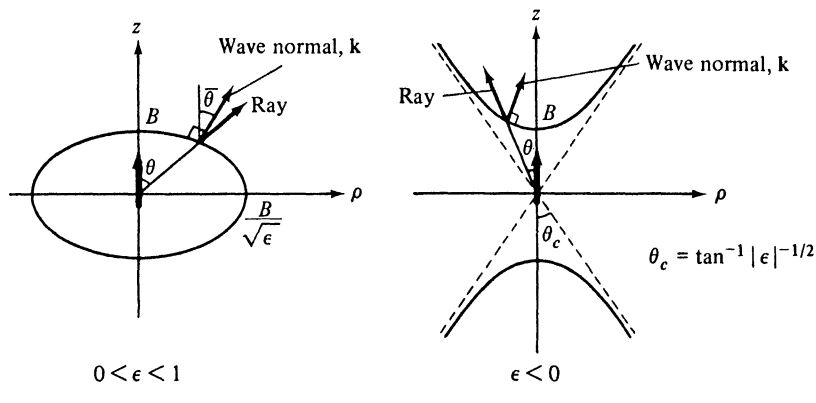
One observes from Eq. (5a) that energy flows *radially outward* from the source, thereby confirming the physical mechanism of energy transport along rays discussed in Sec. 1.6. Propagating rays exist only in the illuminated region wherein  $N(\theta) > 0$ , and no energy is carried into the shadow region  $N(\theta) = i|N(\theta)|$ , where the fields are evanescent. The zones of illumination,  $|\tan \theta| < \tan \theta_c = |\epsilon|^{-1/2}$ , and shadow,  $|\tan \theta| > \tan \theta_c$ , are in evidence in Fig. 7.3.1(b). In view of the anisotropy, the rays are not normal to the equiphasic surfaces defined by the equation  $rN(\theta) = \text{constant}$ , or

$$\frac{z^2}{|\epsilon|} \pm \rho^2 = \frac{B^2}{|\epsilon|}, \quad \epsilon \gtrless 0,$$

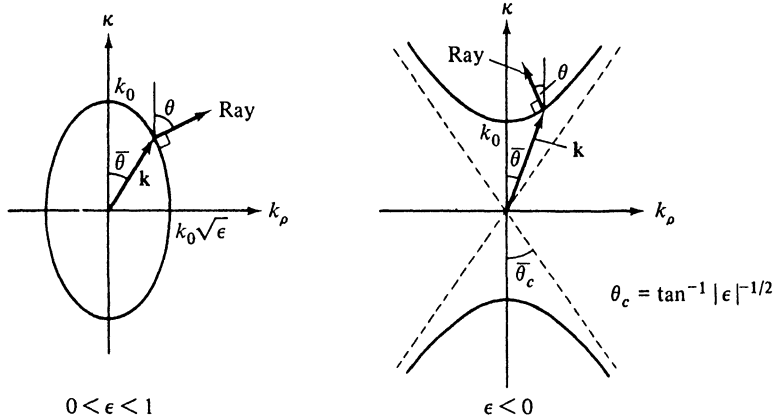
where  $z = r \cos \theta$ ,  $\rho = r \sin \theta$ , and  $B$  is a positive constant. Evidently, the surfaces are elliptical when  $\epsilon > 0$  and hyperbolic when  $\epsilon < 0$ , as shown in Fig. 7.3.2(a). It is instructive to compare these plots with the wavenumber diagrams in Fig. 7.3.2(b), from which one may also deduce directly certain salient features of the radiation field (see Sec. 1.6). For example, from the configuration of normals (rays) that can be drawn to the surfaces in Fig. 7.3.2(b), it follows that all space is accessible to radiation when  $\epsilon > 0$ , whereas only the region  $|\tan \theta| < |\epsilon|^{-1/2}$  is illuminated when  $\epsilon < 0$ .

#### *Modal procedure*

While the point-source radiation problem in the infinite, homogeneous, uniaxially anisotropic medium can be solved in closed form as in Eq. (3b), no such simple solution is possible for partially bounded regions. Instead, one



(a) Equiphase surfaces, wave normals, and rays



(b) Wavenumber surfaces

FIG. 7.3.2 Equiphase and wavenumber surfaces.

must resort to a modal representation of the fields and then attempt an approximate evaluation by asymptotic methods. It is instructive to apply this procedure to an infinite medium problem in order to gain insight into the difficulties encountered in the asymptotic evaluation and to establish the accuracy of the approximate solution by comparison with the exact one. Because of the symmetry of the fields about the  $z$ -axis, a circular waveguide description of the transverse cross section is appropriate, and the corresponding mode functions are given in Eq. (3.2.78b):

$$\Phi_i(\rho) \equiv \phi_i(\rho) = \sqrt{\frac{\xi}{2\pi}} J_0(\xi\rho), \quad 0 < \xi < \infty; \quad k_n \equiv \xi; \quad \sum_i \rightarrow \int_0^\infty d\xi. \quad (7a)$$

Since the region is unbounded along  $z$ , one has from a simple network calculation,

$$Y'_i(z, z') = \frac{1}{2Z'_i} e^{i\kappa'_i|z-z'|}, \quad (7b)$$

with  $Z'_i$  and  $\kappa'_i$  specified in Eq. (7.2.8a). Upon substituting these results into Eq. (7.2.18a) and extending the  $\xi$  integration interval to run from  $-\infty$  to  $+\infty$ , one obtains the desired representation [see Eq. (5.4.7a) for the analogous formulation in an isotropic medium; note the different time dependence  $\exp(j\omega t)$ ]:†

$$G'_f(\mathbf{r}, \mathbf{r}') = \frac{i}{8\pi\epsilon} \int_{-\infty}^{\infty} \xi H_0^{(1)}(\xi\rho) \frac{e^{i\kappa(\xi)|z-z'|}}{\kappa(\xi)} d\xi, \quad \kappa(\xi) = \sqrt{k_0^2 - \frac{\xi^2}{\epsilon}}. \quad (8)$$

The radiation condition, as in Eq. (7.2.10d), requires that  $\kappa > 0$  when real, and  $\kappa = i|\kappa|$  when imaginary, whence the integration path is the same as in Fig. 5.3.6; the branch points are located at  $\xi_b = \pm k_0\sqrt{\epsilon}$ , and the choice of branch cuts assures that  $\text{Im } \kappa > 0$  on the entire top Riemann sheet. When  $\epsilon = 1$ , Eq. (8) reduces to the isotropic Green's-function representation in Eq. (5.4.7a).

It is of interest to point out that the radiation condition on the integrand in Eq. (8) may also be imposed from a study of the refractive index curves in Fig. 7.3.2(b) (with  $k_\rho \equiv \xi$ ). The cylindrical waves in the integral representation degenerate into plane waves far from the source, and when  $z > z'$ , these waves must carry energy toward  $z = +\infty$ . Hence the vectors  $\mathbf{v}_g$  or  $\bar{\mathbf{S}}$  associated with these waves must have a component along the  $+z$  direction. From general considerations [see Eq. (1.7.53a)] it is known that the angle between the  $\mathbf{k}$  and  $\mathbf{v}_g$  vectors is less than  $90^\circ$ , so the required portions of the dispersion curves in Fig. 7.3.2(b) are those for which  $\kappa \geq 0$ . This alternative method of imposing the radiation condition through use of the refractive index plots is frequently to be preferred in more complicated situations (gyrotropic media) where the analytical form of the characteristic admittances  $Y_i$  is much more involved than in the present case.

When  $\epsilon$  is positive real, the integral in Eq. (8) evidently converges uniformly and absolutely since  $H_0^{(1)}(\xi\rho) \sim (\xi\rho)^{-1/2} \exp(i\xi\rho)$ ,  $-\pi < \arg \xi < 2\pi$ , and  $\text{Im } \kappa > 0$  as  $\xi \rightarrow \infty$ . The case of negative real  $\epsilon$  is approached unambiguously by assuming losses in the medium, whence  $0 < \arg \epsilon < \pi$ . One observes from Fig. 5.3.3(b) applied to  $\text{Im } k > 0$  that  $\arg \sqrt{k_0^2\epsilon - \xi^2}$  varies from  $(\arg \epsilon)/2$  to  $\pi/2$  as  $\xi$  moves from zero to infinity along the real axis. From  $\kappa = \epsilon^{-1/2}(k_0^2\epsilon - \xi^2)^{1/2}$ , one has

$$0 \leq \arg \kappa \leq \frac{\pi - \arg \epsilon}{2} \quad \text{for real } \xi, \quad (9)$$

with the lower and upper limits corresponding to  $\xi = 0$  and  $\xi = \pm\infty$ , respectively. Thus, for  $0 \leq \arg \epsilon < \pi$ ,  $\text{Im } \kappa > 0$  as  $|\xi| \rightarrow \infty$  along the real axis

†For the calculation of radiated power, a plane-wave representation as in Sec. 1.2c may be more convenient than the guided-wave representation employed here.

and the convergence of the integral remains unaffected. In consequence, the formula in Eq. (8) may be employed over the extended range  $\text{Im } \epsilon > 0$ .

When  $\arg \epsilon = \pi$ ,  $\kappa$  is positive real along the entire real  $\xi$  axis and the integral in Eq. (8) is no longer absolutely, but instead conditionally, convergent. Since the derivation of the electromagnetic fields requires the repeated differentiation of  $G'$ , it is desirable to obtain a representation that retains the exponential convergence as  $\xi \rightarrow \infty$ . Evidently, such a formulation involves the deformation of the integration path into the complex plane. If branch cuts are introduced along the lines  $\text{Re } \kappa = 0$  (see Fig. 7.3.3), then  $\text{Re } \kappa > 0$  on the entire top sheet of the two-sheeted  $\xi$  plane. Thus, as  $\xi \rightarrow \infty$ ,  $\kappa \sim \pm \xi \sqrt{|\epsilon|}$  for  $\text{Re } \xi \geq 0$ , so that in the right half-plane, the exponential dependence in the integrand is  $\exp(i\Psi)$ , with  $\Psi = \xi\rho + \kappa|z - z'| \sim \xi(\rho + |z - z'|/\sqrt{|\epsilon|})$ , while in the left half-plane,  $\Psi \sim \xi(\rho - |z - z'|/\sqrt{|\epsilon|})$ . Thus,  $\text{Im } \Psi > 0$  when

$$\text{Im } \xi > 0, \quad \text{as } |\xi| \rightarrow \infty \text{ with } \text{Re } \xi > 0, \quad (10a)$$

$$\begin{aligned} \text{Im } \xi > 0, \quad & |\tan \theta| > \tan \theta_c \\ \text{Im } \xi < 0, \quad & |\tan \theta| < \tan \theta_c \end{aligned} \} \text{ as } |\xi| \rightarrow \infty \text{ with } \text{Re } \xi < 0, \quad (10b)$$

where the observation angle  $\theta$  and the limiting angle  $\theta_c$  are defined in Eqs. (4) and in Fig. 7.3.2(b), respectively. A distortion of the endpoints of the integration path away from the real  $\xi$  axis according to Eqs. (10) then assures the exponential convergence of the integral in Eq. (8) when  $\arg \epsilon = \pi$ . The different convergence requirements in Eq. (10b) for  $|\tan \theta| \leq \tan \theta_c$  (i.e., for observation points in the illuminated or shadow regions) are already indicative of the critical role played by the shadow boundary cone  $|\tan \theta| = \tan \theta_c$ . For observation points on the shadow boundary,  $\Psi \sim 0$ , the integrand behaves asymptotically like  $\xi^{-1/2}$ , and the integral diverges.

An asymptotic evaluation of the integral in Eq. (8) can be carried out as in Sec. 5.3, except that we prefer to remain in the complex  $\xi$  plane for the present analysis, in view of the simple interpretation of the saddle-point condition via the refractive index plots. The Hankel function is replaced by its large argument approximation in Eq. (5.3.13b), and the resulting exponential in the integrand has the previously noted form  $\exp(i\Psi) = \exp[ir(\xi \sin \theta + \kappa|\cos \theta|)]$ . For large values of  $r$ , the dominant contribution arises from the vicinity of the saddle point  $\xi_s$ , which is obtained from a solution of the equation  $(d/d\xi)[\xi \sin \theta + \kappa|\cos \theta|] = 0$ ,

$$\frac{d\kappa(\xi)}{d\xi} \Big|_{\xi_s} = -\frac{\xi_s}{\epsilon\kappa(\xi_s)} = -|\tan \theta|. \quad (11a)$$

This relation is easily solved for  $\xi_s$ ,

$$\xi_s = \frac{k_0 \epsilon \sin \theta}{N(\theta)}, \quad \kappa(\xi_s) = \frac{k_0 |\cos \theta|}{N(\theta)}, \quad (11b)$$

with  $N(\theta)$  so defined that  $\arg N(\theta) = -\arg \kappa(\xi_s)$ . Equation (11a) is identical

with Eq. (7.1.7) if  $k_r \equiv \xi_s$ , and therefore has a simple graphical interpretation: the real values of  $\xi_s$ ,  $\kappa(\xi_s)$ , which define a propagating wave, correspond to points on the  $k$  versus  $\bar{\theta}$  plot having a normal inclined to the positive  $z$  axis at an angle  $\theta$  (see Fig. 7.3.2). Since the normal to the surface coincides with the ray direction, one verifies from the saddle-point condition that the rays proceed radially from the source to the observation point. Conversely, the  $k$  versus  $\bar{\theta}$  plots may be employed for the location of the saddle point(s): the saddle points  $\xi_s$  correspond to those surface points that have a normal  $\mathbf{v}$  directed along  $\theta$ , with  $\mathbf{k} \cdot \mathbf{v} \geq 0$ . As noted in Sec. 1.6, this fundamental condition remains valid for propagation problems in more general media where  $\kappa(\xi)$  is no longer the simple function specified in Eq. (8).

The saddle point  $\xi_s$  lies on the positive real  $\xi$  axis when  $\epsilon$  is positive, on the negative real  $\xi$  axis when  $\epsilon < 0$  and  $N(\theta) > 0$ , and in the upper half of the complex  $\xi$  plane when  $\epsilon < 0$  and  $N(\theta)$  is positive imaginary. The two first-mentioned conditions could also have been predicted from a study of Figs. 7.1.1(a) and 7.1.1(b). A closer examination of the expression for  $\xi_s$  in Eq. (11b) for a slightly dissipative medium with  $0 < \text{Im } \epsilon \ll 1$  reveals that the saddle point lies slightly above the real  $\xi$  axis when  $N(\theta)$  is essentially real, and lies slightly to the left of the imaginary axis, in the interval  $|\xi_s| > k_0\sqrt{|\epsilon|}$ , when  $N(\theta)$  is essentially imaginary. For positive real  $\epsilon$ , Eq. (8) is very similar to Eq. (5.4.7a), and the asymptotic evaluation of the integral along the steepest-descent path through the saddle point proceeds as for a source in vacuum. For negative real  $\epsilon$ , with  $|\tan \theta| < \tan \theta_c$ , the endpoints of the integration path are deformed into the first and third quadrants of the  $\xi$  plane, as noted in Eqs. (10). Since

$$\frac{d^2\kappa}{d\xi^2}\Big|_{\xi_s} = \frac{-N^3(\theta)}{k_0\epsilon|\cos^3 \theta|}, \quad (12)$$

this quantity is positive in the present instance and represents a measure of the curvature  $K$  of the refractive index plots via the relation  $K = (d^2\kappa/d\xi^2)_{\xi_s} \cdot |\cos^3 \theta|$ ; both its algebraic sign, and an estimate of its magnitude, may be inferred directly from an inspection of the curves in Fig. 7.1.1. Because  $d^2\kappa/d\xi_s^2 > 0$ , the steepest-descent path (SDP) through the saddle point is inclined at a  $+45^\circ$  angle with the positive  $\xi$  direction [see Eq. (4.2.5)]. The SDP is defined by the equation  $\text{Re } \Psi(\xi) = \text{Re } \Psi(\xi_s)$  (see Sec. 4.1b), so

$$\text{Re } (\kappa|\cos \theta| + \xi \sin \theta) = k_0 N(\theta), \quad \kappa = \sqrt{k_0^2 + \frac{\xi^2}{|\epsilon|}}. \quad (13a)$$

If the branch cuts from  $\xi_b = \pm ik_0\sqrt{|\epsilon|}$  are chosen along the straight lines  $\text{Re } \kappa = 0$ , then  $\text{Re } \kappa > 0$  on the entire top sheet of the two-sheeted  $\kappa$  surface, and, as noted earlier,  $\kappa \sim \pm \xi/\sqrt{|\epsilon|}$  as  $\xi \rightarrow \infty$  in the half-planes  $\text{Re } \xi \gtrless 0$ . Consequently, the SDP is asymptotic to the straight lines

$$\text{Re } \xi^{\pm} \equiv \xi_r^{\pm} = \pm \sqrt{|\epsilon|} k_0 [|\cos \theta| \mp \sqrt{|\epsilon|} \sin \theta]^{1/2}; \quad (13b)$$

one easily verifies that  $\xi_r^- < \xi_s$ , and that the path crosses the imaginary  $\xi$  axis below the branch point  $\xi_b = ik_0\sqrt{|\epsilon|}$ . The SDP therefore takes the form shown

in Fig. 7.3.3(a); it passes through the branch cut arising from the Hankel function in the integrand of Eq. (8). Since the integrand decays exponentially in the first and third quadrants of the complex  $\xi$  plane, the original integration path may be deformed into the SDP without intercepting any singularities.

The resulting first-order asymptotic approximation of the integral for  $\epsilon \gtrless 0, N(\theta) > 0$ , may be obtained from Eq. (4.2.1b) and yields [see also Eq. (1.6.21)]

$$G'_f(\mathbf{r}, \mathbf{r}') \sim \frac{e^{ik_0 r N(\theta)}}{4\pi r N(\theta)}, \quad r \gg 1, \quad N(\theta) \text{ real}, \quad (14)$$

the same expression as the exact result in Eq. (3). Although Eq. (14) happens to agree with the exact formula, it was derived subject to the assumptions that the  $r$ -independent factors in the integrand of Eq. (8) are slowly varying and that  $\kappa''(\xi_s) \not\approx 0, \xi_s \not\approx 0$ ; the condition  $\xi_s \not\approx 0$  arises from the replacement of the Hankel function by its asymptotic form, valid only when  $|\xi\rho| \gg 1$  along the entire path. One observes from Eq. (12) that  $\kappa''(\xi_s) \rightarrow 0$  as  $N(\theta) \rightarrow 0$ , so the validity of the asymptotic expression breaks down as the observation point approaches the shadow boundary. In this region, the saddle point moves to  $\xi_s = -\infty$ , where the curvature  $K$  of the refractive index diagram tends to zero—an indication that difficulties may arise in the asymptotic evaluation. From the exact field expressions in Eqs. (4), it is noted that the asymptotic result to  $O(1/r)$  is meaningful only when  $r \gg 1$  implies also  $k_0 r N(\theta) \gg 1$ , and this requirement must be imposed here to delimit the range of validity of the first-order asymptotic formula. Since  $\xi_s \propto k_0/N(\theta)$ , the condition

$$\frac{k_0^2 r}{|\xi_s|} \gg 1 \quad (14a)$$

serves to restrict the admissible range of saddle-point locations. These observa-

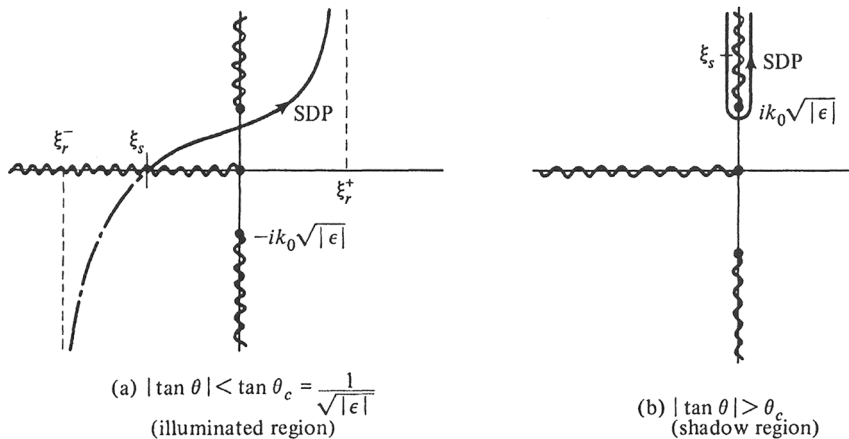


FIG. 7.3.3 Steepest-descent paths in the complex  $\xi$  plane.

tions will also apply to asymptotic calculations in gyrotropic media (see Sec. 8.3c) if the refractive index surface contains an open branch.

If  $|\tan \theta| > \tan \theta_c$ , the saddle point lies slightly to the left of the imaginary axis and above the branch point at  $\xi_b = ik_0\sqrt{|\epsilon|}$ . In the interval  $\xi = i|\xi|$ ,  $|\xi| > k_0\sqrt{|\epsilon|}$ , the propagation constant  $\kappa$  is imaginary, and if the branch cuts are drawn as before,  $\kappa = i|\kappa|$  when  $\arg(\xi - \xi_b) = \pi/2$  while  $\kappa = -i|\kappa|$  when  $\arg(\xi - \xi_b) = -3\pi/2$ . Thus, Eq. (13a), with the right-hand side set equal to zero, is satisfied along a path SDP that surrounds the branch cut [Fig. 7.3.3(b)]. In view of Eqs. (10), the exponential function in the integrand of Eq. (8) decays in the upper half of the  $\xi$  plane, so the original integration path may be deformed into the SDP without encountering any singularities. The resulting first-order asymptotic evaluation yields

$$G'_f(\mathbf{r}, \mathbf{r}') \sim \frac{e^{-k_0 r |N(\theta)|}}{4\pi i r |N(\theta)|}, \quad k_0 r |N(\theta)| \gg 1, \quad (15)$$

an expression that represents the analytic continuation of Eq. (14) to positive imaginary values of  $N(\theta)$ . The asymptotic evaluation therefore confirms the previously observed division into illuminated and shadow regions when  $\epsilon < 0$ , but gives no information about the field behavior in the immediate vicinity of the shadow boundary.

For the dissipative case with  $\text{Im } \epsilon > 0$ , the saddle point is located in the upper half of the  $\xi$  plane and the resulting asymptotic results are found to be the same as in Eq. (14), with  $\text{Im } N(\theta) > 0$ .

#### *Time-harmonic magnetic source current density*

$$\hat{\mathbf{M}}(\mathbf{r}, t) = Vl\delta(\mathbf{r})e^{-i\omega t}\mathbf{z}_0. \quad (16)$$

The relevant scalar  $H$ -mode Green's function  $G''_f(\mathbf{r}, \mathbf{r}')$  is, in view of Eqs. (1) and (7.2.17b), identical with the one in vacuum [see Eq. (3), with  $N(\theta) = 1$ ] and the fields derived therefrom are also the same as in vacuum [see Eq. (5.4.16) et seq.].

#### **7.3b Dipoles Oriented Transverse to the Optic Axis**

##### *Time-harmonic electric source current density*

$$\hat{\mathbf{J}}(\mathbf{r}, t) = Il\delta(\mathbf{r})e^{-i\omega t}\mathbf{x}_0. \quad (17)$$

A dipole oriented transverse to the optic ( $z$ ) axis in the uniaxially anisotropic medium of Eq. (1) excites both  $E$ - and  $H$ -mode fields which are derivable via Eqs. (7.2.14) from the scalar potential functions  $\mathcal{S}'_d(\mathbf{r}, \mathbf{r}')$  and  $\mathcal{S}''_d(\mathbf{r}, \mathbf{r}')$ , respectively; these functions satisfy the differential equations [see Eqs. (7.2.16) and (7.2.17)]

$$\left[ \epsilon \left( \frac{\partial^2}{\partial z^2} + k_0^2 \right) + \nabla_t^2 \right] \nabla_t^2 \mathcal{S}'_f(\mathbf{r}, \mathbf{r}') = \epsilon \delta(\mathbf{r} - \mathbf{r}'), \quad -\mathcal{S}'_f = \frac{\mathcal{S}'_d}{i\omega\epsilon_0}, \quad (18a)$$

$$(\nabla^2 + k_0^2) \nabla_t^2 \mathcal{S}''_f(\mathbf{r}, \mathbf{r}') = \delta(\mathbf{r} - \mathbf{r}'), \quad -\mathcal{S}''_f = \frac{\mathcal{S}''_d}{i\omega\mu_0}, \quad (18b)$$

subject to radiation conditions at infinity, with  $k_0 = \omega\sqrt{\mu_0\epsilon_0}$ . The  $H$ -mode potential function in Eq. (18b) is identical with the function  $\mathcal{S}_f(\mathbf{r}, \mathbf{r}')$  defined in Eq. (5.4.18) for an unbounded isotropic space with wavenumber  $k = k_0$ . The  $E$ -mode potential function may be related to  $\mathcal{S}_f$  via the coordinate scale transformation  $\zeta = z\epsilon^{-1/2}$  when  $\epsilon$  is positive real, since from

$$\left( \frac{\partial^2}{\partial \zeta^2} + \nabla_t^2 + k_0^2 \epsilon \right) \nabla_t^2 \mathcal{S}'_f = \sqrt{\epsilon} \delta(\mathbf{p} - \mathbf{p}') \delta(\zeta - \zeta'), \quad (19)$$

it is recognized that

$$\mathcal{S}'_f(\mathbf{r}, \mathbf{r}') = \sqrt{\epsilon} \mathcal{S}_f\left(\mathbf{p}, \frac{z}{\sqrt{\epsilon}}; \mathbf{p}', \frac{z'}{\sqrt{\epsilon}}\right), \quad (20)$$

provided that  $\mathcal{S}_f$  is evaluated in a medium with wavenumber  $k = k_0\sqrt{\epsilon}$ . As in Sec. 7.3a, analytic continuation may be invoked to validate the resulting function for  $0 < \arg \epsilon \leq \pi$ .

The electromagnetic fields may now be deduced directly from the isotropic medium formulas in Sec. 5.4b. The  $H$ -mode constituents are identical with those in Sec. 5.4b, whereas the  $E$ -mode constituents can be determined from their isotropic medium counterparts by applying the above-mentioned scale transformation.<sup>7</sup> The details are left as an exercise for the reader.

#### Time-harmonic magnetic source current density

$$\hat{\mathbf{M}}(\mathbf{r}, t) = Vl\delta(\mathbf{r})e^{-i\omega t}\mathbf{x}_0. \quad (21)$$

The fields are derivable via Eqs. (7.2.14) from the scalar functions  $\mathcal{S}'_f$  and  $\mathcal{S}''_f$  in Eqs. (18).

### 7.3c Linearly Phased Line Currents Oriented Along the Optic Axis

#### Time-harmonic electric source current density

$$\hat{\mathbf{J}}(\mathbf{r}, t) = Ie^{i\alpha z}\delta(\mathbf{p})e^{-i\omega t}\mathbf{z}_0. \quad (22)$$

Since the current distribution in Fig. 7.3.4 is directed along the optic axis, the electromagnetic fields can be derived from a two-dimensional scalar  $E$ -mode Green's function (see Sec. 7.2)

$$[\nabla_t^2 + (k_0^2 - \alpha^2)\epsilon] \tilde{G}'_f(\mathbf{p}, \mathbf{p}') = -\delta(\mathbf{p} - \mathbf{p}'), \quad \nabla_t^2 = \nabla^2 - \frac{\partial^2}{\partial z^2}, \quad (23)$$

subject to an energy radiation condition at infinity.  $\mathbf{p}$  is the vector coordinate transverse to  $z$  and  $k_0 = \omega\sqrt{\mu_0\epsilon_0}$ . All field components vary like  $\exp(i\alpha z)$  whence  $\partial^2/\partial z^2 \rightarrow -\alpha^2$ . The solution is given by<sup>6</sup>

$$\tilde{G}'_f(\mathbf{p}, \mathbf{p}') = \begin{cases} \frac{i}{4} H_0^{(1)}(\sqrt{\epsilon}\sqrt{k_0^2 - \alpha^2}\rho) & \text{when } \epsilon > 0, \end{cases} \quad (24a)$$

$$\begin{cases} -\frac{i}{4} H_0^{(2)}(\sqrt{|\epsilon|}\sqrt{\alpha^2 - k_0^2}\rho) & \text{when } \epsilon < 0, \end{cases} \quad (24b)$$

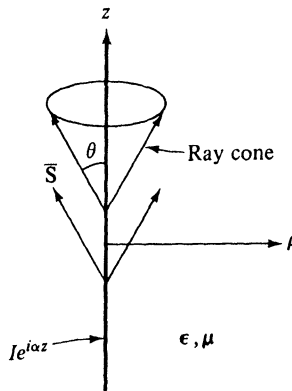


FIG. 7.3.4 Progressively phased line current,  $Ie^{iaz}$ ,  $\alpha > 0$ ;  $\epsilon = \epsilon_0(\mathbf{1}_t + z_0 z_0 \epsilon)$ ,  $\mu = \mu_0 \mathbf{1}$ .

with the square roots defined as follows:

$$\begin{aligned}\sqrt{k_0^2 - \alpha^2} &> 0 \quad \text{when } k_0 > \alpha, & \text{Im } \sqrt{k_0^2 - \alpha^2} &> 0 \quad \text{when } k_0 < \alpha, \\ \sqrt{\alpha^2 - k_0^2} &> 0 \quad \text{when } k_0 < \alpha, & \text{Im } \sqrt{\alpha^2 - k_0^2} &< 0 \quad \text{when } k_0 > \alpha.\end{aligned}\quad (24c)$$

The fields are derived from  $\bar{G}'_f$  via Eqs. (7.2.14):

$$E_\rho = \frac{iI\sqrt{\epsilon}\hat{\kappa}}{4\omega\epsilon_0} e^{i\alpha z} H_1^{(1)}(\sqrt{\epsilon}\hat{\kappa}\rho), \quad (25a)$$

$$E_z = -\frac{\hat{\kappa}^2 I}{4\omega\epsilon_0} e^{i\alpha z} H_0^{(1)}(\sqrt{\epsilon}\hat{\kappa}\rho), \quad (25b)$$

$$H_\phi = \frac{iI\sqrt{\epsilon}\hat{\kappa}}{4} e^{i\alpha z} H_1^{(1)}(\sqrt{\epsilon}\hat{\kappa}\rho), \quad (25c)$$

$$E_\phi = H_\rho = H_z = 0, \quad (25d)$$

where  $\hat{\kappa} = \sqrt{k_0^2 - \alpha^2}$ . These results apply when  $0 \leq \arg \epsilon \leq \pi$ , provided that  $\text{Im } \hat{\kappa} > 0$  when  $\hat{\kappa}$  is non-real; for negative real  $\epsilon$ , one may employ the alternative formulation in Eq. (24b).

The average radiated power density is given for real  $\epsilon$  by

$$\bar{S}_\rho = \begin{cases} -\text{Re}(E_\phi H_\phi^*) = \frac{|\hat{\kappa}|^2}{8\pi k_0 \rho} \sqrt{\frac{\mu_0}{\epsilon_0}} |I|^2, & \sqrt{\epsilon}\hat{\kappa} \text{ real}, \\ 0, & \sqrt{\epsilon}\hat{\kappa} \text{ imaginary}, \end{cases} \quad (26a)$$

$$\quad (26b)$$

$$\bar{S}_z = \text{Re}(E_\rho H_\phi^*) = \frac{\alpha |\sqrt{\epsilon}\hat{\kappa}|}{8\pi k_0 \rho} \sqrt{\frac{\mu_0}{\epsilon_0}} |I|^2, \quad \sqrt{\epsilon}\hat{\kappa} \text{ real or imaginary}. \quad (26c)$$

The radiated power flow direction  $\theta$  and the wavevector direction  $\bar{\theta}$  with respect to the  $z$  axis are defined by

$$\tan \theta = \frac{\bar{S}_\rho}{\bar{S}_z} = \frac{|\hat{\kappa}|}{\alpha |\sqrt{\epsilon}|} = \frac{1}{\epsilon} \tan \bar{\theta}, \quad (27)$$

where  $\bar{\theta}$  is the direction of the wavevector  $\mathbf{k} = \mathbf{z}_0 \alpha + \mathbf{p}_0 \sqrt{\epsilon} \hat{\kappa}$ .

For large values of  $|\sqrt{\epsilon} \hat{k}| \rho$ , Eqs. (25) may be simplified through use of the asymptotic formula  $H_n^{(1)}(w) \sim (2/\pi w)^{1/2} \exp[i(w - \pi/4 - n\pi/2)]$ .

### Discussion

The solution in Eq. (24a) follows directly from the analogous isotropic medium result in Eq. (5.4.47), and the formula in Eq. (24b) is deduced therefrom by analytic continuation via Eq. (24c) and  $H_0^{(1)}(we^{i\pi}) = -H_0^{(2)}(w)$ .

Since the Hankel functions denote propagating wave solutions in a lossless medium only when the argument is real, one observes that the source distribution in Fig. 7.3.4 radiates when

$$(a) \quad \epsilon > 0, k_0 > \alpha \quad \text{and} \quad (b) \quad \epsilon < 0, k_0 < \alpha. \quad (28)$$

These restrictions for cases (a) and (b) imply that the phase speeds along the source are larger and smaller, respectively, than the speed of light in vacuum; thus, different excitation functions are required to produce radiation when  $\epsilon > 0$  and  $\epsilon < 0$ . While, from Eq. (27), the energy propagation vector always has an outward radial component in accord with the energy radiation condition, the corresponding phase fronts move outward when  $\epsilon > 0$  but toward the source axis (backward wave) when  $\epsilon < 0$ , as is observed either from Eq. (27) or from Eqs. (24a) and (24b).

These conclusions may also be arrived at directly from the wavenumber surfaces. In view of the translational invariance of the physical configuration with respect to the  $z$  axis, the radiated fields (i.e., the local plane-wave fields at a large distance from the axis) are characterized by the dependence  $\exp(i\alpha z)$  impressed along the source.  $\alpha$  therefore assumes for the relevant wave constituents the role of the longitudinal wavenumber  $\kappa$ , and one observes from Fig. 7.3.5 that propagation (i.e., intersection of the plane  $\kappa = \alpha$  and the wavenumber surface) occurs for  $\alpha < k_0$  when  $\epsilon > 0$  and for  $\alpha > k_0$  when  $\epsilon < 0$ .

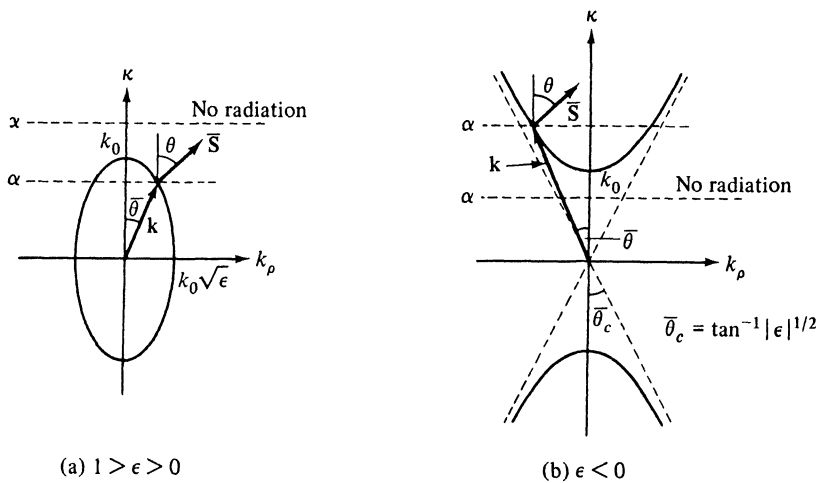


FIG. 7.3.5 Interpretation via wavenumber surfaces.

Evidently, when  $\tilde{S}_\rho > 0$ , as required by the radiation condition, the transverse wavenumber  $k_\rho > 0$  for  $\epsilon > 0$ , but  $k_\rho < 0$  for  $\epsilon < 0$ , thereby confirming the conclusions reached earlier; in discussing the local plane-wave behavior of the far field,  $k_\rho$  may be regarded as a *rectilinear* wavenumber, thereby making negative values of  $k_\rho$  meaningful. Since the wavenumber surfaces are symmetric about the source axis, the rays along  $\tilde{\mathbf{S}}$  defined by the intersection with the  $\kappa = \alpha$  plane emerge from the source at the constant angle  $\theta = \tan^{-1} [|\hat{k}|/(\alpha\sqrt{|\epsilon|})]$ , so the ray configuration forms a right circular cone (Fig. 7.3.4). This symmetry is destroyed when the source axis is inclined with respect to the optic axis in the medium.

#### Time-harmonic magnetic source current density

$$\hat{\mathbf{M}}(\mathbf{r}, t) = V e^{i\alpha z} \delta(\mathbf{p}) e^{-i\omega t} \mathbf{z}_0. \quad (29)$$

The source configuration excites only  $H$  modes, so the fields are identical with those in vacuum (Sec. 5.4d).

#### 7.3d Point Charge in Uniform Straight Motion Along the Optic Axis

The source current density is given by

$$\hat{\mathbf{J}}(\mathbf{r}, t) = qv\delta(z - vt)\delta(\mathbf{p})\mathbf{z}_0, \quad (30)$$

where  $q$  is the charge and  $v = \text{constant}$  is the particle speed (see Fig. 7.3.6). On introducing the Fourier transform

$$Q(\mathbf{r}, \omega) = \int_{-\infty}^{\infty} e^{i\omega t} \hat{Q}(\mathbf{r}, t) dt, \quad (31a)$$

one finds for the source function

$$\mathbf{J}(\mathbf{r}, \omega) = qe^{i(\omega/v)z} \delta(\mathbf{p})\mathbf{z}_0, \quad (31b)$$

which is the same harmonic source as in Eq. (22), with  $I = q$ ,  $\alpha = \omega/v$ . With this identification, the fields follow from Eqs. (25), and the radial harmonic power density is given from Eq. (26a) by

$$\tilde{S}_\rho(\mathbf{r}, \omega) = \frac{(\frac{1}{\beta^2} - 1)k_0\sqrt{\mu_0/\epsilon_0}q^2}{8\pi\rho}, \quad \beta < 1, \quad (32)$$

where  $\beta = v/c$  and  $k_0 = \omega/c$ , with  $c$  denoting the speed of light in vacuum.

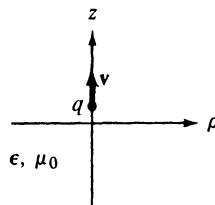


FIG. 7.3.6 Point charge moving along optic axis. Constitutive parameters:  $\epsilon = \epsilon_0(1_t + \mathbf{z}_0\mathbf{z}_0\epsilon)$ ,  $\mu = \mathbf{1}\mu_0$ .

Since  $\beta < 1$ , it follows that  $k_0 < \alpha (= k_0/\beta)$  and radiation takes place only for negative values of  $\epsilon$  [see Eq. (28)]. The total energy radiated per unit length along the trajectory is obtained from Eq. (5.2.30) as

$$W_1 = \frac{1}{\pi} \int_0^\infty \bar{S}_\rho(\mathbf{r}, \omega) \cdot 2\pi\rho d\omega. \quad (33)$$

In general, this result cannot be evaluated unless the frequency dependence of  $\epsilon$  is stated. If, as is the case for certain plasmas,  $\epsilon = 1 - \omega_p^2/\omega^2$  is negative only for  $\omega < \omega_p$ , the upper integration limit is  $\omega_p$ , whence<sup>7</sup>

$$W = \frac{q^2 \mu_0 \omega_p^2}{8\pi} \left( \frac{1}{\beta^2} - 1 \right). \quad (34)$$

This result implies somewhat surprisingly that slower moving particles radiate more strongly than those in rapid motion, a behavior quite different from that encountered in isotropic dielectrics (Sec. 5.4e). It must, of course, be kept in mind that the particle speed is assumed uniform in the above calculation, a condition incompatible with the non-negligible deceleration that accompanies substantial radiation.

The basic features of the radiation process may again be inferred directly from the wavenumber plots in Fig. 7.3.5. From Eq. (31b), the relevant wave constituents excited by the particle have  $\alpha = \omega/v = k_0/\beta > k_0$ , so no radiation occurs for  $\epsilon > 0$  in Fig. 7.3.5(a). When  $\epsilon < 0$ , the sketch in Fig. 7.3.5(b) implies that radiation is of the backward-wave type, with phase progression toward the particle trajectory. The graph illustrates also the basic “Cerenkov coherence condition,” which states that in a small frequency interval about  $\omega$ , the particle excites those waves whose wavevector component along the trajectory matches the spectral component  $\omega/v$ .

### 7.3e Line Currents Oriented Perpendicular to the Optic Axis

*Magnetic source current density*

$$\hat{\mathbf{M}}(\mathbf{r}, t) = V\delta(\hat{\mathbf{p}} - \hat{\mathbf{p}}')e^{-i\omega t}\mathbf{x}_0. \quad (35)$$

With the line current oriented as in Fig. 7.3.7, the electromagnetic fields can be derived from the two-dimensional scalar *E*-mode Green's function  $\tilde{G}'_f(\hat{\mathbf{p}}, \hat{\mathbf{p}}')$  that satisfies the differential equation

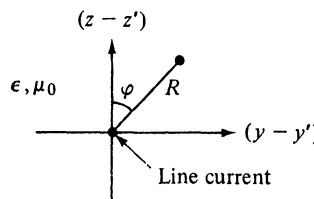


FIG. 7.3.7 Line current transverse to optic axis;  
 $\epsilon = \epsilon_0(\mathbf{1}_t + \mathbf{z}_0\mathbf{z}_0\epsilon)$ ,  $\mu = \mu_0\mathbf{1}$ .

$$\left( \frac{\partial^2}{\partial z^2} + \frac{1}{\epsilon} \frac{\partial^2}{\partial y^2} + k_0^2 \right) \tilde{G}'(\hat{\mathbf{p}}, \hat{\mathbf{p}}') = -\delta(\hat{\mathbf{p}} - \hat{\mathbf{p}}'), \quad \hat{\mathbf{p}} = (y, z), \quad (36)$$

subject to an energy radiation condition at infinity. The solution for  $0 \leq \arg \epsilon \leq \pi$  is given by

$$\tilde{G}'_f = \frac{i}{4} \sqrt{\epsilon} H_0^{(1)}[k_0 R N(\phi)], \quad N(\phi) = \sqrt{\cos^2 \phi + \epsilon \sin^2 \phi}, \quad (37)$$

where  $k_0 = \omega \sqrt{\mu_0 \epsilon_0}$ ,  $R = \sqrt{(y - y')^2 + (z - z')^2}$ , and  $\operatorname{Im} N(\phi) \geq 0$ . The field components are derived from  $\tilde{G}'_f$  as follows:

$$H_x \equiv H = i\omega \epsilon_0 V \tilde{G}'_f = -\frac{\omega \epsilon_0 \sqrt{\epsilon} V}{4} H_0^{(1)}[k_0 R N(\phi)], \quad (38a)$$

$$E_y = -V \frac{\partial \tilde{G}'_f}{\partial z} = \frac{i k_0 \sqrt{\epsilon} V \cos \phi}{4 N(\phi)} H_1^{(1)}[k_0 R N(\phi)], \quad (38b)$$

$$E_z = \frac{V}{\epsilon} \frac{\partial \tilde{G}'_f}{\partial y} = -\frac{i k_0 \sqrt{\epsilon} V \sin \phi}{4 N(\phi)} H_1^{(1)}[k_0 R N(\phi)], \quad (38c)$$

$$H_y = H_z = E_x = 0. \quad (38d)$$

In a cylindrical coordinate system, Eqs. (38b) and (38c) may be combined to yield for the field components,

$$E_R = E_z \cos \phi + E_y \sin \phi = 0, \quad (38e)$$

$$E_\varphi = E_y \cos \phi - E_z \sin \phi = \frac{i k_0 \sqrt{\epsilon} V}{4 N(\phi)} H_1^{(1)}[k_0 R N(\phi)]. \quad (38f)$$

The average radiated power density for real  $\epsilon$  is given by

$$\bar{S}_R = -\operatorname{Re}(E_\varphi H_x^*) = \begin{cases} \sqrt{\frac{\epsilon_0}{\mu_0}} \frac{|\epsilon| k_0}{8\pi R N^2(\phi)} |V|^2, & N \text{ real}, \\ 0, & N \text{ imaginary}, \end{cases} \quad (39a)$$

$$\bar{S}_\varphi = \bar{S}_x = 0, \quad (39c)$$

and the total radiated power is

$$P = R \int_0^{2\pi} \bar{S}_R d\phi = \begin{cases} \text{finite,} & \epsilon > 0, \\ \infty, & \epsilon < 0. \end{cases} \quad (40a)$$

$$(40b)$$

Asymptotic expressions for the field components are found from Eqs. (38) by replacing the Hankel functions by their large-argument approximation,

$$H_n^{(1)}(w) \sim (2/\pi w)^{1/2} \exp[i(w - \pi/4 - n\pi/2)].$$

### Discussion

The formulation of the field in terms of the Green's function  $\tilde{G}'_f$  as in Eqs. (38) is accomplished by proceeding directly from the Maxwell field equations subject to the constraint  $\partial/\partial x \equiv 0$ . Alternatively, the results may be deduced by simplification of Eqs. (7.2.14), (7.2.16), and (7.2.17) [see also the analogous

treatment for the isotropic case, Eqs. (5.4.31)]. In the derivation of Eqs. (39), use is made of the Wronskian for the cylinder functions; it has also been recognized for imaginary  $N$ , that  $H_v^{(1)}(iw) = (2/\pi i) \exp(-v\pi i/2) K_v(w)$ , where the modified Hankel function  $K_v(w)$  is real when  $v$  and  $w$  are real. One observes from Eq. (39a) that the source illuminates all regions of space when  $\epsilon > 0$ , while the region  $|\tan \varphi| > |\epsilon|^{-1/2}$  constitutes for  $\epsilon < 0$  a shadow region wherein the fields are evanescent ( $N$  imaginary). On the shadow boundary  $|\tan \varphi| = \tan \varphi_c = |\epsilon|^{-1/2}$ , where  $N = 0$ , the fields and the radiated power density are infinite. The infinities are weaker than those for point-source excitation [see Eqs. (5a) and (39a)] but still strong enough to render the total radiated power, and therefore the radiation conductance  $\bar{S}/|V|^2$ , infinite.

The interpretation of these results follows also from the wavenumber surfaces. Since the fields are independent of  $x$ , the constituent plane waves in the far zone are characterized by a vanishing wavenumber  $\xi$  (or  $k_x$ ) along the  $x$  direction. The only relevant portions of the wavenumber surfaces are therefore the curves obtained by intersection with the  $k_x = 0$  plane, and these curves are the same as in Fig. 7.3.2(b) if  $k_\rho$  is interpreted as the wavenumber  $k_y \equiv \eta$  along the  $y$  direction. Since the normals to the wavenumber surface at  $k_x = 0$  lie in the  $\eta\kappa$  plane, the rays (trajectories of energy flow) are perpendicular to the  $x$  axis and emanate radially from the source, as noted also from Eqs. (39). Various aspects discussed in connection with Fig. 7.3.2 therefore remain applicable, subject to the identification  $k_\rho \rightarrow \eta$ ,  $\rho \rightarrow y$ .

#### *Removal of the infinity in the radiated power*

It has been found that the fields radiated either by a point source or a line source in a uniaxially anisotropic medium characterized by an open-branched wavenumber surface exhibit infinities along the shadow boundary  $\theta_c$  or  $\varphi_c = \tan^{-1}|\epsilon|^{-1/2}$ , and that the *total* radiated power is also infinite. While we have noted in Sec. 7.3a that these singularities disappear for a more realistic description of the physical medium, it will now be shown that even within the confines of the lossless uniaxially anisotropic model, finite fields and power are obtained for a *distributed* source configuration.<sup>6,8,9</sup> Although the calculation is performed for the two-dimensional case, analogous conclusions apply also to the three-dimensional field.

It may be anticipated on physical grounds that a distributed source softens the singular point-source field behavior since the presence of neighboring elements in the source distribution tends to diffuse the shadow boundary. This effect may be observed from a comparison of the point-source and line-source results in Eqs. (4), (5), and (38), (39), respectively, since the line-source field exhibits a weaker singularity than the point-source field.

It is convenient to employ an integral representation for  $\tilde{G}'_f$ , analogous to that in Eq. (8). The appropriate modal basis involves the plane waves  $\Phi_n(y) = (2\pi)^{-1/2} \exp(i\eta y)$ ,  $-\infty < \eta < \infty$ , and utilization of Eq. (7.2.18a) yields, for the magnetic field,

$$H = C \int_{-\infty}^{\infty} \frac{e^{i\eta y + i\kappa|z-z'|}}{\kappa} d\eta, \quad \kappa(\eta) = \sqrt{k_0^2 - \frac{\eta^2}{\epsilon}}, \quad (41)$$

where  $C$  includes various constants. The convergence properties of this integral are essentially the same as in Eq. (8), and the previous observations apply here as well. If the source is distributed in the plane  $z = z'$  with an amplitude variation given by  $f(y')$ , the corresponding magnetic field  $\hat{H}$  is given by

$$\hat{H} = C \int_{-\infty}^{\infty} \frac{e^{i\eta y + i\kappa|z-z'|}}{\kappa} F(\eta) d\eta, \quad (42)$$

where  $F(\eta)$  is the Fourier transform of the source function  $f(y')$ ,

$$F(\eta) = \int f(y') e^{-i\eta y'} dy', \quad (42a)$$

and the integration extends over the source region. For a line source,  $f(y') = \delta(y')$ ,  $F(\eta) = 1$ , and one recovers Eq. (41). A more regular, distributed source has a spectrum  $F(\eta)$  that decays as  $\eta \rightarrow \infty$  and therefore deemphasizes the contribution from these regions to the integral in Eq. (42). If the integral is then absolutely convergent, although  $\kappa$  is real over the entire integration interval, the previously noted divergence in the fields (as  $\varphi \rightarrow \varphi_c$ ) disappears. If  $F(\eta_s)$ , where  $\eta_s$  denotes the saddle point as in Eqs. (11), drops off sufficiently rapidly, an asymptotic evaluation of the integral for  $\epsilon < 0$  will yield a vanishing result as  $\varphi \rightarrow \varphi_c$  since the decay of  $F(\eta_s)$  overcomes the growth of the earlier asymptotic approximation as  $\eta_s \rightarrow \infty$ .

These considerations may also be applied to the total radiated power. The  $y$  component of electric field is calculated from Eq. (38b):

$$\hat{E}_y = \frac{-C}{\omega\epsilon_0} \int_{-\infty}^{\infty} e^{i\eta y + i\kappa(z-z')} F(\eta) d\eta, \quad z > z', \quad (43)$$

and the total power flow in the  $+z$  direction is then given by

$$\tilde{S}_z = \frac{|C|^2}{\omega\epsilon_0} \operatorname{Re} \left[ \int_{-\infty}^{\infty} dy \int_{-\infty}^{\infty} d\eta \int_{-\infty}^{\infty} d\eta' \frac{e^{i(\eta'-\eta)y + i(\kappa'-\kappa)(z-z')}}{\kappa} F^*(\eta') F(\eta) \right] \quad (44)$$

$$= \frac{2\pi|C|^2}{\omega\epsilon_0} \operatorname{Re} \int_{-\infty}^{\infty} \frac{|F(\eta)|^2}{\sqrt{k_0^2 - (\eta^2/\epsilon)}} d\eta. \quad (45)$$

In Eq. (44),  $\kappa' \equiv \kappa(\eta')$ , and evaluation of the  $y$  integration in terms of the delta function  $\delta(\eta - \eta')$  leads to Eq. (45), which could also have been written down directly from Eq. (7.2.10b). If  $\epsilon > 0$ , the integration extends only over the range  $|\eta| \leq k_0\sqrt{\epsilon}$  and the integral is finite for all reasonably behaved  $F(\eta)$ . If  $\epsilon < 0$ , the integration interval is infinite and  $\tilde{S}_z$  is finite only when

$$\int_{-\infty}^{\infty} \frac{|F(\eta)|^2}{\eta} d\eta < \infty, \quad (46)$$

a mild restriction satisfied by most source distributions. For example, if

$$f(y') = \begin{cases} A = \text{constant} & \text{when } -a < y' < a, \\ 0 & \text{when } |y'| > a, \end{cases} \quad (47)$$

then

$$F(\eta) = \frac{2A \sin \eta a}{\eta}, \quad (48)$$

and the inequality (46) certainly applies. The total radiated power  $P$  is equal to  $2\bar{S}_z$ , and is calculated by integrating the average power flow density  $\bar{S}$  over a surface completely enclosing the source. In the present instance, the surface comprises two infinite parallel planes at  $z = z' \pm \Delta$ ,  $\Delta > 0$ , and two segments of width  $2\Delta$  located at  $y = \pm\infty$ . Since the far field decays like  $1/\sqrt{R}$  [see asymptotic form of Eqs. (38)], the only non-vanishing contribution arises from the planes at  $z = z' \pm \Delta$ , whence  $P = 2\bar{S}_z$ .

Thus, finiteness of radiated power in a lossless anisotropic region with an open-branched wavenumber surface is achieved when the *spatial transform of the source distribution decays sufficiently rapidly at infinity*, and this general conclusion remains valid even for gyrotropic media and for three-dimensional configurations although the *specific requirements may vary for different situations*.

#### *Electric line source current density*

$$\hat{\mathbf{J}}(\mathbf{r}, t) = I\delta(\hat{\mathbf{p}} - \hat{\mathbf{p}}')e^{-i\omega t}\mathbf{x}_0. \quad (49)$$

This source configuration excites only  $H$  modes with respect to the optic axis, and the resulting fields are the same as in vacuum (see Sec. 5.4c).

#### *Electric dipolar source current density*

$$\hat{\mathbf{J}}(\mathbf{r}, t) = A\delta(\hat{\mathbf{p}} - \hat{\mathbf{p}}')e^{-i\omega t}(y_0 \cos \alpha + z_0 \sin \alpha). \quad (50)$$

This source arrangement consists of a line distribution of electric current elements oriented perpendicular to the line axis  $z$ , at an angle  $\alpha$  with respect to the  $y$  axis (Fig. 7.3.8).

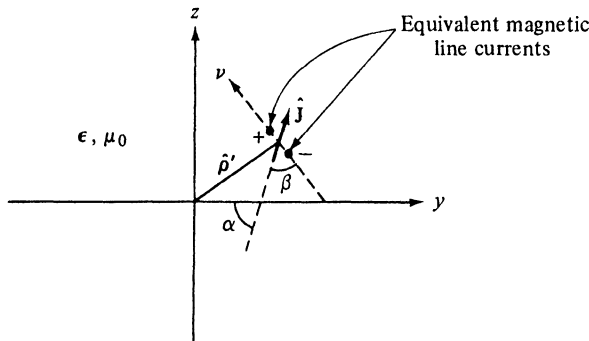


FIG. 7.3.8 Electric dipole line current;  $\epsilon = \epsilon_0(1 + z_0 z_0 \epsilon)$ ,  $\mu = \mu_0 \mathbf{1}$ .

Since  $\partial/\partial x \equiv 0$ , the non-vanishing field components are easily shown to be  $H_x \equiv H$ ,  $E_y$ ,  $E_z$ , and the Maxwell field equations reduce to

$$\frac{\partial E_z}{\partial y} - \frac{\partial E_y}{\partial z} = i\omega\mu_0 H, \quad (51a)$$

$$\frac{\partial H}{\partial z} = -i\omega\epsilon_0 E_y + J_y, \quad \frac{\partial H}{\partial y} = i\omega\epsilon_0 \epsilon E_z - J_z. \quad (51b)$$

Upon substituting for  $\partial E_z/\partial y$  and  $\partial E_y/\partial z$  from Eq. (51b) into Eq. (51a), one obtains the inhomogeneous wave equation

$$\left( \frac{\partial^2}{\partial z^2} + \frac{1}{\epsilon} \frac{\partial^2}{\partial y^2} + k_y^2 \right) H = -A \left( \frac{1}{\epsilon} \sin \alpha \frac{\partial}{\partial y} - \cos \alpha \frac{\partial}{\partial z} \right) \delta(y - y') \delta(z - z'), \quad (52)$$

which can be solved in terms of the two-dimensional Green's function  $\tilde{G}'_f$  in Eq. (37):

$$H = -A \left( \frac{1}{\epsilon} \sin \alpha \frac{\partial}{\partial y'} - \cos \alpha \frac{\partial}{\partial z'} \right) \tilde{G}'_f, \quad (53)$$

with the recognition that  $\partial/\partial y = -\partial/\partial y'$ ,  $\partial/\partial z = -\partial/\partial z'$ , in view of the dependence of  $\tilde{G}'_f$  on  $y - y'$  and  $z - z'$ . The operator inside the brackets in Eq. (53) may be interpreted as  $\mathbf{v} \cdot \nabla' = v(\partial/\partial v)$ , where  $\mathbf{v}$  is a vector with components  $v_y = (1/\epsilon) \sin \alpha$ ,  $v_z = -\cos \alpha$ . Consequently,

$$\mathbf{v} \cdot (\mathbf{y}_0 \cos \alpha + \mathbf{z}_0 \sin \alpha) = [(1/\epsilon) - 1] \sin \alpha \cos \alpha = v \cos \beta,$$

$$v = \sqrt{\cos^2 \alpha + (1/\epsilon^2) \sin^2 \alpha}, \quad (54)$$

where  $\beta$  is the angle between  $\mathbf{v}$  and the source direction  $\hat{\mathbf{j}}$ .

For non-dissipative media with real  $\epsilon$ ,  $\beta$  is a real angle, and in view of Eq. (37), the result in Eq. (53) may be interpreted as the field due to two closely spaced, oppositely directed magnetic currents—a magnetic “line dipole” directed along  $\mathbf{v}$ . In the isotropic case  $\epsilon = 1$ ,  $\mathbf{v}$  and  $\hat{\mathbf{j}}$  are mutually perpendicular, and Eq. (53) reduces to Eq. (5.4.39a). In the uniaxial medium,  $\mathbf{v} \cdot \hat{\mathbf{j}} = 0$  only when the electric dipole direction is parallel or perpendicular to the optic axis ( $\alpha = 0, \pi/2$ ). A source distribution of the type considered here is induced, for example, when a narrow conducting strip centered at  $\hat{\mathbf{p}}'$  and oriented along  $\alpha$  is excited by an incident field with  $H \equiv H_x$ .

*Highly directive, distributed magnetic current source :*

$$\hat{\mathbf{M}}(\mathbf{r}, t) = \begin{cases} \cos \frac{\pi u}{a} e^{iu\zeta} \delta(v) e^{-i\omega t} \mathbf{x}_0, & -a \leq u \leq a, \\ 0, & \text{elsewhere,} \end{cases} \quad (55a)$$

$$(55b)$$

with the coordinates  $u$  and  $v$  defined in Fig. 7.3.9. This functional dependence of  $\hat{\mathbf{M}}$  simulates the excitation due to a progressively phased antenna with a tapered amplitude distribution, and is certainly smooth enough to assure avoidance of the shadow boundary singularities that arise for the isolated line

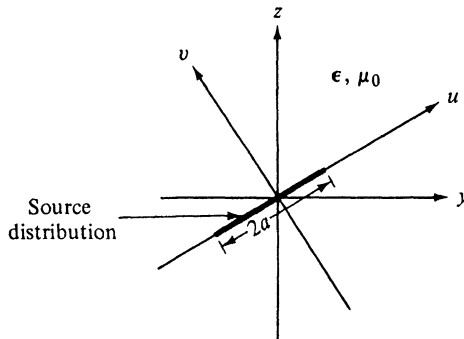


FIG. 7.3.9 Physical configuration;  $\epsilon = \epsilon_0(1_t + z_0 z_0 \epsilon)$ ,  $\mu = \mu_0 \mathbf{1}$ .

source when  $\epsilon < 0$  (see earlier discussion in this section). When the antenna extends over many wavelengths ( $k_0 a \gg 1$ ), the radiated field is highly directive. Such sources find important application in antenna engineering and may be realized either by a series of closely spaced individual elements or by a continuous distribution, as considered here.

The radiation pattern of this antenna is obtained by integrating the far-field form of Eq. (38a),

$$H \sim \frac{-\omega \epsilon_0 \sqrt{\epsilon} e^{-i\pi/4}}{2\sqrt{2\pi} \sqrt{k_0 R N(\varphi)}} e^{i k_0 R N(\varphi) - i \mathbf{k} \cdot \mathbf{u}_0 u}, \quad (56)$$

over the source region. In this equation,  $R = \sqrt{y^2 + z^2} \rightarrow \infty$ ,  $\varphi$  is the angle between  $R$  and the positive  $z$  axis,  $\mathbf{u}_0$  is a unit vector along  $u$ , and  $\mathbf{k}$  is the phase propagation vector corresponding to the ray progressing in the  $\varphi$  direction. The resulting magnetic field  $H_T$  is then given by

$$H_T \sim H|_{u=0} F, \quad (57)$$

where  $F$  is the array factor

$$F = \pi a \frac{\cos [a(\zeta - \mathbf{k} \cdot \mathbf{u}_0)]}{(\pi/2)^2 - [a(\zeta - \mathbf{k} \cdot \mathbf{u}_0)]^2}. \quad (58)$$

Since  $\mathbf{k} \cdot \mathbf{u}_0 a = (\mathbf{z}_0 \kappa + \mathbf{y}_0 \eta) \cdot \mathbf{u}_0 a$  is proportional to  $1/N(\varphi)$ , the ratio  $F/\sqrt{N(\varphi)}$  vanishes as  $N(\varphi) \rightarrow 0$ , so one verifies the regularity of the field near the shadow boundary when  $\epsilon < 0$ . It is recalled from Eq. (11b) that  $k_0 R N(\varphi) = \eta y + \kappa z = \mathbf{k} \cdot \mathbf{R}$  since  $\eta = k_0 \epsilon \sin \varphi / N(\varphi)$ ,  $\kappa = k_0 \cos \varphi / N(\varphi)$ ; the relation between  $\mathbf{k}$  and the radius vector  $\mathbf{R}$  (which is parallel to the group velocity vector  $\mathbf{v}_g$ ) may also be inferred from Fig. 7.3.2.

If  $k_0 a \gg 1$ , the array factor has sharp maxima at those angular locations for which

$$\zeta = \mathbf{k} \cdot \mathbf{u}_0. \quad (59)$$

The corresponding ray angles define the major lobes in the radiation pattern, and they may be easily inferred from the  $\mathbf{k}$  versus  $\varphi$  plot. Evidently, condition

(59) selects those values of  $\mathbf{k}$  whose projection onto the positive  $u$  axis has a length equal to  $\zeta$ , the wavenumber of the progressively phased source distribution in Eq. (55a). The procedure is schematized in Fig. 7.3.10 for the case

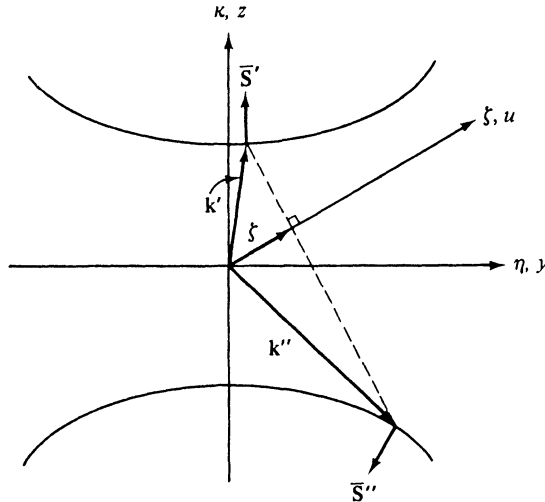


FIG. 7.3.10 Directive, distributed source: directions of pattern maxima ( $\epsilon > 0$ ).

$\epsilon < 0$ ,  $\zeta > 0$ , and one observes that two values  $\mathbf{k}'$  and  $\mathbf{k}''$  satisfy Eq. (59). The corresponding rays  $\bar{S}'$  and  $\bar{S}''$  point essentially in the directions of the major lobes in the radiation pattern since, except near the shadow boundary, the angularly dependent factor  $1/\sqrt{N(\varphi)}$  in  $H|_{u=0}$  of Eq. (57) is slowly varying over the angular width of a narrow beam and introduces only a small shift in the location of the pattern maxima determined from these considerations. Owing to the anisotropy, the radiation pattern is asymmetric about the source axis  $u$ , and the lobe corresponding to  $\bar{S}''$  actually points in the backward direction, although the phase of the antenna progresses along  $+u$ . The construction in Fig. 7.3.10 may also be employed for the inverse problem of determining the values of  $\zeta$  and the directions  $u_0$  that yield a pattern maximum along a specified angle.

The above procedure for determining the locations of the pattern maxima due to highly directive sources in an anisotropic medium is also useful under conditions when the wavenumber surface has a more complicated shape or has additional branches. In essence, one looks for the directions of the rays whose wavenormal projections on the antenna axis match the wavenumber of the phase progression along the source.

A numerical example (Fig. 7.3.11) illustrates the validity of the preceding remarks for a special case in which  $u_0 = z_0$ ,  $\epsilon = -1$ ,  $a = 4\lambda_0$ , and  $\zeta$  takes on

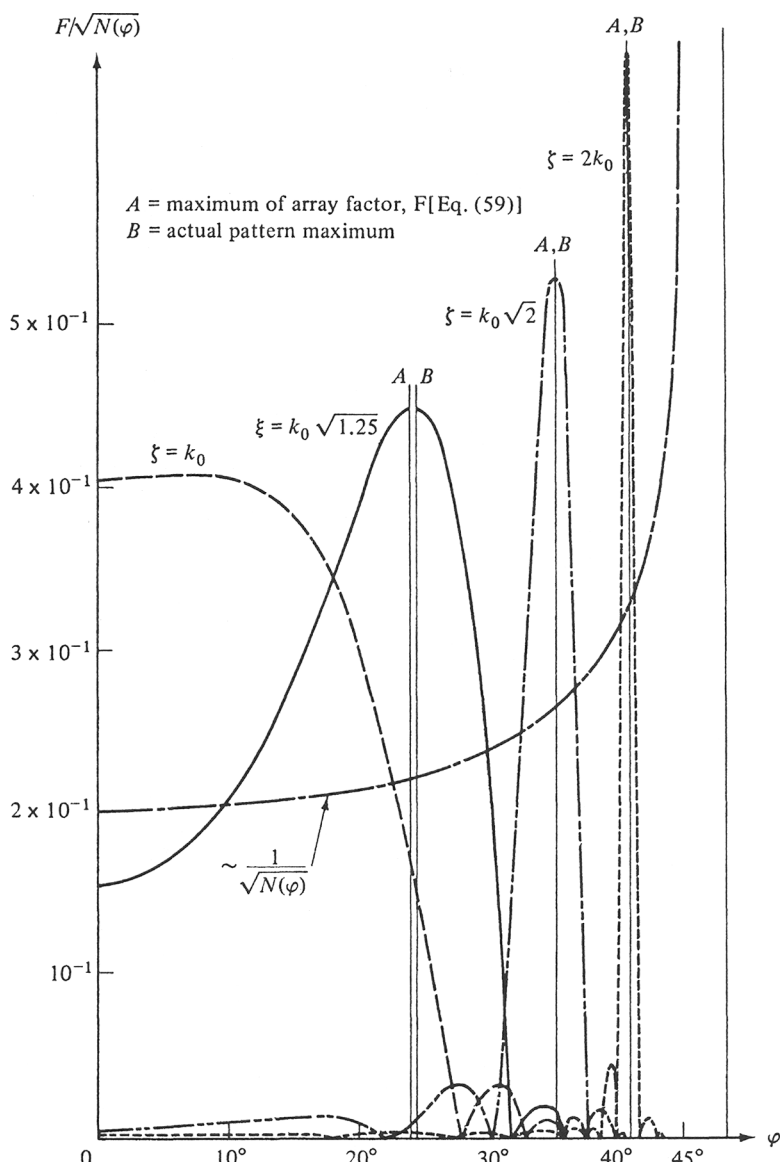


FIG. 7.3.11 Radiation pattern of a highly directive antenna.

the values  $\zeta/k_0 = 1, \sqrt{1.25}, \sqrt{2}, 2$ . A comparison between the actual magnetic field patterns calculated from Eq. (57) and the location of the pattern maxima predicted from Eq. (59) shows good agreement when the pattern is sufficiently narrow.

#### 7.4 DIFFRACTION BY STRUCTURES EMBEDDED IN AN INFINITE, HOMOGENEOUS PLASMA

The calculation of the effect of a perturbing structure on radiation from a source distribution is complicated substantially if the surrounding medium is anisotropic. Simplifications arise under special conditions; in uniaxially anisotropic regions, one may distinguish two special classes of diffraction problems that are easily reduced via scaling to equivalent problems in an isotropic space.

##### 7.4a Optic Axis Parallel to Axis of a Perfectly Conducting Cylindrical Obstacle

In the first class of scattering problems, the scattering object is a perfectly conducting cylinder of *arbitrary* cross section (e.g., a circular, elliptic, or parabolic cylinder; a wedge, half-plane, or strip; etc.) excited by an *arbitrary* source configuration, with the cylinder axis oriented parallel to the optic axis of the medium. This cylindrical scatterer forms the boundaries of a uniform waveguide region, and the resulting radiation or diffraction problem is then solved by the procedure described in Sec. 7.2. From Eqs. (7.2.24), the solutions may be expressed directly in terms of those for the isotropic case, whence one may construct results for a whole class of uniaxial diffraction problems by a simple scaling of the axial ( $z$ ) coordinate in the conventional isotropic expressions. An analysis of these results in the limit of short and long wavelengths, valuable in providing an insight into some of the diffraction effects encountered in anisotropic regions, is left as an exercise for the reader. It may be recalled that the  $H$ -mode constituents of the field are *identical* with those in the isotropic case, and that the coordinate scaling need be applied only to the  $E$ -mode constituents.

##### 7.4b Optic Axis Perpendicular to Axis of a Perfectly Conducting Cylindrical Obstacle

###### *Formulation and reduction of the boundary-value problem*

The second class of problems, involving cylindrical scatterers of arbitrary cross section oriented perpendicular to the optic axis in the medium, is also reducible to equivalent isotropic problems provided that the source distribution does not vary along the direction of the cylinder axis. The solutions may incorporate effects caused by a continuous change in direction of the optic ( $z$ ) axis over the obstacle boundary when the latter is curved, whereas in the problems of Sec. 7.4a, the optic axis is always parallel to the boundary.

Let the cylinder axis be parallel to  $x$  and let the excitation be comprised of a line source of magnetic currents

$$\hat{\mathbf{M}}(\mathbf{r}, t) = V\delta(\hat{\mathbf{p}} - \hat{\mathbf{p}}')e^{-i\omega t}\mathbf{x}_0, \quad \hat{\mathbf{p}} = (y, z). \quad (1)$$

Parenthetically, we note that a line source of electric currents excites only  $H$

modes in the direction perpendicular to  $x$ ; these are not affected by the presence of the uniaxially anisotropic medium. The medium is described again by the constitutive parameters

$$\epsilon = \epsilon_0(1 + z_0 z_0 \epsilon), \quad \mu = \mu_0 1. \quad (2)$$

As in the absence of the scatterer, the non-vanishing field components are  $H_x \equiv H, E_y, E_z$ . On the obstacle surface  $A$  specified by the equation  $A(y, z) = 0$ , the impedance boundary condition

$$E_{\tan} = ZH \quad (3a)$$

is assumed, where  $Z(y, z)$  denotes the surface impedance and  $E_{\tan}$  is the electric field component tangential to  $A$ . If  $n$  represents the direction normal to  $A$  and  $\alpha$  is the angle between the tangent to  $A$  and the positive  $y$  axis [see Fig. 7.4.1(a)], then  $E_{\tan} = (E_z \sin \alpha + E_y \cos \alpha)$  and the relations  $E_y =$

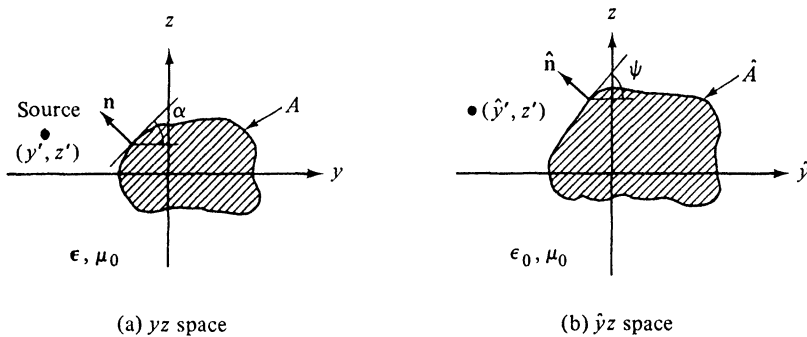


FIG. 7.4.1 Equivalent configurations.

$-(i\omega\epsilon_0)^{-1}\partial H/\partial z, E_z = (i\omega\epsilon_z)^{-1}\partial H/\partial y, \epsilon_z = \epsilon\epsilon_0$ , may be used to rewrite Eq. (3a) as [see also Eqs. (7.3.38)]

$$\frac{\partial H}{\partial y} - \epsilon \cot \alpha \frac{\partial H}{\partial z} = i\omega\epsilon\epsilon_0 \frac{Z}{\sin \alpha} H \quad \text{on } A. \quad (3b)$$

In an isotropic medium ( $\epsilon = 1$ ), the expression on the left-hand side of the equation is equal to  $-\csc \alpha \partial H/\partial n$ , and the impedance boundary condition then takes the familiar form  $\partial H/\partial n \propto ZH$  on  $A$ . This condition does not hold in the anisotropic medium, where the normal derivative of  $H$  is replaced by an “oblique derivative” whose direction may be inferred from considerations analogous to those following Eq. (7.3.53).

The boundary-value problem can now be stated as follows. As in Eqs. (7.3.36) and (7.3.38a), the magnetic field  $H$  is defined by the differential equation

$$\left( \frac{\partial^2}{\partial z^2} + \frac{1}{\epsilon} \frac{\partial^2}{\partial y^2} + k_0^2 \right) H(\hat{p}, \hat{p}') = -i\omega\epsilon_0 V \delta(\hat{p} - \hat{p}'), \quad (4)$$

subject to an energy radiation condition at infinity, and to the boundary condition (3b) on the obstacle surface  $\hat{A}$ .

To reduce this boundary-value problem to one in an isotropic medium, it is again suggestive to introduce a coordinate scaling transformation that yields a Laplacian instead of a differential operator as in Eq. (4). Evidently, either the  $z$  or  $y$  coordinates may be scaled. The former has already been utilized (Sec. 7.2) and involves an equivalent isotropic medium with wavenumber  $k_0\sqrt{\epsilon}$ . For the present application, the alternative procedure is employed via the definition

$$\hat{y} = \sqrt{\epsilon} y, \quad (5)$$

which furnishes the Laplacian in  $\hat{y}z$  space, with the medium properties described by the wavenumber  $k_0$ . The boundary condition in Eq. (3b) becomes, accordingly,

$$\frac{\partial \hat{H}}{\partial \hat{y}} - \cot \psi \frac{\partial \hat{H}}{\partial z} = i\omega \epsilon_0 \frac{\sqrt{\epsilon}}{\sin \alpha} Z \hat{H} \quad \text{on } \hat{A}, \quad (6a)$$

where  $\hat{H}$  and  $\hat{G}$  are, respectively, the equivalent isotropic field solution and Green's function

$$\hat{H}(\hat{y}, z; \hat{y}', z') = i\omega \epsilon_0 \sqrt{\epsilon} V \hat{G}(\hat{y}, z; \hat{y}', z') = H\left(\frac{\hat{y}}{\sqrt{\epsilon}}, z; \frac{\hat{y}'}{\sqrt{\epsilon}}, z'\right), \quad (6b)$$

with

$$\cot \psi = \sqrt{\epsilon} \cot \alpha, \quad (6c)$$

and  $\hat{A}$  defining the surface

$$\hat{A}(\hat{y}, z) = A\left(\frac{\hat{y}}{\sqrt{\epsilon}}, z\right) = 0. \quad (6d)$$

$\psi$  is the angle between the tangent to the transformed surface  $\hat{A}$  and the positive  $\hat{y}$  axis [see Fig. 7.4.1(b)], and if  $\hat{n}$  denotes the direction of the outward normal to  $\hat{A}$ , Eq. (6a) may be written as

$$\frac{\partial \hat{H}}{\partial \hat{n}} = -i\omega \epsilon_0 \hat{Z} \hat{H} \quad \text{on } \hat{A}, \quad (7a)$$

where  $\hat{Z}$  is the equivalent surface impedance

$$\hat{Z} = \sqrt{\epsilon} \frac{\sin \psi}{\sin \alpha} Z = \left( \frac{\epsilon}{\sin^2 \alpha + \epsilon \cos^2 \alpha} \right)^{1/2} Z. \quad (7b)$$

Thus, it is found that the boundary conditions on  $\hat{H}$  in the equivalent isotropic problem involving the medium  $\epsilon_0$  and a scatterer  $\hat{A}$  are of the conventional impedance type, so solutions of diffraction problems in the anisotropic medium can be constructed by applying to the customary isotropic Green's function the transformations (5), (6d), and (7b).<sup>6</sup>

In view of Eqs. (6d) and (7b), the auxiliary isotropic problem generally in-

volves both a different obstacle shape† and surface impedance. The obstacle shape is stretched according to Eq. (5), whence a circular cylinder with radius  $a$  (i.e.,  $A = y^2 + z^2 - a^2 = 0$ ) transforms into a elliptic cylinder,  $\hat{A} = (\hat{y}^2/\epsilon) + \hat{z}^2 - a^2 = 0$ ; a wedge formed by the two half-planes  $A_1 = y - z \cot \alpha_1 = 0$ ,  $A_2 = y - z \cot \alpha_2 = 0$ ,  $z \geq 0$ , transforms into an equivalent wedge,  $\hat{A}_1 = \hat{y} - \hat{z} \cot \psi_1 = 0$ ,  $\hat{A}_2 = \hat{y} - \hat{z} \cot \psi_2 = 0$ ,  $z \geq 0$ ; etc. A constant surface impedance  $Z$  in the  $yz$  space generally requires a non-constant surface impedance  $\hat{Z}$  in the isotropic space since  $\alpha$  is variable over a curved obstacle contour  $A$ . The only exceptions occur when

$$(a) \quad Z = 0 \quad \text{or} \quad (b) \quad \alpha = \text{piecewise constant on } A; \quad (8)$$

the former condition for a perfectly conducting surface in the  $yz$  space transforms unchanged into the  $\hat{y}z$  space since  $\hat{Z} = 0$ , while the latter condition applies to an obstacle contour comprised of plane segments (e.g., an infinite plane, half-plane, wedge, or polygon). The validity of the preceding considerations is apparent only when  $\epsilon$  is positive real since the geometrical equivalence between the problems sketched in Figs. 7.4.1(a) and (b) does not apply when  $\sqrt{\epsilon}$  has an imaginary part. However, if a solution constructed for positive real  $\epsilon$  can be continued analytically into  $0 \leq \arg \epsilon \leq \pi$ , the result will be valid throughout this extended range.

This procedure is now applied to various examples which illustrate some of the diffraction phenomena encountered in anisotropic media.

### 7.4c Half-Space Bounded by a Perfect Conductor

Consider a line source of magnetic current located at  $(0, z')$  in the presence of an infinite, perfectly conducting plane inclined at an angle  $\alpha$  with the  $z=0$  plane as shown in Fig. 7.4.2(a). This boundary is described by the equation  $u = 0$ , where the  $uv$  coordinate system is rotated through the angle  $\alpha$  with respect to  $y$  and  $z$ . The auxiliary problem in the isotropic  $\hat{y}z$  space, involving a perfectly conducting plane inclined at the angle  $\psi = \cot^{-1}(\sqrt{\epsilon} \cot \alpha)$ , with the source location unaltered, may evidently be solved by the method of images. The location  $(\hat{y}', \hat{z}')$  of the image point is obtained by reflection,

$$\hat{y}' = z' \sin 2\psi, \quad \hat{z}' = -z' \cos 2\psi, \quad (9)$$

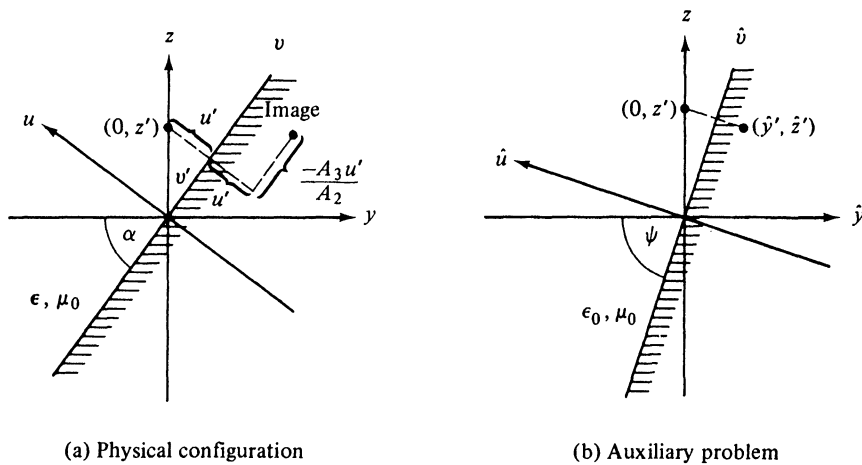
and the resulting magnetic field in the half-space  $u > 0$  is given by

$$H(y, z; 0, z') = H_i(y, z; 0, z') + H_i(y, z; \frac{\hat{y}'}{\sqrt{\epsilon}}, \hat{z}'), \quad (10)$$

where  $H_i$  denotes the infinite space solution in Eq. (7.3.38a).

---

†The transformation  $\hat{z} = z/\sqrt{\epsilon}$  in Sec. 7.2 applied to a cylindrical obstacle oriented parallel to the  $z$  axis leaves the obstacle shape unchanged. This invariance is not maintained by scaling either  $z$  or  $y$  in the present configuration oriented perpendicular to the  $z$  axis.

FIG. 7.4.2 Half-space bounded by a perfect conductor ( $0 < \epsilon < 1$ ).

It is of interest to determine the image location in the  $uv$  coordinate space which is natural to the description of the bounding plane  $u = 0$ . From Eqs. (5) and (6c), the image location  $(\bar{y}', \bar{z}')$  in the  $yz$  coordinate system is

$$\begin{aligned}\bar{y}' &= 2z' \frac{\sin \alpha \cos \alpha}{\epsilon A_2}, & \bar{z}' &= \hat{z}' = z' \frac{\sin^2 \alpha - \epsilon \cos^2 \alpha}{\epsilon A_2}, \\ \epsilon A_2 &= \sin^2 \alpha + \epsilon \cos^2 \alpha;\end{aligned}\quad (11)$$

the corresponding point  $(\bar{u}', \bar{v}')$  relative to the  $uv$  coordinates is obtained via the relations

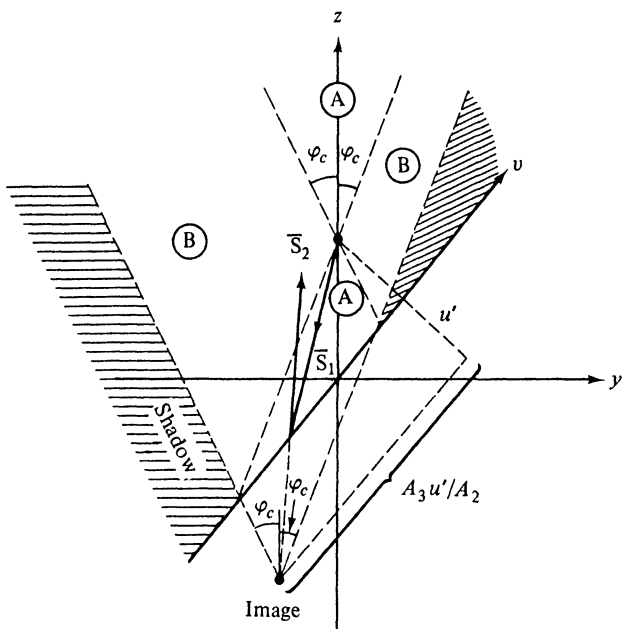
$$\bar{u}' = \bar{z}' \cos \alpha - \bar{y}' \sin \alpha, \quad \bar{v}' = \bar{y}' \cos \alpha + \bar{z}' \sin \alpha, \quad (12)$$

and yields

$$\bar{u}' = -u', \quad \bar{v}' = v' - \frac{A_3 u'}{A_2}, \quad \epsilon A_3 = 2(\epsilon - 1) \sin \alpha \cos \alpha. \quad (13)$$

Thus, the perturbation fields due to the presence of the perfectly reflecting plane in Fig. 7.4.2(a) may be rigorously accounted for in terms of an image source that is, however, displaced from the mirror-image location  $(-u', v')$  by the distance  $-A_3 u' / A_2$  measured parallel to plane.<sup>6</sup> The image location coincides with the conventional one only when  $\epsilon = 1$  (isotropic case) or when  $\alpha = 0, \pi/2$  (optic axis parallel or perpendicular to boundary); in the latter instance, the analysis in Sec. 7.4a shows that the mirror-image construction holds for arbitrary source distributions, as in isotropic regions. Although the solution (10) was obtained on the assumption  $\epsilon > 0$ , it may be continued analytically into the range  $0 \leq \arg \epsilon \leq \pi$  and holds in particular when  $\epsilon < 0$ .

The image displacement has interesting consequences which arise also in media with more general anisotropic properties: it implies the occurrence of non-specular reflections at a plane boundary, as schematized in Fig. 7.4.3 for

FIG. 7.4.3 Incident and reflected rays when  $\epsilon < 0$ .

the case  $\epsilon < 0$ , with  $A_2 > 0$ . Since  $\epsilon < 0$ , the propagating plane-wave spectrum issuing from the source and its image is restricted to ray angles  $\varphi$  which satisfy the condition  $|\tan \varphi| < \tan \varphi_c = 1/\sqrt{|\epsilon|}$ , where  $\varphi$  is measured from the positive  $z$  axis (see Sec. 7.3e). Consequently, the direct radiation  $\bar{S}_1$  from the source illuminates only region A in Fig. 7.4.3, while propagating rays  $\bar{S}_2$  from the image source (i.e., the rays reflected at the boundary) penetrate both regions A and B. The shaded area constitutes the shadow zone in which the fields decay, and one observes that the presence of a reflecting boundary enlarges the illuminated region. The non-specular character of the reflection is evident from the construction and, for the case considered, both the incident and reflected rays lie on the same side of the normal to the surface—a phenomenon not encountered in isotropic media.

The directions of the incident and reflected rays may also be inferred from the refractive index diagrams in Fig. 7.1.1, an aspect that is explored further in Sec. 7.5b.

#### 7.4d Half-space Bounded By a Reactive Surface

We repeat the analysis in the preceding section for the case where the plane boundary at  $u = 0$  is assumed to have a constant surface impedance  $Z \neq 0$ .<sup>6</sup> The transformed isotropic problem then involves the plane surface in Fig.

7.4.2(b), with a constant surface impedance  $\hat{Z}$  inferred from Eq. (7b). The solution for  $\hat{H}$  can no longer be obtained in closed form by the method of images but involves the integral representations in Eqs. (5.7.17) or (5.7.21). For distant observation points, the integrals may be evaluated asymptotically and yield the result in Eq. (5.7.19) which contains three contributions: the infinite space field in the absence of the boundary; the reflected field which appears to arise from the mirror-image point, with an angularly dependent amplitude factor equal to the plane-wave reflection coefficient of the surface; and a surface-wave field that contributes only when the surface impedance is inductive ( $\text{Im } \hat{Z} < 0$ ) and when the observation point lies sufficiently close to the boundary. Upon transforming these field solutions into the anisotropic  $y, z$  space (with  $\epsilon > 0$ ), one obtains a far field comprising the above-mentioned three constituents. The first two may be interpreted exactly as in Fig. 7.4.3, or rather its analogue for  $\epsilon > 0$ , and yield the incident and reflected rays, with the latter weighted by the transformed reflection coefficient.

The surface-wave contribution merits further attention. If  $\hat{u}$  and  $\hat{v}$  denote the coordinates parallel and perpendicular, respectively, to the surface in the equivalent isotropic problem [see Fig. 7.4.2(b)], then the magnetic field  $\hat{H}$ , in the surface wave has the behavior [see Eq. (5.7.21)]

$$\hat{H}_s = \exp(ik_y\sqrt{1 - \hat{Z}^2}\hat{u} - ik_0\hat{Z}\hat{v}), \quad (14)$$

where  $\text{Im } \hat{Z} < 0$ ,  $\text{Re } \hat{Z} \geq 0$ , and  $\hat{v} \geq 0$ . This solution may be transformed into the anisotropic space by noting that  $\hat{u} = \hat{y} \cos \psi + z \sin \psi$ ,  $\hat{v} = z \cos \psi - \hat{y} \sin \psi$ , and applying Eq. (5). The resulting expression is then written in terms of the  $u, v$  coordinates via  $y = v \cos \alpha - u \sin \alpha$ ,  $z = v \sin \alpha + u \cos \alpha$ , and yields the following variation of the surface-wave field  $H_s$ :

$$H_s = e^{iqu+i\beta v}, \quad (15)$$

where  $q$  and  $\beta$  are the wavenumbers along the  $u$  and  $v$  directions, respectively,

$$q = -\beta \frac{A_3}{2A_2} - k_0 \frac{Z'}{A_2}, \quad \beta = k_0 \sqrt{\epsilon(A_2 - Z'^2)}, \quad Z' = \frac{Z}{\sqrt{\mu/\epsilon_0}}, \quad (15a)$$

with  $\epsilon$  assumed positive, and  $Z$  and  $A_2$  defined in Eqs. (7b) and (11). This relation between  $q$  and  $\beta$  is a direct consequence of the dispersion equation (7.1.5) when expressed in terms of the rotated  $u, v$  coordinates [see Eq. (7.5.5)]. If the surface is purely reactive, then  $Z' = -i|Z'|$ , and the field in both Eqs. (14) and (15) decays away from the boundary. However, in the isotropic case, the wavenumber in the perpendicular  $\hat{u}$  direction is purely imaginary, whereas it is complex in the anisotropic problem. The constant-phase planes in the anisotropic medium are therefore inclined with respect to the  $v$  direction along the boundary.

If the field  $H_s$  does indeed define a surface wave, it must carry energy in the  $v$  direction parallel to the surface. Since

$$\frac{\partial}{\partial y} = \cos \alpha \frac{\partial}{\partial v} - \sin \alpha \frac{\partial}{\partial u}, \quad \frac{\partial}{\partial z} = \sin \alpha \frac{\partial}{\partial v} + \cos \alpha \frac{\partial}{\partial u}, \quad (16)$$

and  $E_u = E_z \cos \alpha - E_y \sin \alpha$ ,  $E_v = E_z \sin \alpha + E_y \cos \alpha$ , one obtains from the electric-field expressions in Eq. (7.3.38),

$$E_u = \frac{1}{i\omega\epsilon_0} \left( A_1 \frac{\partial}{\partial v} + \frac{A_3}{2} \frac{\partial}{\partial u} \right) H, \quad E_v = -\frac{1}{i\omega\epsilon_0} \left( \frac{A_3}{2} \frac{\partial}{\partial v} + A_2 \frac{\partial}{\partial u} \right) H, \quad (17)$$

where  $A_2$  and  $A_3$  are defined in Eqs. (11) and (13), respectively, and

$$A_1 = \sin^2 \alpha + \frac{1}{\epsilon} \cos^2 \alpha \equiv \frac{1}{\epsilon} N^2(\alpha). \quad (17a)$$

A calculation of the time-averaged Poynting vector for  $Z' = -i|Z'|$  then shows that

$$\tilde{S}_u = -\operatorname{Re}(E_{vs} H_s^*) = 0, \quad (18a)$$

$$\tilde{S}_v = \operatorname{Re}(E_{us} H_s^*) = \frac{\beta}{\omega\epsilon A_2} |H_s|^2, \quad (18b)$$

thereby confirming the surface-wave character of the field in Eq. (15).

#### 7.4e Wedge and Half-plane

We consider briefly the problem of diffraction by a perfectly conducting wedge, the isotropic version of which, treated in detail in Chapter 6, may be transformed according to Eq. (6) to yield a result in the anisotropic space.<sup>6,10</sup> Any of the various representations listed in Sec. 6.5 may be employed in appropriate parameter ranges. For source or observation points located near the edge, the series in Eq. (6.5.13) is convenient and rapidly convergent, while the far field excited by a distant source is calculated best from the asymptotic formulas in Eqs. (6.5.19).

The far-field approximation in the isotropic medium comprises three parts, each of which possesses a simple physical interpretation in terms of geometric-optical rays: (a) the infinite space field in the absence of the obstacle; (b) the reflected field comprising all rays that are reflected specularly from the sides of the wedge (Fig. 6.5.1); and (c) the diffracted field which takes the form of an inhomogeneous cylindrical wave (radially diverging rays) emanating from the wedge apex (see Fig. 6.3.1). This simple description fails in the vicinity of the geometrical shadow and reflected-wave boundaries and must be augmented by a transition solution, as discussed in Chapter 6. No difficulty arises in transforming these solutions into the anisotropic medium when  $\epsilon > 0$ ; the wedge angle is changed thereby according to the remarks made in the paragraph following Eq. (7), and the source location is also affected when  $y' \neq 0$ . The resulting asymptotic field comprises the same contributions as above, and has an analogous physical interpretation. The primary field (a) is as in Eq. (7.3.37) and exists only in the illuminated region; the shadow boundary is defined by the ray that just grazes the apex, as illustrated for the half-plane in Fig. 7.4.4. As in Fig. 7.4.2, the reflected wave field (b) may be viewed as arising from a displaced image source, one for each of the singly and multiply re-

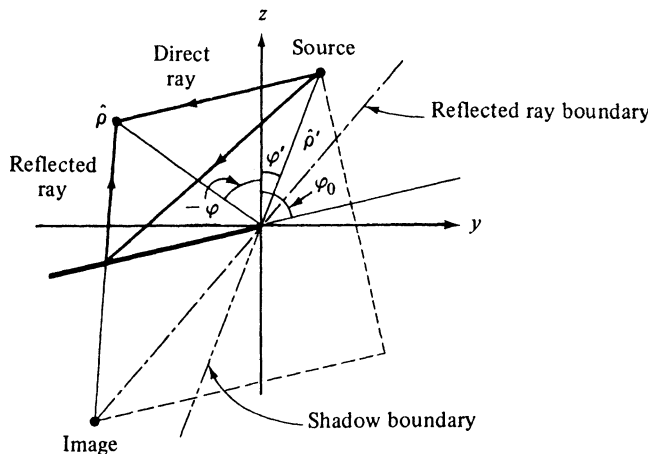


**FIG. 7.4.4** Domains of existence of direct and reflected rays.

flected rays, and its domain of existence is bounded by the ray from the image that just grazes the edge. The diffracted field (c) appears to emanate from a line source at the edge and reaches all observation points; it is excited by the incident ray that grazes the edge, its angular intensity being dependent upon the transformed diffraction coefficient as well as on the  $1/\sqrt{N(\varphi)}$  term arising from the asymptotic approximation to Eq. (7.3.37) [see Eq. (19)]. Most important in this quasi-optic interpretation of the scattered field is the recognition that the *rays*, and not the wavenormals, enter into the identification of the various field constituents—a property that continues to apply in more general types of anisotropic media. These simple physical ray concepts, in conjunction with the image construction, or more generally the refractive index curves (see Sec. 1.6), may be employed to derive detailed information about the nature of the high-frequency field.

It is also of interest to take note of the edge condition in the anisotropic case. In the isotropic problem, the electric field at a distance  $\hat{\rho}$  from the edge diverges like  $\hat{\rho}^{(\pi/\delta)-1}$  as  $\hat{\rho} \rightarrow 0$ , where  $\delta$  is the exterior angle subtended by the wedge. Through the transformation (5),  $\hat{\rho} \rightarrow \rho N(\varphi)$ ,  $\rho = (y^2 + z^2)^{1/2}$ , and

$$\delta = \cot^{-1}(\sqrt{\epsilon} \cot \varphi_2) - \cot^{-1}(\sqrt{\epsilon} \cot \varphi_1), \quad \epsilon > 0,$$

with the angles  $\varphi_{1,2}$  specifying the location of the wedge faces in the  $y, z$  space. The resulting behavior of the electric fields near the edge,  $O[\rho^{(\pi/\delta)-1}]$ , may be more violent than that observed when the identical structure is embedded in an isotropic medium. For example, if  $\varphi_2 = 3\pi/2$  and  $-\pi/2 < \varphi_1 < 0$ , then  $\delta = (3\pi/2) - \cot^{-1}(\sqrt{\epsilon} \cot \varphi_1)$ . For  $0 < \epsilon < 1$ ,  $\cot^{-1}(\sqrt{\epsilon} \cot \varphi_1) < \varphi_1$ , so  $\delta > \delta_0 = 3\pi/2 + |\varphi_1|$ , with  $\delta_0$  denoting the exterior wedge angle. In an isotropic medium the electric field near the edge behaves like  $\rho^{(\pi/\delta_0)-1}$  and therefore grows less rapidly than  $\rho^{(\pi/\delta)-1}$ .

When  $\epsilon$  is complex or negative real, the solutions are obtained from those for positive  $\epsilon$  by analytic continuation. Since the scaling procedure [Eq. (6c)] then transforms real into complex angles, questions of interpretation arise which have been clarified for the special case of a perfectly conducting half plane.<sup>10</sup> It is found that for  $\epsilon \geq 0$ , the incident and reflected fields in their domains of existence are the same as for an infinitely extended plane, with the reflected field derivable from an image source as in Fig. 7.4.3. The boundary of the domain of existence of the incident field (shadow boundary) is still given by the ray that grazes the edge regardless of whether the field along this ray is propagating or evanescent; a similar statement applies to the boundary of the domain of existence of the reflected rays (Fig. 7.4.4). The diffracted field  $H_d$  obtained by application of coordinate scaling to the isotropic-medium formula in Eq. (6.5.19a) yields the asymptotic result:

$$H_d \sim [VQ(\hat{\mathbf{p}}')][f(\varphi, \varphi', \varphi_0)Q(\hat{\mathbf{p}})], \quad \hat{\mathbf{p}} = (\hat{\rho}, \varphi), \quad \hat{\mathbf{p}}' = (\hat{\rho}', \varphi'), \quad (19)$$

where  $V$  is the strength of the magnetic line current [Eq. (1)], while

$$Q(\hat{\mathbf{p}}') = -\frac{\omega\epsilon_0\sqrt{\epsilon}}{4} \sqrt{\frac{2}{\pi k_0 \hat{\rho}' N(\varphi')}} e^{ik_0 \hat{\rho}' N(\varphi') - i\pi/4} \quad (19a)$$

is the magnetic field at the edge of the half-plane, generated by a line current of unit strength at  $\hat{\mathbf{p}}'$  [asymptotic form of Eq. (7.3.38)];  $Q(\hat{\mathbf{p}})$  is the field at the observation point  $\hat{\mathbf{p}}$  generated by a virtual line current of unit strength at the edge, and  $f(\varphi, \varphi', \varphi_0)$  is the pattern function associated with the edge-diffracted field:

$$f(\varphi, \varphi', \varphi_0) = \frac{1}{2} \frac{f_1(\varphi, \varphi_0)f_1(\varphi', \varphi_0)}{f_2(\varphi, \varphi_0) + f_2(\varphi', \varphi_0)}, \quad (19b)$$

where

$$f_1(\varphi, \varphi_0) = \left[ 1 - \frac{\epsilon \sin \varphi_0 \sin \varphi + \cos \varphi_0 \cos \varphi}{N(\varphi_0)N(\varphi)} \right]^{1/2},$$

$$f_2(\varphi, \varphi_0) = \frac{\epsilon \sin \varphi_0 \sin \varphi + \cos \varphi_0 \cos \varphi}{N(\varphi_0)N(\varphi)}, \quad (19c)$$

and  $N(\varphi) = \cos^2 \varphi + \epsilon \sin^2 \varphi$ . In these formulas, which remain valid for positive or negative  $\epsilon$  provided that  $\text{Im } N \geq 0$ , the angles  $\varphi$ ,  $\varphi'$ , and  $\varphi_0$  measure, respectively, the angular locations of the observation point, source point, and half-plane with respect to the optic ( $z$ ) axis (Fig. 7.4.4). Near the geometrical shadow and reflected ray boundaries where  $f_2(\varphi, \varphi_0) \rightarrow -f_2(\varphi', \varphi_0)$ , one must employ a modified description in terms of Fresnel integrals [see Eq. (6.5.20)]. When  $\epsilon < 0$ , the formula fails along the shadow boundaries  $N(\varphi_c) = 0$  and  $N(\varphi_c) = 0$  associated with the anisotropy in the medium.

The factors inside the brackets in Eq. (19) have a direct physical interpretation;  $fQ(\hat{\mathbf{p}})$  represents the diffracted field due to an incident field having unit amplitude at the edge while  $VQ(\hat{\mathbf{p}}')$  accounts for deviations of the incident field strength from unity. It follows from these considerations that an incident *plane*

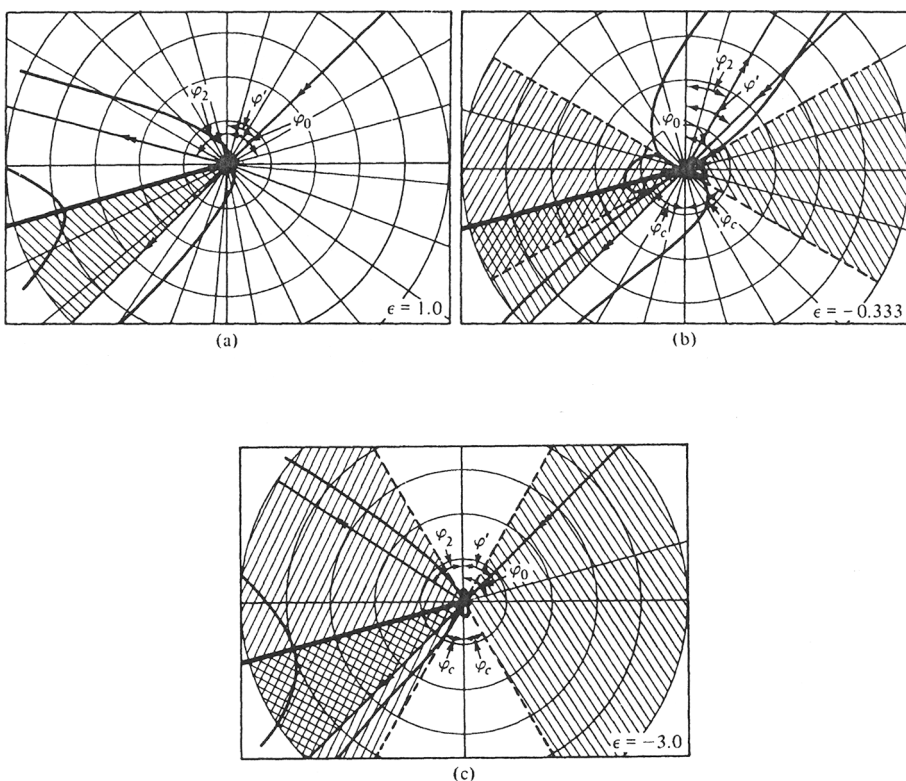
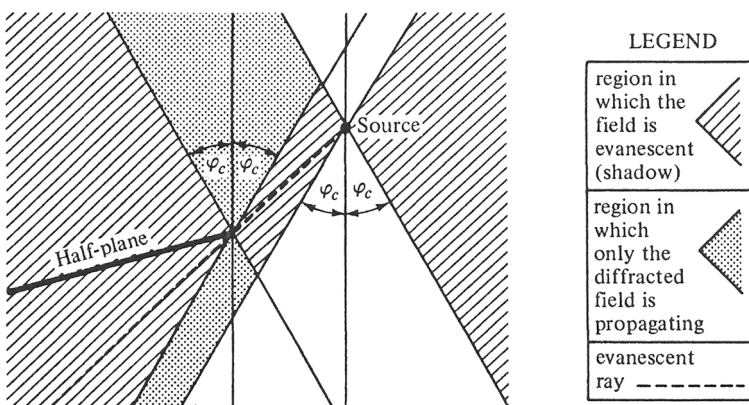


FIG. 7.4.5 Plot of the pattern function  $f(\phi, \phi', \phi_0)$  for  $\phi' = 45^\circ$ ,  $\phi_0 = 75^\circ$ , and various  $\epsilon$ .

wave of the form  $\exp[-i(\eta_i y + \kappa_i z)]$  carrying energy along  $\phi'$  gives rise to an edge diffracted field  $fQ(\hat{p})$ . The influence of an anisotropic environment on the pattern function may be assessed from Fig. 7.4.5, which contains a plot of  $f$  for (a)  $\epsilon = 1$ , (b)  $\epsilon = -\frac{1}{3}$ , (c)  $\epsilon = -3$ , with the incidence and half-plane angles remaining fixed at  $\phi' = 45^\circ$  and  $\phi_0 = 75^\circ$ , respectively.  $\phi_2$  locates the boundary of the reflected waves. Case (a) corresponds to an isotropic medium; since  $\epsilon < 0$  in cases (b) and (c), the medium supports propagating fields only in the restricted angular domain  $|\tan \phi| < \tan \phi_c = |\epsilon|^{-1/2}$ , whence the incident field is propagating in case (b) but evanescent in case (c). Two shadow zones, shown shaded in Fig. 7.4.5, must be distinguished: the first is due to the geometrical blocking effect of the half-plane, whereas the second, the double-wedge-shaped region  $|\tan \phi| > |\epsilon|^{-1/2}$ , arises from anisotropy in the medium. Inside the latter region,  $f$  describes the angular variation of the evanescent field. Evidently, the presence of anisotropy may introduce substantial distortion of the isotropic medium pattern which is symmetrical about the half-plane. It



**FIG. 7.4.6** Various wave domains when half-plane is in the shadow region of the source in a medium with  $\epsilon = \epsilon_0(1_t + z_0 z_0 \epsilon)$ ,  $\epsilon < 0$ .

is of interest to observe that although the incident field may be evanescent when  $\epsilon < 0$  [ $N(\varphi')$  imaginary], the diffraction field due to the edge couples to propagating waves in the region  $|\tan \varphi| < |\epsilon|^{-1/2}$  wherein  $N(\varphi)$  is real. Thus, diffraction may extract real energy from an incident evanescent field, by a mechanism somewhat reminiscent of that encountered in the operation of a microwave cutoff attenuator or the tunnel effect in quantum mechanics. Figure 7.4.6 contains a representative sketch, wherein the regions illuminated by the source and by diffraction are delineated.

## 7.5 RADIATION FROM A HOMOGENEOUS PLASMA HALF-SPACE

To observe radiation phenomena associated with an interface bounding a uniaxially anisotropic region, we consider a source embedded in a plasma half-space. If the interface is perpendicular to the  $z$  axis, the fields excited by arbitrary source distributions may be constructed via the simple procedure in Sec. 7.2; the equivalent modal network problem is directly analogous to that for the isotropic half-space, shown in Figs. 5.5.3 or 5.5.6. The modal description is in terms of transmission along the  $z$  direction, and because of the reflection symmetry with respect to the optic axis, longitudinal wavenumbers  $\pm \kappa$  exist for the same transverse wavenumber  $k$ , or  $-k$ , [see Eq. (7.2.8)]. Interface effects are similar to those in isotropic regions, and such peculiarly anisotropic phenomena as non-specular reflections do not occur. The latter are present when the optic axis is inclined with respect to the interface; hence it is instructive to examine a problem of this kind since it is not amenable to a simple network treatment.

Even for the two-dimensional case corresponding to excitation by a magnetic line source as in Sec. 7.4, when the optic axis is not perpendicular to the

interface, coordinate scaling does not facilitate the solution since the originally isotropic medium becomes anisotropic in the scaled coordinate frame. Thus, it is necessary to resort to a representation in terms of plane-wave modes propagating along the direction perpendicular to the interface; owing to the obliquity of the optic axis in the anisotropic half-space, these modes do not possess reflection symmetry. After formulation of this problem in Sec. 7.5a, attention is given in Sec. 7.5b to the reflection and transmission properties of the plane-wave modes, and to the interpretation of nonspecular reflection, etc., through use of the wavenumber surfaces for the two media. The solution for the line-source field, obtained by modal synthesis in Sec. 7.5c, is simplified subsequently for distant observation points. In the plasma half-space, the asymptotic evaluation of the radiation integral by the steepest-descent method yields saddle-point and branch-point contributions that can be identified as geometric-optical and diffracted (lateral-wave) fields, respectively (Sec. 7.5d). The geometric-optical fields are similar to those obtained in Sec. 7.4c for a perfectly conducting boundary. As in the isotropic problem discussed in Sec. 5.5, the lateral-wave fields are excited by a ray incident at the critical angle. However, their behavior is modified substantially by anisotropy, especially when the uniaxial wavenumber surface is open branched; in this event, lateral rays are refracted backward with respect to the incident critical ray. The simple asymptotic calculation providing a ray-optical interpretation must be modified for observation points in the transition region surrounding the angle of total reflection. This parameter regime is characterized by proximity of a saddle point and branch point in the representation integral and thus requires use of the uniform asymptotic procedure discussed in Sec. 4.4c.

Fields in the vacuum half-space are evaluated asymptotically in Sec. 7.5e, and are found to propagate along refracted rays. When the uniaxial wavenumber surface is open branched, the family of refracted rays is found to form a caustic indicative of a kind of field enhancement or focusing not exhibited in an isotropic medium. For observation points near the caustic, modified asymptotic procedures (Secs. 4.5a and 4.5b) must be employed to account for the proximity of two or three saddle points in the refracted field integral. The chapter concludes in Sec. 7.5f with a brief treatment of radiation from a transverse electric dipole source.

### 7.5a Formulation of the Problem (Line-source Excitation)

The physical configuration is shown in Fig. 7.5.1, where the uniaxially anisotropic half-space occupies the region  $u < 0$ , and the region  $u > 0$  is filled with an isotropic dielectric of permittivity  $\epsilon_0$ . The  $uv$  coordinate system, natural to the description of this geometrical configuration, is inclined at an angle  $\alpha$  with respect to the  $yz$  axes along which the medium anisotropy is described most directly. On suppressing the  $\exp(-i\omega t)$  factor and normalizing the source strength, the single component of magnetic field satisfies in the anisotropic

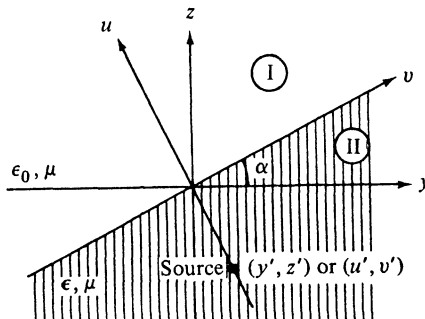


FIG. 7.5.1 Physical configuration.

region II the inhomogeneous wave equation (7.3.36) which, when transformed into the  $uv$  frame, reads (with  $\epsilon_0$  replaced by  $\epsilon_y$  for generality)<sup>11</sup>

$$\left( A_1 \frac{\partial^2}{\partial v^2} + A_2 \frac{\partial^2}{\partial u^2} + A_3 \frac{\partial^2}{\partial u \partial v} + k_y^2 \right) H_2 = -i\omega\epsilon_y \delta(u - u') \delta(v - v'), \quad u < 0, \quad (1)$$

and the electric-field components  $E_{u2}$  and  $E_{v2}$  are then determined from Eq. (7.4.17). The constants  $A_{1,2,3}$  were defined in Eqs. (7.4.11), (7.4.13), and (7.4.17a). In the isotropic region I, characterized by the scalar dielectric constant  $\epsilon_0$  and permeability  $\mu$ , the magnetic field  $H_1$  satisfies the homogeneous equation

$$\left( \frac{\partial^2}{\partial u^2} + \frac{\partial^2}{\partial v^2} + k_0^2 \right) H_1 = 0, \quad u > 0, \quad (2)$$

and the corresponding electric fields are

$$E_{u1} = \frac{1}{i\omega\epsilon_0} \frac{\partial H_1}{\partial v}, \quad E_{v1} = -\frac{1}{i\omega\epsilon_0} \frac{\partial H_1}{\partial u}. \quad (2a)$$

The solutions in regions I and II are connected by the continuity conditions  $H_1 = H_2$ ,  $E_{v1} = E_{v2}$  at  $u = 0$ , and imposition of a radiation condition at infinity completes the unique specification of  $H$ .

### 7.5b Reflection and Transmission of Plane Waves, and the Radiation Condition

The radiation problem specified in the preceding section is solved most naturally by viewing the configuration as a waveguide whose axis is parallel to  $u$ , with the mode functions taken as plane waves with cross-sectional dependence  $\exp(i\beta v)$ ,  $-\infty < \beta < \infty$ . Thus, we seek a representation for  $H_2$  in terms of a continuous spectrum of plane waves of the form

$$\exp(i\mathbf{k} \cdot \mathbf{R}) = \exp[iq(\beta)u + i\beta v]. \quad (3)$$

Because of their importance in the analysis, these wave solution are subjected

to further study. It will be found that the longitudinal wavenumbers  $q_1(\beta)$  and  $q_2(\beta)$  corresponding to a plane wave that carries energy along the  $+u$  and  $-u$  directions, respectively, are not connected by the simple relation  $q_1 = -q_2$  which applies in regions with reflection symmetry. Thus, as noted in Sec. 7.1, it is no longer possible to schematize propagation phenomena by a bilateral transmission line with a given propagation constant  $q$ ; instead, unidirectional transmission lines with different properties are required, one for each forward and backward propagating wave. Because of this complication, which is generally characteristic of wave propagation in anisotropic media, the traveling-, and not the standing-, wave description is the more fundamental; in consequence, a network representation in terms of transmission lines loses much of the appeal it possesses in reflection symmetric problems.

The plane wave in Eq. (3) satisfies the homogeneous wave equation (1), and hence the wavenumbers  $q$  and  $\beta$  are connected by the dispersion equation

$$A_2 q^2 + A_1 \beta^2 + A_3 q\beta = k_y^2 = k_0^2 \epsilon'_y, \quad \epsilon'_y = \frac{\epsilon_y}{\epsilon_0}, \quad (4)$$

which has the two solutions

$$q_{1,2}(\beta) = \frac{-\beta A_3 \pm 2\sqrt{k_y^2 A_2 - (\beta^2/\epsilon)}}{2A_2}, \quad \epsilon = \frac{\epsilon_z}{\epsilon_y}. \quad (5)$$

Equation (4) contains the same information as Eq. (7.1.5), but the latter has a simpler form since its wavenumbers  $k_r = \eta$  and  $\kappa$  are expressed with respect to the principal axes of the wavenumber surface. A plot of the real solutions of Eq. (5) therefore reproduces the curves in Fig. 7.1.1, with  $q$  and  $\beta$  measured in the rotated coordinate system shown in Fig. 7.5.2. If the square root in Eq.

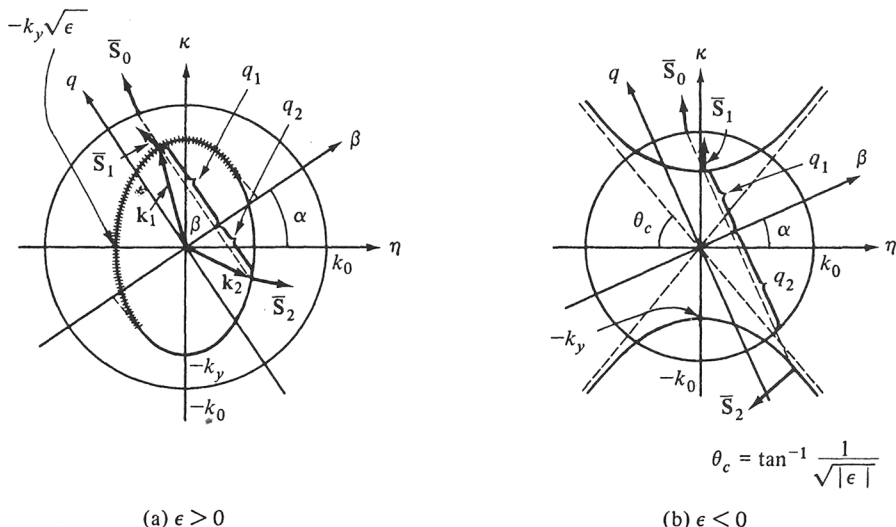


FIG. 7.5.2 Wavenumber surfaces.

(5) is defined to be positive when real, one observes from Fig. 7.5.2(a) that the solution designated as  $q_1$  defines the shaded portion of the ellipse while  $q_2$  specifies the unshaded portion. Since the outward normals on the  $q_1$  branch have a component parallel to the  $+q$  axis while those on the  $q_2$  branch have a component parallel to the  $-q$  axis, plane waves with wave vector  $\mathbf{k}_1 = q_1 \mathbf{u}_0 + \beta \mathbf{v}_0$  carry energy along the  $+u$  direction, and those with wave vector  $\mathbf{k}_2 = q_2 \mathbf{u}_0 + \beta \mathbf{v}_0$  carry energy along the  $-u$  direction. Evidently,  $q_1 \neq -q_2$ , and  $q_1$  may be negative or  $q_2$  positive—another example of a “backward wave” with respect to the  $u$  axis. Analogous considerations apply when  $\epsilon < 0$ .

In the presence of an interface parallel to the  $v$  axis, the continuity of the tangential field components requires that the incident, reflected, and transmitted waves all have the same dependence  $\exp(i\beta v)$ . If the wave is incident from the anisotropic half-space  $u < 0$ , then

$$\bar{H}_2 = g(\beta) e^{i\beta v} [e^{iq_1 u} - \Gamma(\beta) e^{iq_2 u}], \quad u < 0, \quad (6a)$$

and

$$\bar{H}_1 = f(\beta) e^{i\beta v} e^{iq_0 u}, \quad q_0 = \sqrt{k_0^2 - \beta^2}, \quad u > 0, \quad (6b)$$

where  $g(\beta)$ ,  $g\Gamma(\beta)$ , and  $f(\beta)$  represent the amplitudes of the incident, reflected, and transmitted (refracted) waves, respectively;  $q_0$ , which is positive when real, is the conventional longitudinal propagation constant in an isotropic waveguide. Upon imposing the boundary conditions  $H_1 = H_2$  and  $E_{v1} = E_{v2}$  at  $u = 0$ , one obtains the expressions for the reflection and transmission coefficients,

$$\Gamma = 1 - T = \frac{2\epsilon' q_0 + A_2(q_2 - q_1)}{2\epsilon' q_0 - A_2(q_2 - q_1)}, \quad T = \frac{f}{g}. \quad (7)$$

In view of the preceding remarks, the plane-wave solutions in Eqs. (6) satisfy the energy radiation condition when  $q_1$ ,  $q_2$ , or  $q_0$  are real. If these quantities are complex, the required decay of the field solutions is assured if

$$\operatorname{Im} q_1 > 0, \quad \operatorname{Im} q_2 < 0, \quad \operatorname{Im} q_0 > 0, \quad (8)$$

thereby completing the specification of the multivalued propagation constants  $q$ . If  $\epsilon = 1$ , the resulting expression for  $\Gamma$  agrees with that listed in Eq. (5.5.3d) for the isotropic half-space problem.

The ray directions, along which energy is transported in the plane waves characterized by the wave vectors  $\mathbf{k}_1$ ,  $\mathbf{k}_2$ , and  $\mathbf{k}_0 = q_0 \mathbf{u}_0 + \beta \mathbf{v}_0$ , may be determined either analytically or from an inspection of the wavenumber curves in Fig. 7.5.2. The values of  $q_1$  and  $q_2$  belonging to a specified value of  $\beta$  are obtained directly from the graphs, and the corresponding incident- and reflected-ray directions  $\bar{\mathbf{S}}_1$  and  $\bar{\mathbf{S}}_2$  in the  $uv$  coordinate space are determined by constructing the normals to the curves at the points  $(q_1, \beta)$  and  $(q_2, \beta)$ , respectively; it is recalled from Eq. (1.7.53a) that the angle between  $\mathbf{k}$  and  $\bar{\mathbf{S}}$  is less than  $90^\circ$ . Since the dispersion curve for the vacuum region II is the circle described by the equation  $q_0^2 + \beta^2 = k_0^2$ , the transmitted ray  $\bar{\mathbf{S}}_0$  follows the direction of the

radius vector at the point on the circle having an abscissa equal to  $\beta$ . This “ray-tracing” procedure applies also when the medium has more general anisotropic properties; it is particularly useful in inhomogeneous regions that may be approximated by piece-wise constant layers having different refractive index diagrams (see Fig. 1.6.7).

An analytical expression relating the ray angles  $\varphi_1$ ,  $\varphi_2$ , and  $\varphi_0$ , which are measured from the positive  $u$  axis toward the positive  $v$  axis and specify the directions on the incident, reflected, and refracted rays, respectively, is obtained from the analogue of Eq. (7.1.7):

$$\tan \varphi = -\frac{dq}{d\beta} \quad (9a)$$

Evaluation of the derivative from Eq. (5) and use of  $\beta = k_0 \sin \varphi_0$  yields

$$\tan \varphi_{1,2} = \frac{A_3}{2A_2} \pm \frac{\sin \varphi_0}{\epsilon A_2 \sqrt{\epsilon'_y A_2 - (\sin^2 \varphi_0)/\epsilon}}, \quad (9b)$$

the generalization of the Snell reflection and refraction law for the rays at a uniaxially anisotropic interface. Unless  $A_3 = 0$  (i.e.,  $\epsilon = 1$ , or  $\alpha = 0, \pi/2$ ),  $\varphi_2 \neq \pi - \varphi_1$  so reflection at the interface is generally non-specular. This phenomenon has already been encountered in the problem of reflection from a perfectly conducting plane, analyzed by a different method in Sec. 7.4c, wherein the relation between the incident- and reflected-ray directions has been schematized by an image construction. The present discussion also applies to an anisotropic half-space bounded by a perfectly conducting plane if the current reflection coefficient  $-\Gamma$  is set equal to unity, thereby assuring that  $E_v = 0$  at  $u = 0$ .

When  $\epsilon < 0$ , the algebraic signs of  $\varphi_1$  and  $\varphi_0$  may be opposite, and the associated phenomenon is one of backward refraction of the rays with respect to the direction perpendicular to the interface (i.e., the refracted and incident rays both lie on the same side of the surface normal). This does not apply to the wavevectors, since  $\mathbf{k}_1 = q_1 \mathbf{u}_0 + \beta \mathbf{v}_0$  and  $\mathbf{k}_0 = q_0 \mathbf{u}_0 + \beta \mathbf{v}_0$  both have the same tangential component  $\beta \mathbf{v}_0$ . Moreover, if  $\sqrt{\epsilon'_y A_2 - (1/\epsilon)}$  is real, total reflection is possible in the plasma half-space. The angles of total reflection are obtained by putting  $\varphi_0 = \pm \pi/2$  in the expression for  $\varphi_1$  in Eq. (9b).

It is relevant to ascertain possible pole singularities of  $\Gamma$  which, if they exist, may give rise to the appearance of surface-wave or leaky-wave contributions in the radiated field. While the discussion so far has been concerned with an anisotropic medium specified by the permittivity parameters  $\epsilon_y$  and  $\epsilon_z$ , and an exterior isotropic medium characterized by a different permittivity  $\epsilon_0$ , it will now be assumed that the anisotropic medium is a plasma and the exterior region is vacuum. In this instance,  $\epsilon'_y = 1$ . The denominator of the expression for  $\Gamma$  in Eq. (7) then has a simple zero  $\beta_p$ , when

$$\sqrt{k_0^2 - \beta_p^2} = -\sqrt{k_0^2 A_2 - (\beta_p^2/\epsilon)}. \quad (10)$$

Squaring and solving for  $\beta_p$ , one finds  $\beta_p = \pm k_0 \sin \alpha$ , so  $\sqrt{k_0^2 - \beta_p^2}$  is positive real. Since the square root on the right-hand side is also defined to be positive when real (on the top sheet of the pertinent Riemann surface),  $\beta_p$  cannot be a solution of Eq. (10) but annuls instead the numerator in Eq. (7). Thus,  $\beta_p$  is a zero of the reflection coefficient and poles do not occur. One observes from Fig. 7.5.2 with  $k_y = k_0$  that a wave with wavenumber  $\beta_p$  propagates along the direction of the optic ( $z$ ) axis in the medium, and experiences no reflection at the interface since  $\Gamma = 0$ . This result may be understood by noting that when the transverse permittivities in both media are the same, the region appears homogeneous to a wave propagating along the  $z$  axis since its electric field has only an  $E_y$  component.

### 7.5c Modal Representation of the Solution

To utilize the plane-wave solutions  $\tilde{H}_1$  and  $\tilde{H}_2$  in the synthesis of the line source fields  $H_1$  and  $H_2$ , we assume the representations

$$H_1 = \int_{-\infty}^{\infty} e^{i\beta v + i q_0 u} f(\beta) d\beta, \quad u > 0, \quad (11)$$

$$H_2 = \begin{cases} \int_{-\infty}^{\infty} g(\beta) e^{i\beta v} [e^{iq_1 u} - \Gamma(\beta) e^{iq_2 u}] d\beta, & 0 > u > u', \\ \int_{-\infty}^{\infty} g(\beta) e^{i\beta v} [h(\beta) e^{iq_2 u} - \Gamma(\beta) e^{iq_1 u}] d\beta, & u < u' < 0. \end{cases} \quad (12a)$$

$$H_2 = \begin{cases} \int_{-\infty}^{\infty} g(\beta) e^{i\beta v} [h(\beta) e^{iq_2 u} - \Gamma(\beta) e^{iq_1 u}] d\beta, & u < u' < 0. \end{cases} \quad (12b)$$

The radiation condition has already been satisfied in these formulations since the constituent plane waves describing the primary (i.e.,  $\Gamma = 0$ ) field in Eqs. (12) carry energy away from the source region while the reflected and transmitted waves carry energy away from the interface. Equation (7) gives the expression for  $\Gamma$  and the relation between  $f$  and  $g$ . One may determine the incident-wave amplitudes by writing the primary field as

$$H_{2i} = \int_{-\infty}^{\infty} e^{i\beta v} Q(u, \beta) d\beta, \quad (13)$$

substituting this Fourier integral representation into Eq. (1), recalling that  $2\pi\delta(v - v') = \int_{-\infty}^{\infty} e^{i\beta(v-v')} d\beta$ , and then deriving the differential equation for the transform  $Q(u, \beta)$ :

$$\left( A_2 \frac{d^2}{du^2} + i\beta A_3 \frac{d}{du} - A_1 \beta^2 + k_y^2 \right) Q = \frac{-i\omega\epsilon_y}{2\pi} e^{-i\beta v'} \delta(u - u'). \quad (14)$$

A solution of this equation that satisfies continuity at  $u = u'$  and the radiation condition is given by (for an alternative procedure utilizing first-order transmission-line equations, see Sec. 8.2g)

$$Q = \begin{cases} ae^{i(q_1 u + q_2 u')}, & u > u', \\ ae^{i(q_2 u + q_1 u')}, & u < u', \end{cases} \quad (15)$$

with the constant  $a$  evaluated from the jump condition on the derivative,

$$A_2 \frac{dQ}{du} \Big|_{u'=0}^{u'+0} = -\frac{i\omega\epsilon_y}{2\pi} e^{-i\beta v'}. \quad (16)$$

Consequently,

$$a = \frac{-\omega\epsilon_y e^{-i(q_1 u' + q_2 u' + \beta v')}}{2\pi A_2 (q_1 - q_2)}, \quad (17)$$

and a comparison of Eqs. (12), (13), (15), (17) leads to the identification,

$$g(\beta) = \frac{-\omega\epsilon_y e^{-i(q_1 u' + \beta v')}}{2\pi A_2 (q_1 - q_2)}, \quad (18a)$$

$$h(\beta) = e^{i(q_1 - q_2)u'}, \quad (18b)$$

thereby completing the integral representation for the primary field whose closed-form solution is given in Eq. (7.3.38a). Since each of the constituent plane waves in Eqs. (12a) and (11) satisfies the boundary conditions at the interface, so does the total magnetic field, whence the integral representations in Eqs. (11) and (12) constitute the desired solution; the convergence properties of the integrals when  $\epsilon < 0$  are discussed in connection with Eq. (7.3.10). The multivalued functions  $q_{0,1,2}$  are defined uniquely on the integration path, in view of the specifications given in Sec. 7.5b.

#### 7.5d Asymptotic Evaluation in the Plasma Half-space

While the infinite space contribution arising from the first term in the integrand of Eq. (12a) can be written in the closed form in Eq. (7.3.38a), no such simple evaluation is possible for the remaining term. Hence, we employ asymptotic methods to derive simple expressions for the fields observed at great distances from the source. As noted previously, it will be assumed that  $k_y = k_0$ ; in addition,  $A_2$  in Eq. (7.4.11) is restricted to be positive. This evidently places no constraint on  $\alpha$  or  $\epsilon$  when  $\epsilon > 0$ . For  $\epsilon < 0$ , however, it is implied that  $\tan \alpha < \sqrt{|\epsilon|}$  [i.e., the  $q$  axis in Fig. 7.5.2(b) intersects the branches of the hyperbolic dispersion curve]. If  $A_2 > 0$ , the requirements  $\text{Im } q_1 > 0$ ,  $\text{Im } q_2 < 0$ , when  $q$  is complex, are met by specifying that  $\text{Im } \sqrt{k_0^2 A_2 - (\beta^2/\epsilon)} > 0$  when the radicand is negative; the square root is positive when real. The  $\epsilon > 0$  case is similar to the previously treated problem of radiation from an isotropic half-space (Sec. 5.5) and is therefore not considered in detail. When  $\epsilon < 0$ , however, the analysis contains distinctive features that merit further attention. In this instance, the branch points at  $\beta_b = \pm k_0 \sqrt{\epsilon A_2}$  lie on the imaginary axis; the integration path in the complex  $\beta$  plane appears as in Fig. 7.5.3(a), with the branch cuts drawn so that the various square roots have positive imaginary parts on the entire top sheet of the four-sheeted  $\beta$  surface.

As in the isotropic problems in Sec. 5.5, it is convenient to introduce a new variable  $w$  via

$$\beta = k \sin w, \quad k = k_0 \sqrt{\epsilon A_2} > 0, \quad (19)$$

so that we have

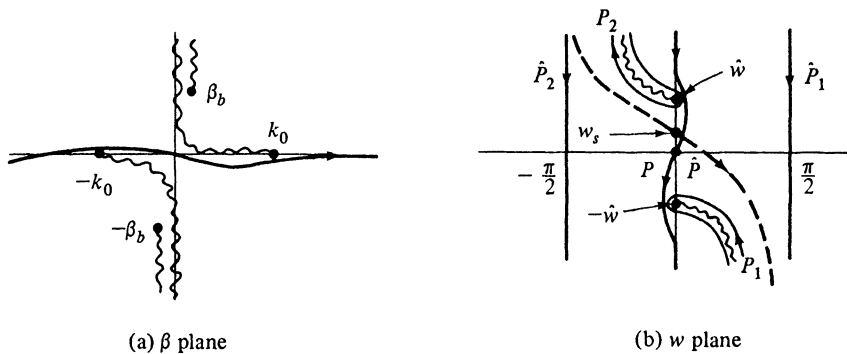


FIG. 7.5.3 Integration paths and singularities in the complex  $\beta$  and  $w$  planes ( $\epsilon < 0$ ).

$$q_{1,2} = \frac{-kA_3 \sin w \pm 2(k/\sqrt{\epsilon}) \cos w}{2A_2}. \quad (20)$$

For positive  $\epsilon$ , the integration path in the  $w$  plane is then essentially the same as  $\tilde{P}$  in Fig. 5.3.6(b), while  $P$  in Fig. 7.5.3(b) is the corresponding path when  $\epsilon$  is negative, with  $\sqrt{\epsilon} = i\sqrt{|\epsilon|}$ . In order to cast the reflected-field contribution in Eq. (12) into a form that exhibits an exponential dependence  $\exp[iy \cos(w - w_s)]$ , where  $y$  and  $w_s$  do not depend on  $w$ , it is useful to define the parameter  $w_s$  via

$$\tan w_s = \frac{(v - v') - (A_3/2A_2)(u - u')}{|u + u'|/\sqrt{\epsilon}A_2}. \quad (21)$$

The integral representation for the reflected field in region II may then be written as

$$H_{2r} = -\frac{\omega\epsilon_0\sqrt{\epsilon}}{4\pi} \int_P \Gamma(k \sin w) e^{iy \cos(w - w_s)} dw, \quad y = \frac{k_0}{\sqrt{A_2} \cos w_s} |u + u'|, \quad (22)$$

which is in the familiar form suitable for asymptotic evaluation when  $y$  is large.

The only pertinent singularities in the  $w$  plane are branch points located at  $\hat{w} = \pm \sin^{-1}(k_0/k)$ .  $w_s \pm n\pi$ ,  $n = 0, 1, 2, \dots$ , specifies the saddle points of the integrand. For positive  $\epsilon$ ,  $w_s$  is real and the pertinent saddle point is located in the interval  $-\pi/2 < w_s < \pi/2$ , while the pertinent branch points  $\hat{w}$  are complex and lie on the lines  $|\operatorname{Re} w| = \pi/2$ . The deformation of  $P$  into the steepest-descent path through  $w_s$ , and the subsequent asymptotic evaluation of the integral, proceeds therefore as in Sec. 5.3. When  $\epsilon < 0$ ,  $w_s$  is complex and it is convenient to introduce a real parameter  $\delta$ ,

$$w_s = i \tanh^{-1} \delta, \quad \delta = \frac{(v - v') - (A_3/2A_2)(u - u')}{|u + u'|/\sqrt{|\epsilon|}A_2}. \quad (23)$$

If  $-1 < \delta < 1$ , then  $w_s = i\phi_s$ , where  $\phi_s$  is real and varies between  $-\infty$  and  $+\infty$ ; if  $\pm\delta > 1$ , then  $w_s = \pm\pi/2 + i \coth^{-1} \delta$ . Since  $w_s$  represents the

saddle point of the integrand in Eq. (22), one must distinguish between the cases  $|\delta| < 1$  and  $|\delta| > 1$  in the asymptotic evaluation. For  $|\delta| < 1$ ,  $\gamma$  is real, and  $\text{Im} \cos(w - w_s) = \sin w_r \sinh(\phi_s - w_i)$  is positive either when  $\sin w_r > 0$ ,  $w_i < \phi_s$ , or when  $\sin w_r < 0$ ,  $w_i > \phi_s$ , where  $w_r$  and  $w_i$  denote the real and imaginary parts of  $w$ , respectively. Hence, the integral converges exponentially along a path such as  $\hat{P}$  in Fig. 7.5.3(b). For  $\pm\delta > 1$ ,  $\gamma = i|\gamma|$ , whence  $\text{Im}[\gamma \cos(w - w_s)] > 0$  when  $\sin w_r \gtrless 0$ , and the integral converges exponentially along paths  $\hat{P}_{1,2}$  when  $\pm\delta > 1$ .

For an asymptotic evaluation when  $|\gamma|$  is large, the integration path  $P$  is deformed into the steepest-descent path (SDP) through the appropriate saddle points. When  $|\delta| < 1$ , the SDP is defined by the requirement  $\text{Re} \cos(w - w_s) = 1$ , which yields the contour  $\hat{P}$  in Fig. 7.5.3(b).  $P$  can be deformed into  $\hat{P}$  by the addition of path segments  $P_1$  and (or)  $P_2$  around the branch-point singularities (the branch cuts have been drawn conveniently as shown) and at  $|w_i| = \infty$ . In view of the preceding discussion concerning the exponential decay of the integrand, no contribution accrues from the latter. Thus,<sup>11</sup>

$$H_{2r} = -\frac{i\omega\epsilon_0\sqrt{|\epsilon|}}{4\pi} [I + U(|\hat{w}| + \phi_s)I_1 + U(|\hat{w}| - \phi_s)I_2], \quad |\delta| < 1, \quad (24)$$

where

$$I = \int_{\hat{P}} F dw, \quad I_1 = \int_{P_1} F dw, \quad I_2 = \int_{P_2} F dw, \quad (24a)$$

with  $F$  representing the integrand in Eq. (22).  $U(x) = 1$ ,  $x > 0$ , and  $U(x) = 0$ ,  $x < 0$ .

When  $|\delta| > 1$ ,  $\gamma$  is imaginary and the saddle point  $w_s$  lies on the line  $w_r = \pi/2$  for  $\delta > 1$ , and  $w_r = -\pi/2$  for  $\delta < -1$ . The steepest-descent path for  $\delta > 1$  is defined by the equation  $\text{Im} \cos(w - w_s) = 0$ , which determines the line  $w_r = \pi/2$ . Since the integrand in Eq. (22) converges exponentially in the strip  $\sin w_r > 0$ , the contour  $P$  can be deformed into the path  $\hat{P}_1$  provided that the branch-cut integral over  $P_1$  is included. Thus, for  $\delta > 1$ ,

$$H_{2r} = -\frac{i\omega\epsilon_0\sqrt{|\epsilon|}}{4\pi} [\hat{I}_1 + I_1], \quad \hat{I}_1 = \int_{\hat{P}_1} F dw, \quad (25a)$$

while, from analogous considerations for  $\delta < -1$ ,

$$H_{2r} = -\frac{i\omega\epsilon_0\sqrt{|\epsilon|}}{4\pi} [\hat{I}_2 + I_2], \quad \hat{I}_2 = \int_{\hat{P}_2} F dw. \quad (25b)$$

### The geometric-optical field

The asymptotic evaluation of the steepest-descent path integral can now be carried out directly, and from the formula in Eq. (4.2.7), one obtains the lowest-order approximation,

$$H_{2r}|_{\text{SDP}} \sim -\frac{\omega\epsilon_0\sqrt{\epsilon}}{2\sqrt{2\pi}} \Gamma(k \sin w_s) \frac{e^{i(y-\pi/4)}}{\sqrt{\gamma}} + O(\gamma^{-3/2}), \quad (26)$$

valid for positive or negative  $\epsilon$ ; if  $\gamma$  is imaginary, one takes  $\gamma = i|\gamma|$ . This contribution is subsequently interpreted as the geometric-optical part of the reflected field, and with the asymptotic approximation of the primary field in Eq. (7.3.38a), the total geometric-optical field  $H_{2g}$  in the plasma half-space may be written as

$$H_{2g} \sim -\frac{\omega\epsilon_0\sqrt{\epsilon}e^{-in/4}}{2\sqrt{2\pi}} \left\{ \frac{e^{ix}}{\sqrt{\chi}} \left[ 1 + O\left(\frac{1}{\chi}\right) \right] + \Gamma(k \sin w_s) \frac{e^{iy}}{\sqrt{\gamma}} \left[ 1 + O\left(\frac{1}{\gamma}\right) \right] \right\}, \quad (27)$$

valid when  $|\chi|$  and  $|\gamma|$  are large. The higher-order terms, not shown explicitly, may be evaluated by the procedure in Sec. 4.2. Here

$$\chi = k_0 R N(\varphi), \quad N(\varphi) = \sqrt{\cos^2(\varphi - \alpha) + \epsilon \sin^2(\varphi - \alpha)}, \quad (27a)$$

while alternative expressions for  $\gamma$  are

$$\begin{aligned} \gamma &= \frac{k_0}{\sqrt{A_2}} |u + u'| \sqrt{1 + \tan^2 w_s} \\ &= k_0 \sqrt{\epsilon A_2} \left\{ \frac{|u + u'|^2}{\epsilon A_2^2} + \left[ (v - v') - \frac{A_3}{2A_2}(u - u') \right]^2 \right\}^{1/2} = L_1 + L_2, \end{aligned} \quad (27b)$$

$$L_1 = k_0 R_1 N(\varphi_1) = \beta_s \bar{v} + q_1(\beta_s) |u'|, \quad (27c)$$

$$L_2 = k_0 R_2 N(\varphi_2) = \beta_s (v - \bar{v}) - q_2(\beta_s) |u|. \quad (27d)$$

$R$  is the distance from the source to the observation point,  $\varphi$  is the angle between  $R$  and the positive  $u$  axis, and  $N(\varphi)$  is the ray refractive index [see Eq. (7.3.37), where  $\varphi$  is measured from the  $z$  axis].  $L_1$  represents the phase change along a ray  $\bar{S}_1$  which leaves the source at an angle  $\varphi_1$  and travels the distance  $R_1$  to the interface, while  $L_2$  is the phase change along a reflected ray  $\bar{S}_2$  which travels the distance  $R_2$  from the interface to the observation point  $P$ , with an inclination specified by the angle  $\varphi_2$  (see Fig. 7.5.4).

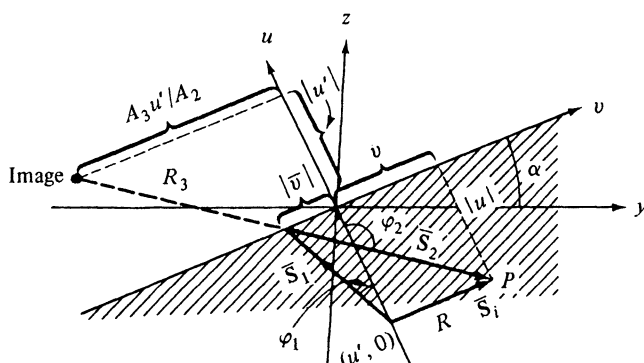


FIG. 7.5.4 Physical interpretation of far fields in the plasma ( $\epsilon > 0$ ): geometrical-optical contribution.

When  $\epsilon < 0$ , both the primary and reflected fields are confined to illuminated regions in which  $\chi$  and  $\gamma$ , respectively, are real; the disposition of these regions is the same as in the problem of reflection from an infinite, perfectly conducting plane (Fig. 7.4.3). Equation (27) fails in the vicinity of the incident or reflected field shadow boundaries on which  $\chi$  or  $\gamma$  vanishes. The transition through the former is accomplished via the exact expression in Eq. (7.3.38a). Since the major contribution to the reflected field integral in the vicinity of its shadow boundary arises from a saddle point at very large distance from the origin, and since  $\Gamma(k \sin w)$  is a well-behaved function which may be approximated by  $\Gamma(k \sin w_s)$  and removed from the integrand in Eq. (22), the remaining integral may be evaluated exactly in terms of  $H_0^{(1)}(\gamma)$ . This latter expression may be employed in the transition region where  $\gamma \rightarrow 0$  and exhibits a singularity similar to that in the primary field.

Since  $\varphi_1$  and  $\varphi_2$  are precisely the angles required to satisfy the reflection law in Eq. (9b), the asymptotic field solution has a simple physical interpretation: the field energy leaves the source along radial rays that, many wavelengths away from the source, behave locally like plane waves. These incident rays are reflected at the interface, the amplitude and direction of the emerging ray being the same as for the corresponding plane wave. The ray amplitudes decay in accord with the divergence coefficients  $|\chi|^{-1/2}$  or  $|\gamma|^{-1/2}$  that are also explained in terms of the energy conserved in a ray tube (see Sec. 1.6b), and the factor outside the braces in Eq. (27) has to do with the normalization of the primary field. Thus, the first-order asymptotic solution confirms the predictions of geometric-optical "ray tracing" in an anisotropic medium. To substantiate this interpretation, it is convenient to return to Eqs. (12) and to examine the saddle-point condition for the reflected field in the  $\beta$  plane. If  $v' = 0$  for simplicity, the pertinent exponential function is  $\exp[i\beta v + iq_2 u - iq_1 u']$ , and the saddle points  $\beta_s$  are defined by

$$-\frac{dq_2}{d\beta} + \frac{dq_1}{d\beta} \frac{|u'|}{|u|} + \frac{v}{|u|} = 0, \quad \beta = \beta_s. \quad (28)$$

In view of relation (9a) between the ray angle and the derivative of  $q$ , one may write, instead of Eq. (28),

$$\tan \varphi_2 - \frac{|u'|}{|u|} \tan \varphi_1 + \frac{v}{|u|} = 0, \quad (29)$$

where

$$\tan \varphi_1 = -\left. \frac{dq_1}{d\beta} \right|_{\beta_s}, \quad \tan \varphi_2 = -\left. \frac{dq_2}{d\beta} \right|_{\beta_s}. \quad (29a)$$

Equation (29) may be interpreted graphically as in Fig. 7.5.4, with  $\tan \varphi_1 = \bar{v}/|u|$ ,  $\tan \varphi_2 = -(v - \bar{v})/|u|$ . Since  $\beta$  remains fixed at  $\beta_s$ , Eq. (29a) is evidently equivalent to Eq. (9b). Thus, the saddle-point condition (28) selects that value of  $\beta_s$  for which the incident and reflected ray directions are such that the reflected ray  $\bar{S}_2$  passes through the observation point  $P$ . The phase variation of

the reflected field corresponding to the saddle point  $\beta_s$ ,  $\gamma = \beta_s v + q_1(\beta_s)|u'| - q_2(\beta_s)|u|$ , is equivalent to Eq. (27b).

It is of interest to observe that the image construction for the reflected field, rigorously applicable when reflection takes place from a perfect conductor (Sec. 7.4c), is also valid for the asymptotic field solution in Eq. (27). For verification, it suffices to show that the phase path  $L_1$  from the source to the interface along  $R_1$  in Fig. 7.5.4 is the same as the phase path  $L'_1$  from the image to the interface along  $R_3$ , provided that the anisotropic medium fills all of space. Now,  $L_1$  is given in Eq. (27c), while

$$L'_1 = \beta_s \left( \frac{A_3}{A_2} u' + \bar{v} \right) - q_2(\beta_s)|u'| = k_0 R_3 N(\phi_2). \quad (30)$$

But since  $q_1 + q_2 = -\beta A_3/A_2$  [see Eq. (5)], one confirms easily that  $L'_1 = L_1$ . In view of the image construction, the region illuminated by the reflected field, and the extent of the shadow region, may also be inferred as in Fig. 7.4.3 when  $\epsilon < 0$ . The reader may verify that the directions of incident-reflected ray pairs described analytically in Eq. (29) may also be inferred from the wave-number surfaces in Fig. 7.5.2.

#### *The lateral waves*

The branch-cut integrals  $I_1$  and  $I_2$  in Eqs. (24) and (25) yield field contributions that can be identified as lateral waves. When  $1 > \epsilon > 0$ , the branch points  $\hat{w} = \pm \sin^{-1}(1/\sqrt{\epsilon A_2}) = \pm \sin^{-1}(1/\sqrt{\sin^2 \alpha + \epsilon \cos^2 \alpha})$  are complex and unless both the source and observation points lie on the interface, the resulting branch-cut integral is exponentially small, as in the analogous isotropic problem discussed in Sec. 5.5e. When  $\epsilon < 0$ , however, the branch points lie on the imaginary axis in Fig. 7.5.3(b) where the exponential term in the integrand of Eq. (22) is undamped, and their contribution to the field in the plasma half-space may be important. In fact, the branch-cut integral contributions are found to be dominant in the shadow regions wherein both  $\chi$  and  $\gamma$  in Eq. (27) are imaginary; their role is more significant here than in the analogous isotropic case (Fig. 5.5.2), where the geometric-optical fields are always stronger (it is recalled that the branch-cut integral is  $O[(\text{distance})^{-3/2}]$ ; however, when losses are present, the geometric-optical fields are exponentially damped and may then be smaller than the lateral-wave fields). Thus, the branch-cut integrals for  $\epsilon < 0$  merit detailed investigation. Their subsequent physical interpretation in terms of lateral waves exhibits features quite different from those encountered in the isotropic problem.<sup>11</sup>

The asymptotic evaluation of the branch-cut integral  $I_1$  in Eq. (24a) may be carried out exactly as in Eqs. (5.5.17)–(5.5.22) provided that the saddle point does not lie near the branch point (i.e.,  $-\phi_s \not\approx |\hat{w}|$ ). For  $|\delta| < 1$ , one introduces the change of variable

$$\cos(w - w_s) = \cos(w + \hat{w}) + is^2, \quad -\infty < s < \infty, \quad (31)$$

where  $P_1$  in Fig. 7.5.3(b) denotes the resulting path on which  $s$  is real and in-

creases from  $-\infty$  to  $+\infty$  along the direction indicated by the arrow. Near  $s = 0$ , from which region the major contribution to the integral originates when  $\gamma \gg 1$ ,

$$\frac{dw}{ds} = \frac{2s}{\sinh(\phi_s + |\hat{w}|)} + O(s^3), \quad (32a)$$

$$s \cong \sqrt{\sinh(\phi_s + |\hat{w}|)} \sqrt{w + \hat{w}}, \quad 0 < \arg(w + \hat{w}) < 2\pi, \quad (32b)$$

$$\Gamma(k \sin w) = 1 + \frac{2e^{-in/4}}{\cosh|\hat{w}|} \sqrt{\frac{|\epsilon| \sinh 2|\hat{w}|}{\sinh(\phi_s + |\hat{w}|)}} s + O(s^2). \quad (32c)$$

The integral can then be written as

$$I_1 = e^{iy \cosh(\phi_s + |\hat{w}|)} \int_{-\infty}^{\infty} \left( \frac{dw}{ds} \Gamma \right) e^{-rs^2} ds, \quad (33)$$

and the lowest-order term in the asymptotic approximation for large  $\gamma$  arises from the  $s^2$  term in the power-series expansion of  $\Gamma dw/ds$ . The resulting formula is [see Eq. (4.2.17)]

$$I_1 \sim \frac{2\sqrt{\pi} e^{-in/4} e^{iy \cosh(\phi_s + |\hat{w}|)}}{\cosh|\hat{w}| [\gamma \sinh(\phi_s + |\hat{w}|)]^{3/2}} \sqrt{|\epsilon| \sinh 2|\hat{w}|} + O(\gamma^{-5/2}), \quad (34)$$

and the analogous result for  $I_2$  is the same except for the replacement of  $\phi_s$  by  $-\phi_s$ . With  $w_s = i \tanh^{-1} \delta$ , these expressions may be shown to apply as well when  $|\delta| > 1$ .

For subsequent interpretation,<sup>11</sup> it is useful to employ alternative expressions that are derived most simply in terms of the original  $\beta$  variable. Since the branch points at  $w = \pm i|\hat{w}|$  correspond to  $\beta = \pm k_0$ , one finds that, for  $v' = 0$ ,

$$\gamma \cosh(|\hat{w}| \pm \phi_s) = \pm k_0 v + q_1(\pm k_0)|u'| - q_2(\pm k_0)|u|; \quad (35)$$

it may also be shown that

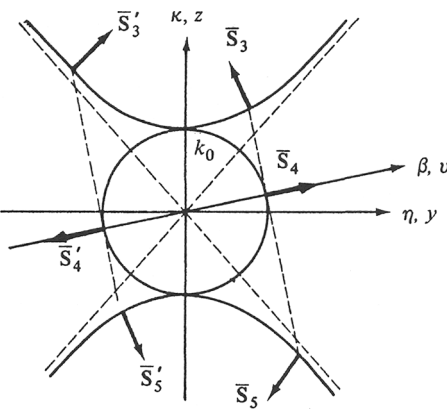
$$\frac{|u + u'|}{\cosh \phi_s} \sinh(|\hat{w}| \pm \phi_s) = \pm \sqrt{|\epsilon| A_2} \cosh |\hat{w}| \left[ v - |u| \left. \frac{dq_2}{d\beta} \right|_{\pm k_0} + |u'| \left. \frac{dq_1}{d\beta} \right|_{\pm k_0} \right]. \quad (36)$$

In each of these branch-cut contributions, the transverse wavenumber  $\beta$  remains *fixed* at  $+k_0$  or at  $-k_0$ , and the various phase increments for different observation points are therefore not achieved by varying the ray directions as in the geometric-optical field. Because  $\beta = \pm k_0$  corresponds to a ray that travels parallel to the interface in the vacuum region, the phenomenon of critical refraction may be expected to play a role. It is suggestive to define phase increments along the critically refracted ray paths and so let

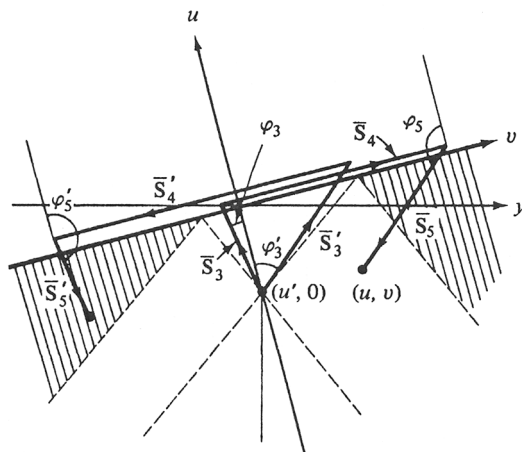
$$L_3(k_0) \equiv L_3 = [k_0 \tan \varphi_3 + q_1(k_0)]|u'|, \quad \tan \varphi_3 = -\left. \frac{dq_1}{d\beta} \right|_{k_0}, \quad (37a)$$

$$L_4(k_0) \equiv L_4 = k_0(v - |u'| \tan \varphi_3 + |u| \tan \varphi_5), \quad \tan \varphi_5 = -\left. \frac{dq_2}{d\beta} \right|_{k_0}, \quad (37b)$$

$$L_5(k_0) \equiv L_5 = -[k_0 \tan \varphi_5 + q_2(k_0)]|u|. \quad (37c)$$



(a) Dispersion curves



(b) Ray paths

FIG. 7.5.5 Lateral rays ( $\epsilon < 0$ ).

$L_3$  is the phase change along ray  $\bar{S}_3$  in Fig. 7.5.5(b) which travels from the source to the interface at the first critical angle  $\varphi_3$  [see Eq. (27c), with  $\beta_s = k_0$ ],  $L_4$  is the phase change along ray  $\bar{S}_4$  which travels in the *vacuum* region parallel to the interface, and  $L_5$  is the phase change along ray  $\bar{S}_5$  which travels from the interface to the observation point  $(u, v)$  in the plasma at the second critical angle  $\varphi_5$  [see Eq. (27d), with  $\beta_s = k_0$  and  $\bar{v}$  equal to the value of  $v$  at the starting point of  $\bar{S}_5$ ]. The directions of  $\bar{S}_3$ ,  $\bar{S}_4$ , and  $\bar{S}_5$  may also be inferred from the wavenumber diagram in Fig. 7.5.5(a); note the backward refraction since  $\epsilon < 0$ .

Along the ray path  $(L_3 + L_4 + L_5)$ , it is possible to reach different observation points by changing the length, but not the direction, of  $L_4$  or  $L_5$ , and keeping  $L_3$  fixed. The entire trajectory then corresponds to the constant value  $\beta_s = k_0$  as required, and defines a “lateral wave” on an anisotropic interface (see Fig. 5.5.2 for the isotropic case).

With these definitions, the branch-cut integral contributions  $H_{2b}$  to the reflected field in the plasma half-space may be written as

$$H_{2b} \sim -\frac{\omega\epsilon_0 e^{i\pi/4}}{\sqrt{2\pi}} \left( \frac{|\epsilon|}{1+|\epsilon|A_2} \right) \left[ \frac{e^{i(L_3+L_4+L_5)}}{L_4^{3/2}} U(L_4) + \frac{e^{i(L'_4+L'_5+L'_6)}}{L'_4^{3/2}} U(L'_4) \right], \quad (38)$$

where  $U(x)$  is the Heaviside unit function, and

$$L'_3 = L_3(-k_0), \quad L'_4 = L_4(-k_0), \quad L'_5 = L_5(-k_0), \quad (38a)$$

are the phase increments along the lateral ray path corresponding to  $\beta_s = -k_0$ . Thus, the branch-cut integrals may be interpreted as representing the fields along lateral rays that propagate parallel to the interface in the vacuum region, are excited by a ray incident at the critical angle, and shed energy back into the plasma by refraction. In contrast to lateral waves on an isotropic interface, it is observed that backward refraction obtains, as a result of which a certain range of observation points may be reached by two lateral rays. Moreover, the lateral rays penetrate the shadow zone, one ray for each of the areas shown shaded in Fig. 7.5.5(b), thereby providing a means of transferring energy into an otherwise inaccessible region; in this zone, the geometric optical field  $H_{2g}$  in Eq. (27) is exponentially small. The magnitude of the lateral ray field varies like  $L_4^{-3/2}$  or  $L'_4^{-3/2}$ , and for distant observation points in the illuminated region, this decay with distance is stronger than that of the geometric optical field. An exception occurs near the angles of total reflection defined by  $L_4 = 0$  or  $L'_4 = 0$ . In their vicinity, Eq. (38) becomes invalid and must be replaced by the more precise formula in Eq. (45), which permits the field calculation in or near this transition region.

#### *Fields in the vicinity of the angle of total reflection*

For an asymptotic evaluation of the integral  $I_1$  in the vicinity of the angle of total reflection where  $\phi_s \rightarrow -|\hat{w}|$ , the change of variable introduced in Eq. (31) is inappropriate since  $dw/ds$  in Eq. (32a) is then not slowly varying near  $s = 0$ . The difficulty arises since the branch point is located near the saddle point. It is convenient to employ as a new variable the function<sup>†</sup>

$$\tau = \sqrt{1 + \frac{\sin^2 w}{\sinh^2 |\hat{w}|}}, \quad \sinh |\hat{w}| = \frac{1}{\sqrt{|\epsilon|A_2}}, \quad \epsilon < 0, \quad (39)$$

so the branch point  $w = -\hat{w}$  maps into  $\tau = 0$ . The mapping derivative,

$$\frac{dw}{d\tau} = \frac{\tau}{(\sin w \cos w)|\epsilon|A_2}, \quad (40)$$

<sup>†</sup>The integration variable  $\tau$  here is not to be confused with the function  $\tau(s) = q(z)$  employed in Chapter 4.

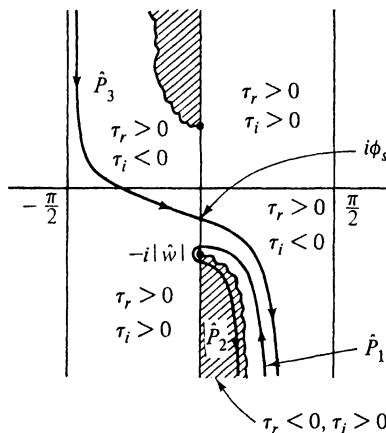
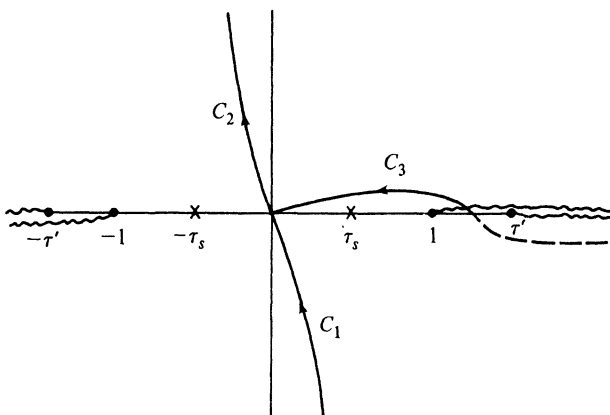
is now well behaved near  $\tau = 0$ , and, for  $w \approx -i|\hat{w}|$ ,

$$\begin{aligned}\cos w &= \cosh |\hat{w}| \sqrt{1 - \frac{\tau^2}{1 + |\epsilon|A_2}} \\ &\approx \cosh |\hat{w}| \left[ 1 - \frac{\tau^2}{2(1 + |\epsilon|A_2)} - \frac{\tau^4}{8(1 + |\epsilon|A_2)^2} - \dots \right],\end{aligned}\quad (41a)$$

$$\sin w = -i(\sinh |\hat{w}|) \sqrt{1 - \tau^2} \approx -i \sinh |\hat{w}| \left( 1 - \frac{\tau^2}{2} - \frac{\tau^4}{8} - \dots \right), \quad (41b)$$

$$\frac{dw}{d\tau} \Gamma = i \left( 1 - \frac{2\tau}{\sqrt{A_2} \cosh |\hat{w}|} \right) \tau \tanh |\hat{w}| + O(\tau^3), \quad (41c)$$

with the square roots defined to be positive when the radicands are positive.

(a)  $w$  plane(b)  $\tau$  plane**FIG. 7.5.6** Contours and singularities in the  $w$  and  $\tau$  planes.

The behavior of  $\tau_r = \operatorname{Re} \tau$  and  $\tau_i = \operatorname{Im} \tau$  in the various sections of the complex  $w$  plane is shown in Fig. 7.5.6(a), whence one infers that the path  $\hat{P}_1 + \hat{P}_2$  maps into the contour  $C_1 + C_2$  in Fig. 7.5.6(b). Since

$$\cos(w - w_s) = \sinh|\hat{w}| (\cosh \phi_s \sqrt{1 + |\epsilon| A_2 - \tau^2} + \sinh \phi_s \sqrt{1 - \tau^2}), \quad (42)$$

the integrand of  $I_1$  in Eq. (24a) has saddle points at

$$\tau = 0, \pm \tau_s, \quad \text{with } \tau_s = \sqrt{1 - (\sinh \phi_s / \sinh |\hat{w}|)^2} \geq 0, \quad (43)$$

so there exists on the real  $\tau$  axis a confluence of three equally spaced, first-order saddle points as  $\phi_s \rightarrow -|\hat{w}|$ . The integrand, which decays away from  $\tau = 0$  along  $C_{1,2}$ , also possesses branch points at  $\tau = \pm 1$  and  $\pm \tau' = \pm \coth |\hat{w}|$  [see Fig. 7.5.6(b)] which are, however, far removed from the saddle-point region  $\tau \approx 0$ . The problem of performing an integration when a saddle point and a branch point tend to coalesce has thus been transformed into one of integration in the presence of three adjacent saddle points (see Sec. 4.4c). With the indicated choice of branch cuts,  $\sqrt{1 - \tau^2}$  and  $\sqrt{\coth^2 |\hat{w}| - \tau^2}$  have positive real parts on the entire top sheet of the four-sheeted Riemann surface, and positive (negative) imaginary parts in the second and fourth (first and third) quadrants.

For large  $\gamma$ , the dominant contribution to the integral  $I_1$  arises from the vicinity of  $\tau = 0$ , and since the saddle-point configuration is similar to the one occurring in the integral representation for the parabolic cylinder function,  $I_1$  may be approximated in terms of this function (for related problems in isotropic media, see Reference 12). The required analysis has been presented in Sec. 4.5b, and in terms of the notation employed there,  $\tau \rightarrow z$ ,  $\Omega = \gamma$ ,  $q(\tau) = i \cos(w - w_s)$ . Since the integration path  $C_1 + C_2$  is symmetrical with respect to  $\tau = 0$ , and  $\Gamma dw/d\tau \sim \tau$  as  $\tau \rightarrow 0$  [see Eq. (41c)], the lowest-order contribution arises from the  $\tau^2$  term in the power-series expansion of  $\Gamma dw/d\tau$ , and the corresponding parabolic cylinder function is of order  $-\frac{3}{2}$ . From Eqs. (42) and (43),

$$q(\tau_s) - q(0) = -2i \sinh^2 \left( \frac{\phi_s + |\hat{w}|}{2} \right), \quad (44a)$$

$$q(\tau_s) + q(0) = 2i \cosh^2 \left( \frac{\phi_s + |\hat{w}|}{2} \right), \quad (44b)$$

so, from an application of Eq. (4.5.44)<sup>11</sup>,

$$I_1 \sim \overset{\circ}{I}_1 e^{-i3\pi/8 - i\zeta^{3/4}} \zeta^{3/2} D_{-3/2}(\zeta e^{-i\pi/4}), \quad \zeta = 2\sqrt{\gamma} \sinh \left( \frac{\phi_s + |\hat{w}|}{2} \right) \geq 0, \quad (45)$$

where  $\overset{\circ}{I}_1$  is the simple asymptotic formula in Eq. (34). The terms multiplying  $\overset{\circ}{I}_1$  provide a correction that approaches unity when  $\zeta \gg 1$  [see Eq. (66a)], and compensate for the singularity in  $\overset{\circ}{I}_1$  when  $\zeta \rightarrow 0$ . Because  $\gamma$  is assumed to be

large, it is possible to have  $\zeta \gg 1$ , although  $\phi_s + |\hat{w}|$  is small; thus, Eq. (45) is required only when  $\phi_s + |\hat{w}| = O(\gamma^{-1/2})$ , and Eq. (34) suffices for larger values of  $\phi_s + |\hat{w}|$ . On the boundary confining the domain of existence of the totally reflected waves,  $\zeta = 0$ , and use of the formula for  $D_{-3/2}(0)$  [Eq. (4.5.41)] yields the result

$$I_1 \sim \left( \frac{2}{\gamma} \right)^{3/4} \frac{4\pi\sqrt{|\epsilon|} \tanh |\hat{w}| e^{-i5\pi/8} e^{i\gamma}}{\Gamma(\frac{1}{4})}. \quad (46)$$

No confusion should arise between the gamma function  $\Gamma(\frac{1}{4})$  and the same symbol  $\Gamma$  employed elsewhere for the reflection coefficient. The distance dependence in the branch-cut integral contribution is seen to increase from  $\gamma^{-3/2}$  far from the angle of total reflection to  $\gamma^{-3/4}$  at this angle.

While the asymptotic evaluation of the integral  $I$ , in Eq. (24a), along the steepest-descent path  $\hat{P}$  yields a lowest-order contribution [Eq. (26)] that is not affected as  $\phi_s \rightarrow -|\hat{w}|$ , the higher-order terms are influenced by the proximity of the branch point near the saddle point. As  $\phi_s \rightarrow -|\hat{w}|$ , one has, with reference to Fig. 7.5.6,

$$I = \begin{cases} \left( \int_{\hat{P}_1} - \int_{\hat{P}_2} \right) F dw = \left( \int_{C_1} - \int_{C_2} \right) F \frac{dw}{d\tau} d\tau, & -\phi_s < |\hat{w}|, \\ \int_{\hat{P}_3 + \hat{P}_4} F dw = \int_{C_3 + C_4} F \frac{dw}{d\tau} d\tau, & -\phi_s > |\hat{w}|, \end{cases} \quad (47a)$$

$$(47b)$$

where  $F = \Gamma \exp[iy \cos(w - w_s)]$ . It is convenient to write  $\Gamma = 1 + (\Gamma - 1)$ , since the contribution from the first term can then be evaluated exactly in terms of the Hankel function. For the remaining term, follow the procedure above to express the integral over paths  $C_{1,2}$  in terms of  $D_{-3/2}[\zeta \exp(-i\pi/4)]$ ; the one over path  $C_3$  involves  $D_{-3/2}[-\zeta \exp(-i\pi/4)]$ . Thus,<sup>11</sup>

$$I = I' + I'' \quad (48)$$

$$I' = \int_{\hat{P}} e^{iy \cos(w - w_s)} dw \sim \sqrt{\frac{2\pi}{\gamma}} e^{i(y-\pi/4)} + O(\gamma^{-3/2}), \quad (48a)$$

$$\begin{aligned} I'' &= \int_{\hat{P}} (\Gamma - 1) e^{iy \cos(w - w_s)} dw \sim \frac{-iI_1}{2D_{-3/2}(\zeta e^{-i\pi/4})} \\ &\times [D_{-3/2}(-\zeta e^{-i\pi/4}) \mp iD_{-3/2}(\zeta e^{-i\pi/4})], \quad -\phi_s \leq |\hat{w}|, \end{aligned} \quad (48b)$$

with  $I_1$  given in Eq. (45).

Although  $I''$  is discontinuous across the total reflection boundary  $\phi_s = -|\hat{w}|$ , this is not true of the sum  $\bar{I} = I'' + I_1 U(|\hat{w}| + \phi_s)$  which occurs in Eq. (24). Via the relation

$$D_{1/2}(z) = 2^{-3/2} [e^{iz/4} D_{-3/2}(iz) + e^{-iz/4} D_{-3/2}(-iz)], \quad (49)$$

one may write

$$\bar{I} \sim \overset{\circ}{I}_1 e^{-i5\pi/8 - i\zeta^{3/4}} \zeta^{3/2} \sqrt{2} D_{1/2}(-\zeta e^{i\pi/4}), \quad (50)$$

which expression remains valid for  $-\phi_s \geq |\hat{w}|$ . For  $-\zeta \gg 1$ , Eq. (50) may be

reduced via the asymptotic formula in Eq. (66a), while for  $\zeta \gg 1$ , one uses Eq. (66b). When applied to the above expressions for  $\tilde{I} + I'$ , these asymptotic results reduce to those in Eqs. (27) and (38) in the vicinity of  $-\phi_s \approx |\hat{w}|$ .

### 7.5e Asymptotic Evaluation in the Vacuum Half-Space

#### *Ray interpretation of the saddle-point condition—caustic and cusp*

The field solution in the vacuum region  $u > 0$  is given in Eq. (11):

$$H_1 = -\frac{\omega\epsilon_0}{\pi} \int_{-\infty}^{\infty} F(\beta) e^{i\psi(\beta)} d\beta, \quad (51)$$

where

$$F(\beta) = \frac{1}{2q_0 - A_2(q_2 - q_1)}, \quad (51a)$$

and

$$\psi(\beta) = \beta(v - v') + q_0 u + q_1 |u'|. \quad (51b)$$

Instead of transforming to the  $w$  plane as before, it is preferable to carry out the present analysis in the  $\beta$  plane. Upon introducing a change of scale via  $\beta = k_0 \beta'$ , one may write  $\psi(\beta) = k_0 \hat{\psi}(\beta')$  and, if  $k_0$  is large, the integrand is in a form suitable for the application of asymptotic methods. The change to the variable  $\beta'$  will not be carried out but it will be kept in mind that  $\psi(\beta)$  contains a large parameter  $k_0$ . Thus, the stationary points  $\beta_s$ , obtained from  $d\psi/d\beta = 0$ , are expected to play an important role in the asymptotic approximation:

$$v = u \tan \varphi_0 + |u'| \tan \varphi_1, \quad \text{when } \beta = \beta_s, \quad (52)$$

where  $\tan \varphi_0 \equiv -dq_1/d\beta$  and  $\tan \varphi_1 \equiv -dq_0/d\beta = \beta(k_0^2 - \beta^2)^{-1/2}$ . The solution of the latter equation yields  $\beta_s = k_0 \sin \varphi_0$  and the associated value of  $\varphi_1$  is then inferred from Eq. (9b). Subsequent discussion is restricted to the espe-

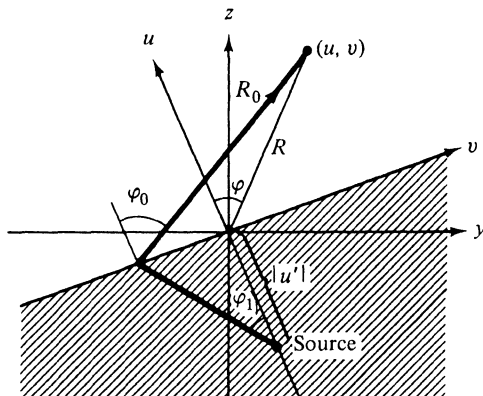


FIG. 7.5.7 Refracted ray when  $\epsilon < 0$ .

cially interesting case  $\epsilon < 0$ , with  $A_2 > 0$ . Also, for simplicity and without loss of generality,  $v'$  has been set equal to zero.

The important saddle points are those for which  $\psi(\beta_s)$  is real since the associated field contribution  $\sim \exp[i\psi(\beta_s)]$  is then undamped. These real solutions correspond to real values of  $\varphi_1$  and  $\varphi_0$ , which represent the angles of incidence and refraction, respectively, of a ray that emerges from the plasma into the vacuum region (see Sec. 7.5b). The equation of the refracted ray is precisely the one given in Eq. (52), and the pertinent ray picture is shown in Fig. 7.5.7. One observes from Eq. (9b) (with  $\epsilon < 0$  and  $A_2 > 0$ ) that  $\varphi_0$  and  $\varphi_1$  may have opposite signs, thereby resulting in backward refraction; an increase in  $\varphi_0$  causes  $\varphi_1$  to decrease (i.e.,  $|\varphi_1|$  increases since  $\varphi_1 < 0$  when  $\varphi_0 > 0$ ), thus leading to a crossing of successive rays. When  $\varphi_0 = \pm\pi/2$ , the corresponding values of  $\varphi_1$ , the angles of critical refraction, are the ones required to launch the lateral waves. It is shown below (see Fig. 7.5.8) that because of the occurrence of

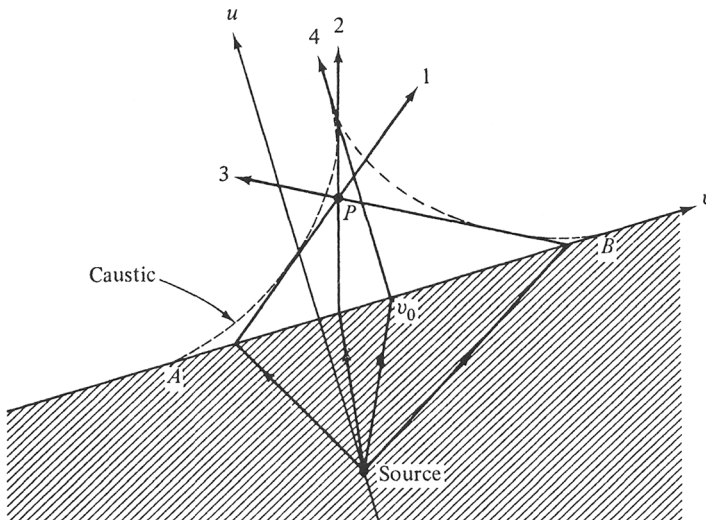


FIG. 7.5.8 Refracted ray configuration when  $\epsilon < 0$ .

backward refraction, a certain region in the vacuum half-space is reached by three propagating rays. This region is bounded by a caustic possessing a cusp at some distance above the interface. Thus, the *straight* interface on the *homogeneous* anisotropic half-space acts like an optical lens that focuses the fields radiated into the vacuum<sup>13</sup>—a phenomenon quite distinct from focusing in isotropic media where inhomogeneities or curved boundaries are required.

The real saddle-point solutions  $\beta_s = k_0 \sin \varphi_0$  of Eq. (52) are best visualized from a plot of the ray configuration shown in Fig. 7.5.8. One notes that an observation point  $P(u, v)$  near the interface may be reached by three rays (e.g., by 1, 2, and 3) but that more distant points are met by only a single ray. In the

former case, the two rays 1 and 2 are refracted on the same side of the normal ray 4 and have positive angles  $\varphi_{01}$  and  $\varphi_{02}$ , while ray 3 is refracted on the opposite side and has a negative angle  $\varphi_{03}$ . The picture is reversed when the observation point lies on the other side of the normal ray 4 whose equation is given by  $\varphi_0 = 0$ , or  $v_0 = |u'|A_3/2A_2$ . The ray configuration in the vacuum region but not in the plasma is, in fact, symmetrical about the line  $v = v_0$ . A caustic (ray envelope), whose shape is found to be a hypocycloid, separates the region of three ray crossings from the exterior region wherein the rays diverge. The contact points  $A$  and  $B$  between the caustic and the interface correspond to  $\varphi_0 = \pm\pi/2$  and are located at

$$v = v_0 \mp \frac{|u'|}{|\epsilon|A_2\sqrt{A_2 + 1/|\epsilon|}}, \quad v_0 = \frac{|u'|A_3}{2A_2}, \quad (53a)$$

the intercept of a ray with the line  $v = v_0$  is given by

$$u = \frac{|u'|\cos\varphi_0}{|\epsilon|A_2\sqrt{A_2 + (\sin^2\varphi_0)/|\epsilon|}},$$

and the cusp  $C$  corresponds to  $\varphi_0 = 0$ , whence

$$u = \frac{|u'|}{|\epsilon|A_2^{3/2}}, \quad v = v_0, \quad \text{at the cusp.} \quad (53b)$$

To determine the equation of the caustic, the parameter  $\varphi_0$  is eliminated between Eq. (52) and the derivative of Eq. (52) with respect to  $\varphi_0$ :

$$\frac{u}{|u'|} = \frac{\sqrt{|\epsilon|}\cos^3\varphi_0}{(|\epsilon|A_2 + \sin^2\varphi_0)^{3/2}}. \quad (54a)$$

After a bit of manipulation, one obtains for  $\varphi_0 > 0$  the equation of one branch of a hypocycloid,<sup>13</sup>

$$\frac{(v_0 - v)^{2/3}}{[a(A_2\sqrt{A_2 + 1/|\epsilon|})^{-1}]^{2/3}} + \frac{u^{2/3}}{A_2^{-1}a^{2/3}} = 1, \quad a = \frac{|u'|}{|\epsilon|}; \quad (54b)$$

for the other branch, corresponding to  $\varphi_0 < 0$ ,  $v_0 - v$  is replaced by  $v - v_0$ . It is evident that Eq. (54b) yields correctly the endpoints in Eqs. (53a) and (53b).

### *Asymptotic field evaluation*

In the evaluation of the integral in Eq. (51) by the saddle-point method, the path of integration is deformed into steepest-descent paths traversing the various contributing saddle points. The division of the complex  $\beta$  plane into “mountain” and “valley” regions in the vicinity of each saddle point depends on the second derivative of  $\psi(\beta)$ :

$$\psi''(\beta) = q_0''(\beta)u + q_1''(\beta)|u'|, \quad (55)$$

where

$$q_0'' = \frac{-k_0^2}{(k_0^2 - \beta^2)^{3/2}}, \quad q_1'' = \frac{k_0^2}{|\epsilon|(k_0^2 A_2 + \beta^2/|\epsilon|)^{3/2}}, \quad \beta = k_0 \sin \varphi_0. \quad (55a)$$

Since  $q_0''$  and  $q_1''$  have opposite signs in the important region  $|\beta| < k_0$ , where both quantities are real,  $\psi''(\beta)$  may be positive, negative, or zero. If one considers a ray with a specified angle of refraction,  $\varphi_0$ , then as the observation point moves along the ray,  $\psi''(\beta)$  is positive at the starting point  $u = 0$  since  $q_1''(\beta) > 0$ , but is negative at sufficiently large values of  $u$  where the  $q_0''u$  term dominates. The change in sign occurs at the point of tangency with the caustic where  $\psi''(\beta) = 0$ . An examination of the ray picture in Fig. 7.5.8 reveals that, of the three rays reaching a given observation point inside the caustic, two have touched the caustic but one has not, and that the angle  $\varphi_0$  for the latter is intermediate between the other two. Thus, at the three corresponding saddle points  $\beta_s = \beta_{1,2,3}$ , one has  $\psi''(\beta_1) < 0$ ,  $\psi''(\beta_2) > 0$ ,  $\psi''(\beta_3) < 0$ , while at the single real saddle-point exterior to the caustic,  $\psi''(\beta_s) < 0$ . The resulting steepest-descent paths in the vicinity of the saddle points then have the direction along the  $45^\circ$  lines shown in Fig. 7.5.9, and, on the remainder of the path,

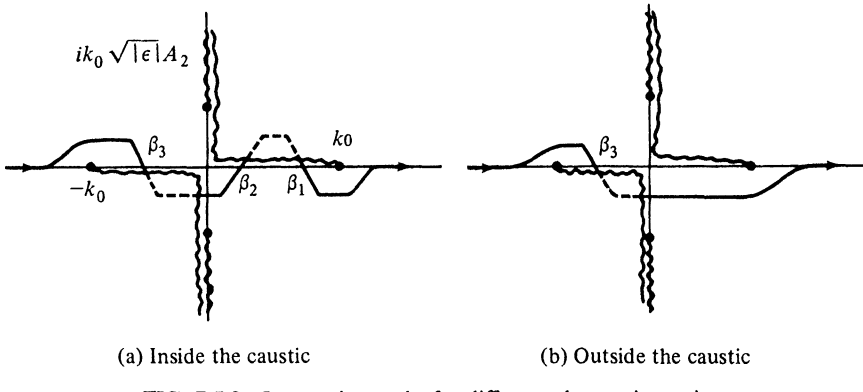


FIG. 7.5.9 Integration paths for different observation points.

the magnitude of the integrand in Eq. (51) may be shown to be exponentially smaller than at the saddle points. Consequently, the integral may be approximated in terms of the contributions arising from the vicinity of the saddle points only. The branch cuts associated with  $\beta = \pm k_0$  have been so chosen that  $\text{Im } q_0 > 0$  on the entire top sheet of the four-sheeted  $\beta$  plane. The branch cuts arising from  $q_1$  in Eq. (5) have been drawn so that  $\text{Re } \sqrt{\cdot} > 0$  on the top sheet.

Figure 7.5.9(a) pertains to an observation point  $P$  as shown in Fig. 7.5.8, while Fig. 7.5.9(b) is relevant when the observation point lies along ray 3 but outside the caustic. If the observer moves along ray 3 (i.e.,  $\beta_3$  is fixed), then  $\beta_1$  and  $\beta_2$  approach one another and coalesce into a double saddle point on the caustic; exterior to the caustic, the saddle points  $\beta_1$  and  $\beta_2$  are complex and the dominant contribution to the integral arises from the vicinity of  $\beta_3$  alone. While the explicit solution of Eq. (52) for the saddle points  $\beta_s$  is somewhat involved when  $u$  and  $v$  are arbitrary, it is easily obtained when the observation

point lies along the normal ray  $v = v_0$ . In this instance,

$$\beta_2 = 0, \quad \beta_1 = -\beta_3 = k_0 \left( \frac{1 - A_2 b^2}{1 + b^2/|\epsilon|} \right)^{1/2}, \quad b = \frac{u|\epsilon|A_2}{|u'|}, \quad (56)$$

and one observes that  $\beta_1$  and  $\beta_3$  are imaginary when  $u > \hat{u}$ , where  $\hat{u} = |u'|[|\epsilon|A_2^{3/2}]^{-1}$  is the ordinate at the cusp. Since  $\beta_1 = \beta_2 = \beta_3 = 0$  at the cusp, one has  $\psi'(0) = \psi''(0) = \psi'''(0) = 0$ , so a third-order saddle-point evaluation is required for the asymptotic approximation.

The asymptotic formulas for the magnetic field in Eq. (51) may now be written down directly.<sup>13</sup> By the ordinary saddle-point procedure [Eq. (4.2.1b)], one obtains for observation points inside the caustic,

$$H \sim -\omega\epsilon_0 \sqrt{\frac{2}{\pi}} \sum_{i=1}^3 \frac{F(\beta_i)}{\sqrt{|\psi'''(\beta_i)|}} e^{i\psi(\beta_i) + i(\pi/4) \operatorname{sgn} \psi''(\beta_i)}, \quad (57)$$

while outside the caustic,

$$H \sim -\omega\epsilon_0 \sqrt{\frac{2}{\pi}} \frac{F(\beta_s)}{\sqrt{|\psi'''(\beta_s)|}} e^{i\psi(\beta_s) - i\pi/4}, \quad (58)$$

where  $\beta_s = k_0 \sin \varphi_0$ . Near the caustic,  $\beta_1 \approx \beta_2$  or  $\beta_3 \approx \beta_2$ , and the required formula must account explicitly for the proximity of two saddle points. When  $\beta_1 \approx \beta_2$  [see Eq. (4.5.7)]

$$\begin{aligned} H \sim & -\omega\epsilon_0 \sqrt{\frac{2}{\pi}} \frac{F(\beta_3)}{\sqrt{|\psi'''(\beta_3)|}} e^{i\psi(\beta_3) - i\pi/4} \\ & - 2\omega\epsilon_0 \left[ \frac{2}{-\psi'''(\beta_0)} \right]^{1/3} e^{i[\psi(\beta_1) + \psi(\beta_2)]/2} \operatorname{Ai}(\xi) F(\beta_0), \end{aligned} \quad (59)$$

where  $\beta_0 = (\beta_1 + \beta_2)/2$ , with  $\psi''(\beta_0) = 0$ ,  $\operatorname{Ai}(\xi)$  is the Airy function

$$\operatorname{Ai}(\xi) = \frac{1}{2\pi i} \int_{\infty e^{-i2\pi/3}}^{\infty e^{i2\pi/3}} e^{\xi t - (t^{3/3})} dt, \quad \operatorname{Ai}(0) = \frac{1}{3^{2/3} \Gamma(\frac{2}{3})}, \quad (59a)$$

and

$$\xi = \left\{ -\frac{3}{4} i [\psi(\beta_1) - \psi(\beta_2)] \right\}^{2/3}, \quad (59b)$$

with

$$\xi = |\xi| e^{+i\pi}, \quad \text{when } \psi(\beta_1) - \psi(\beta_2) > 0. \quad (59c)$$

The last relation specifies the choice of the cube root. When  $-\xi \gg 1$ , one may employ the asymptotic formula in Eq. (4.2.51),

$$\operatorname{Ai}(\xi) \sim \frac{e^{-i\pi/4}}{2\sqrt{\pi(-\xi)^{1/4}}} [e^{i(2/3)(-\xi)^{3/2}} + ie^{-i(2/3)(-\xi)^{3/2}}], \quad (60)$$

to simplify the second expression in Eq. (59). With the relations

$$-\xi \approx \frac{1}{4} \left[ -\frac{\psi'''(\beta_0)}{2} \right]^{2/3} (\beta_1 - \beta_2)^2, \quad \psi'(\beta_0) \approx \left[ -\frac{\psi'''(\beta_0)}{8} \right] (\beta_1 - \beta_2)^2, \quad (61a)$$

and

$$i \left[ -\frac{\psi'''(\beta_0)}{2} \right]^{-1/3} \approx \left[ \frac{-2\xi^{1/2}}{i|\psi''(\beta_{1,2})|} \right]^{1/2}, \quad (61b)$$

the large- $\xi$  approximation of Eq. (59) reduces to Eq. (57), thereby permitting the smooth calculation of  $H$  as the observation point approaches the left branch of the caustic. Analogous considerations apply to the other branch. It is implied in these formulas that the region of overlap between Eqs. (57) and (59) occurs when  $\beta_1 \approx \beta_2 \approx \beta_0$ , so  $F(\beta_1) \approx F(\beta_2) \approx F(\beta_0)$  and  $\psi'''(\beta_1) \approx \psi'''(\beta_2) \approx \psi'''(\beta_0) < 0$ . From Eq. (61a), this restriction is compatible with the requirement  $-\xi \gg 1$  provided that  $-\psi'''(\beta_0) \gg 1$  (i.e., the wavenumber  $k_0$  or the coordinates  $u$  and  $|u'|$  must be sufficiently large). For a uniform approximation not subject to  $\beta_1 \approx \beta_2 \approx \beta_0$ , one employs the more general result in Eq. (4.5.2).

The transition through a point on the left branch of the caustic for which  $\psi'(\beta_0) = \psi''(\beta_0) = 0$  is followed most directly if the observation point approaches along the line

$$u = |u'| \frac{q_1''(\beta_0)}{-q_0''(\beta_0)}, \quad (62)$$

on which  $\psi''(\beta_0) = 0$  [see Eq. (55)]. On this line,  $\psi'(\beta_0) = v + q_0'(\beta_0)u + q_1'(\beta_0)|u'|$  is positive when the observation point lies to the right of the caustic,  $\psi'(\beta_0) = 0$  on the caustic, and  $\psi'(\beta_0) < 0$  after the observation point has passed through the caustic. From Eq. (61a),  $(\beta_1 - \beta_2)^2 < 0$  when  $\psi'(\beta_0) < 0$ , so  $\xi$  is positive. For  $\xi \gg 1$ , the asymptotic approximation in Eq. (4.2.42a)

$$\text{Ai}(\xi) \sim \frac{1}{2\sqrt{\pi}\xi^{1/4}} e^{-(2/3)\xi^{3/2}}, \quad (63)$$

shows that the field decays exponentially on the “dark” side of the caustic, so the resulting contribution is negligible. Thus, Eq. (59) reduces correctly to Eq. (58) since, by the same considerations as above, one may find an overlapping region for these formulas.

The simplest description of the field near the cusp is obtained when the observation point approaches along the line  $v = v_0$ . From Eq. (56), the saddle points  $\beta_1$  and  $\beta_3$  are then located symmetrically with respect to  $\beta_2 = 0$ , either on the real or on the imaginary axis. For real  $\beta_{1,3}$ , the integration path proceeds as in Fig. 7.5.9(a) and the three saddle points contribute, while for imaginary  $\beta_{1,3}$ , only the saddle point  $\beta_2 = 0$  is significant and the path is similar to the one in Fig. 7.5.9(b), with  $\beta_3$  replaced by  $\beta_2$  at the origin. When  $u < \hat{u}$  and not near the cusp, the asymptotic field solution is the same as in Eq. (57), with rays 2 and 4 in Fig. 7.5.8 coincident. Since  $F(\beta)$ ,  $\psi(\beta)$ , and  $\psi''(\beta)$  are even functions of  $\beta$  on the line  $v = v_0$ , one may rewrite Eq. (57) as

$$H \sim -\omega\epsilon_0\sqrt{\frac{2}{\pi}} \left\{ \frac{F(0)}{\sqrt{\psi''(0)}} e^{i[\psi(0)+\pi/4]} + \frac{2F(\beta_1)}{\sqrt{|\psi''(\beta_1)|}} e^{i[\psi(\beta_1)-\pi/4]} \right\}, \quad u < \hat{u}, \quad v = v_0. \quad (64)$$

For  $u$  sufficiently larger than  $\hat{u}$ , Eq. (58) applies with  $\beta_s = 0$  whence the field

along the ray  $v = v_0$  experiences a phase retardation of  $90^\circ$  upon passing through the cusp at  $u = \hat{u}$ . These formulas fail as  $u \rightarrow \hat{u}$  since  $\psi''(0) \rightarrow 0$ ,  $\psi'(0) = 0$  on  $v = v_0$  and  $\psi'''(0)$  vanishes identically so that the first non-vanishing derivative is  $\psi''''(0)$ . Hence, the cusp (focal) region is characterized by a coalescence of three saddle points.

The formula required for the detailed transition through the focal region is

$$H \sim \frac{i\omega\epsilon_0 e^{+i3\pi/8}}{-2^{1/4}\sqrt{\pi}} e^{i[\psi(0)+\psi(\beta_1)]/2} D_{-1/2}\left\{e^{-i(3\pi/4)}\sqrt{2[\psi(\beta_1) - \psi(0)]}\right\} \left[ \frac{24}{-\psi''''(0)} \right]^{1/4} F(0), \quad (65)$$

where  $D_{-1/2}(z)$  is the parabolic cylinder function of order  $-\frac{1}{2}$ ,  $[-\psi''''(0)]$  is positive, and  $\arg [\psi(\beta_1) - \psi(0)]$  equals zero or  $\pi$  when  $u < \hat{u}$  and  $u > \hat{u}$ , respectively. Use of the large-argument approximations,

$$D_{-v}(z) \sim \frac{e^{-z^2/4}}{z^v} \left[ 1 + O\left(\frac{1}{z^2}\right) \right], \quad |\arg z| < \frac{3\pi}{4}, \quad (66a)$$

$$D_{-v}(z) \sim \frac{e^{-z^2/4}}{z^v} - \frac{\sqrt{2\pi} e^{z^2/4+i\nu\pi}}{\Gamma(v) z^{1-v}} + O[z^{v-3}, z^{-(2+v)}], \quad -\frac{\pi}{4} > \arg z > -\frac{5\pi}{4}, \quad (66b)$$

reduces Eq. (65) to Eqs. (58) and (64), respectively, thereby permitting the complete transition through the cusp. In this reduction, the following approximate identities are helpful:

$$\psi''(\beta_1) \approx -2\psi''(0), \quad \left[ \frac{24}{-\psi''''(0)} \right]^{1/4} \approx -\frac{i2\sqrt{2}[\psi(\beta_1) - \psi(0)]^{1/4}}{\sqrt{\psi''(\beta_1)}}, \quad (67)$$

and it is assumed that the argument of the parabolic cylinder function may be large although  $\beta_1$  does not differ greatly from zero (i.e.,  $k_0$  or  $u$  and  $|u'|$  are large). One observes that the field far from the caustic behaves like  $|\psi''|^{-1/2}$ , near the caustic like  $|\psi'''|^{-1/3}$ , and near the cusp like  $|\psi''''|^{-1/4}$ . Since  $\psi$  contains a large parameter, these variations illustrate the successive field-strength enhancement as the observer approaches the caustic and the focal region.

The above-described focusing phenomena occur within a confined region near the interface and are not in evidence at great distances from the boundary. This follows from the ray picture in Fig. 7.5.8 which shows that observation points outside the caustic are reached by a single ray only; the corresponding far-field solution is given by the single term in Eq. (58). It may also be emphasized that analogous considerations are applicable for media with more general anisotropy (e.g., gyrotropic), in which the refractive index curves have a more complicated shape than that shown in Fig. 7.5.2 (see Sec. 8.3b). The transmitted field is generally given by integrals of the type shown in Eq. (51), but the functional dependence of the wavenumber  $q_1$  on  $\beta$  is then specified by a dispersion relation that is usually much more involved than the one in Eq. (4). Focusing effects may arise whenever  $\psi''(\beta) \rightarrow 0$  [see Eq. (55)] (i.e.,

when the real quantities  $q''_0$  and  $q''_1$  have opposite algebraic signs). The sign of  $q''$  is related to the curvature of the  $q(\beta)$  versus  $\beta$  curves, so an inspection of the refractive index plots reveals the possible existence, or not, of focal regions. From these considerations, focusing effects are absent when the uniaxially anisotropic half-space has a refractive index plot as in Fig. 7.5.2(a) since  $q''_0$  and  $q''_1$  then have the same algebraic sign.

### 7.5f Radiation from a Transverse Electric Dipole

The preceding sections have dealt with the radiation from a line source of magnetic current embedded in a uniaxially anisotropic plasma half-space. In view of the symmetries inherent in the physical structure for this special form of excitation, the electromagnetic field problem has been reducible to a single scalar boundary value problem, and a mathematical formulation has been possible in terms of  $E$  modes only. Since the plasma medium generally has a different effect upon the  $E$  and  $H$  modes, as noted from the two different refractive index diagrams in Figs. 7.1.1, it is instructive to treat a configuration in which both mode types must be considered.<sup>13</sup> A transversely directed dipole source belongs in this category, and incorporates, furthermore, certain three-dimensional aspects that are absent in the line-source excitation.

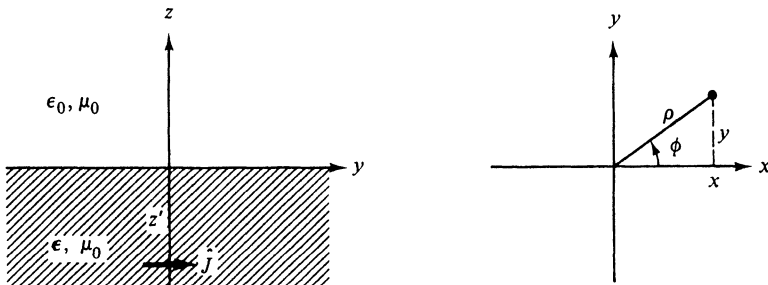


FIG. 7.5.10 Three-dimensional problem.

The physical arrangement is shown in Fig. 7.5.10, where the source distribution is taken as an electric current element oriented along the  $y$  direction,

$$\hat{\mathbf{J}}(\mathbf{r}, t) = y_0 \delta(\mathbf{r} - \mathbf{r}') e^{-i\omega t}, \quad \mathbf{r}' \equiv (x', y', z') = (0, 0, z'), \quad z' < 0. \quad (68)$$

To simplify the analysis, the interface is now assumed to be coincident with the  $z = 0$  plane, corresponding to  $\alpha = 0$  in Fig. 7.5.1. Alternative representations for the electromagnetic fields may be written down directly from the general results in Sec. 7.2. It is convenient to calculate first the voltage and current potentials  $V''(\mathbf{r})$  and  $I'(\mathbf{r})$  in Eqs. (7.2.13a) and (7.2.13b) and then to compute the fields via Eqs. (7.2.11a) and (7.2.11b). To utilize the symmetries inherent in excitation by a point source, it is convenient, as in the isotropic problem in Sec. 5.5b, to regard the infinite cross section transverse to  $z$  as a

cylindrical waveguide, with the scalar mode functions  $\Phi_i$  and  $\psi_i$  taken from Eqs. (3.2.78b). Since the dipole is located on the waveguide axis  $\rho' = 0$ , the resulting integral representations for the functions  $\nabla'_i \mathcal{S}'_d$  and  $\nabla'_i \mathcal{S}''_d$  may be simplified by considerations directly analogous to those employed in Sec. 5.5b, and one may easily derive the expressions for the potential functions. For the  $E$  modes,

$$I'(\mathbf{r}) = \frac{i}{4\pi} \sin \phi \frac{\partial}{\partial z'} \int_0^\infty J_1(\beta\rho) \frac{h(\beta)}{\kappa'_i} d\beta, \quad (69)$$

where

$$h(\beta) = \begin{cases} e^{i\kappa'_i|z-z'|} - \Gamma'(\beta)e^{-i\kappa'_i(z+z')}, & z < 0, \\ [1 - \Gamma'(\beta)]e^{-i\kappa'_i z} e^{i\kappa'_i z}, & z > 0, \end{cases} \quad (69a)$$

and

$$\Gamma'(\beta) = \frac{\kappa'_2 - \kappa'_1}{\kappa'_2 + \kappa'_1}, \quad \kappa'_1 = \sqrt{k_0^2 - \frac{\beta^2}{\epsilon}}, \quad \kappa'_2 = \sqrt{k_0^2 - \beta^2}, \quad \epsilon = \frac{\epsilon_z}{\epsilon_0}, \quad (69b)$$

with the square roots defined to be positive when real, and positive imaginary otherwise. The longitudinal dependence in Eq. (69a) is the same as in Eqs. (6a) and (6b) if one recalls that  $\alpha = 0$  in the present problem, so  $q_1 = \kappa'_1$ ,  $q_2 = -\kappa'_1$ ,  $q_0 = \kappa'_2$ ,  $u = z$ ,  $u' = z'$ . The modal network problem is the same as in Fig. 5.5.6, with the characteristic impedance and propagation constant taken from Eq. (7.2.8a).

For the  $H$  modes, the modal parameters  $\kappa''_i$  and  $Z''_i$  are identical inside and outside the plasma medium [see Eq. (7.2.8b), with  $\mu_i = \mu_z = \mu_0$ ,  $\epsilon_i = \epsilon_0$ ], so the corresponding network problem is the same as for an infinite vacuum. The potential function  $V''$  is then given by

$$V''(\mathbf{r}) = -\frac{\omega\mu}{4\pi} \cos \phi \int_0^\infty J_1(\beta\rho) \frac{e^{i\kappa''_i|z-z'|}}{\kappa''_i} d\beta, \quad \kappa''_i \equiv \kappa'_2, \quad (70)$$

which expression may be evaluated in closed form<sup>7</sup> via the formula [see Eq. (5.4.19) and the first term of Eq. (5.5.31)]

$$\int_0^\infty J_1(\beta\rho) \frac{e^{i\kappa''_i \zeta}}{\kappa''_i} d\beta = \frac{1}{k_0 \rho} [\exp(i k_0 |\zeta|) - \exp(i k_0 \sqrt{\rho^2 + \zeta^2})]. \quad (70a)$$

Such a simple reduction is not possible for the  $E$ -mode integral in Eq. (69). The different effect of the plasma medium on the  $E$ -mode and  $H$ -mode constituents is clearly evident since Eq. (70), in contrast to Eq. (69), shows no dependence on the boundary at  $z = 0$ .

The electromagnetic fields may now be determined from Eqs. (7.2.11a) and (7.2.11b). Some interesting differences between two-dimensional and three-dimensional field solutions, especially in the vicinity of caustics and cusps, may be ascertained from an asymptotic analysis in the vacuum half-space, with the choice  $\epsilon < 0$ . To simplify the discussion, we shall consider the magnetic field in the plane  $x = 0$  which then has only a single component,  $H \equiv H_x$ ; the field components at other points in space exhibit quite a similar behavior, modified

by the azimuthal variation  $\sin \phi$  or  $\cos \phi$ . In the plane  $x = 0$ , with  $z > 0$ , the  $E$ -mode contribution  $H'$  is found to be

$$H' = \frac{1}{2\pi} \int_0^\infty \frac{\kappa'_1}{\kappa'_1 + \kappa'_2} \frac{d}{d\rho} J_1(\beta\rho) e^{i(\kappa'_2 z + \kappa'_1 |z'|)} d\beta, \quad (71)$$

while the closed-form expression for the  $H$ -mode portion of the field is<sup>7</sup>

$$H'' = \frac{1}{4\pi y^2} \left[ e^{ik_0(z+|z'|)} - \frac{z+|z'|}{r} e^{ik_0 r} \right], \quad r = \sqrt{y^2 + (z+|z'|)^2}. \quad (72)$$

Since  $x = 0$ , one has  $\rho = \sqrt{x^2 + y^2} = y$ . The total magnetic field in the  $x = 0$  plane is given by  $H = H' + H''$ .

To facilitate an asymptotic evaluation of the integral in Eq. (71), it is convenient to separate observation points on the  $z$  axis ( $\rho = 0$ ) from those at large distances from this axis. For the former, use of

$$\frac{d}{d\rho} J_1(\beta\rho)|_{\rho=0} = \frac{\beta}{2}, \quad (73)$$

leads to

$$H' = \frac{1}{4\pi} \int_0^\infty \frac{\kappa'_1}{\kappa'_1 + \kappa'_2} \beta e^{i(\kappa'_2 z + \kappa'_1 |z'|)} d\beta, \quad \rho = 0, \quad (74)$$

while for the latter, an infinite integral representation is useful [see Eqs. (3.2.68) et seq.]:

$$H' = \frac{1}{4\pi} \frac{\partial}{\partial \rho} \int_{-\infty}^\infty \frac{\kappa'_1}{\kappa'_1 + \kappa'_2} H_1^{(1)}(\beta\rho) e^{i(\kappa'_2 z + \kappa'_1 |z'|)} d\beta. \quad (75)$$

In the last expression, the integration path is indented into the upper half of the complex  $\beta$  plane to avoid the branch-point singularity at  $\beta = 0$ . For an asymptotic procedure accommodating arbitrary values of  $\rho$ , see Reference 14.

The asymptotic calculation of  $H'$  in Eq. (75) may now proceed in the usual manner with a replacement of the Hankel function by its large-argument approximation in Eq. (5.3.13b), provided that the integration path is deformed away from the region  $\beta = 0$ . The resulting integrand is identical in form with that in Eq. (51), except for a differently defined amplitude function  $F(\beta)$ , whence the saddle-point configuration is the same as in Sec. 7.5e provided that the rectilinear variable  $v$  is identified with the radial variable  $\rho$ . A geometrical interpretation of the saddle-point condition leads to the ray diagram in Fig. 7.5.8, modified so that  $\alpha = 0$ , with observation points lying in the region  $v > 0$  since the radial variable  $\rho$  is always positive. In view of the rotational symmetry of the ray system about the  $\rho = 0$  axis, the caustic in Fig. 7.5.8 is now a surface of revolution and the (line) cusp at  $C$  in the two-dimensional problem becomes a point cusp. Upon noting the angles of inclination  $\varphi_0$  of the refracted rays that pass through an observation point with  $\rho > 0$  (i.e.,  $v > 0$  in Fig. 7.5.8), and recalling the saddle-point condition  $\beta_s = k_0 \sin \varphi_0$ , one may verify that the integration path in Eq. (75) may be deformed into the steepest-descent paths through the various saddle points without encountering any of the

branch-point singularities. The asymptotic approximation of the  $E$ -mode contribution to the field is therefore analogous to that in Eqs. (57) and (58) for observation points off the caustic, and to that in Eq. (59) for observation points near or on the caustic. Since the previously mentioned Hankel function approximation contains a factor  $\rho^{-1/2}$ , the three-dimensional field decays properly according to  $(\text{distance})^{-1}$ , in contrast to the  $(\text{distance})^{-1/2}$  dependence of the two-dimensional field in the line-source problem.

In the preceding considerations, valid for observation points “far” from the axis  $\rho = 0$ , the contributing saddle points have not been located near the origin of the complex  $\beta$  plane. If  $\rho = 0$ , however, the integrand of Eq. (74) has the saddle points

$$\beta_1 = k_0 \left( \frac{1 - b^2}{1 + b^2/|\epsilon|} \right)^{1/2}, \quad \beta_2 = 0, \quad b = \frac{z|\epsilon|}{|z'|}, \quad (76)$$

as noted from Eq. (56), with  $\alpha = 0$ . The asymptotic evaluation of the contribution  $H'_1$  from  $\beta_1$  when  $0 < z < \hat{z}$ , where  $\hat{z} = |z'|/|\epsilon|$  is the coordinate at the cusp, proceeds as in the line-source problem and yields

$$H'_1 \sim \frac{1}{4\pi} \sqrt{\frac{2\pi}{\psi''(\beta_1)}} \frac{\beta_1 \kappa'_1(\beta_1)}{\kappa'_1(\beta_1) + \kappa'_2(\beta_1)} e^{i\psi(\beta_1) - i\pi/4}, \quad \psi(\beta) = \kappa'_2 z + \kappa'_1 |z'|, \quad (77)$$

thereby exhibiting a dependence  $\sim (\text{distance})^{-1/2}$ . This behavior is explained by the observation that points on the axis of the rotationally symmetric ray configuration are reached by refracted rays arriving from all angles  $0 < \phi \leq 2\pi$ , so the  $z$  axis is a caustic of the refracted ray system. Hence, there exists on the axis a field enhancement not evident at off-axis points.

The saddle point  $\beta_2 = 0$  describes a ray that progresses along the  $z$  axis and represents a conventional field contribution uninfluenced by the axial focusing described above. Its decay should therefore be described by the ordinary inverse distance dependence. In an asymptotic evaluation of the integral in Eq. (74) for this case, one must take account of the vanishing of the amplitude function  $g(\beta) = \beta \kappa'_1 [\kappa'_1 + \kappa'_2]^{-1}$  at  $\beta = 0$ . On application of the procedure in Sec. 4.2b to the semiinfinite interval  $0 \leq \beta < \infty$ , the saddle point at  $\beta = 0$  is transformed via  $\psi(\beta) = \psi(0) + is^2$  into a saddle point at  $s = 0$ , and the amplitude function  $G(s) = g(\beta) d\beta/ds$  is then expanded in a power series about  $s = 0$ . Since  $G(0) = 0$ , the first non-vanishing term arises from  $G'(0)s$ , and the corresponding integral to be evaluated is  $\int_0^\infty s e^{-s^2} ds = \frac{1}{2}$ . The first-order asymptotic approximation  $H'_2$  arising from the saddle point at  $\beta_2 = 0$  is then found to be

$$H'_2 \sim \frac{1}{4\pi} \frac{i}{2\psi''(0)} e^{i\psi(0)}, \quad (78)$$

and the total  $E$ -mode contribution to the magnetic field on the  $z$  axis is  $H' \sim H'_1 + H'_2$ . The difference between the three-dimensional field behavior here and the two-dimensional one described previously is to be noted and has been ex-

plained in physical terms. Since  $\psi''(0) \geq 0$  when  $z \leq \hat{z}$ , one notes a phase retardation of  $\pi$  along a ray passing through a point cusp.

Formulas (77) and (78) break down when  $z \approx \hat{z}$  because then  $\beta_1 \rightarrow 0$  and  $\psi''(0) \rightarrow 0$ . In this case, one may employ the more accurate formula derived in Sec. 4.5b, which accounts explicitly for the simultaneous presence of three closely spaced saddle points. The resulting expression for  $H'$  is<sup>13</sup>

$$H' \sim \frac{1}{4\pi} \frac{e^{i(\psi(0)+\psi(\beta_1))/2-i\pi/4}}{4\sqrt{2}} \sqrt{\frac{24}{-\psi'''(0)}} D_{-1}\{e^{-i3\pi/4}\sqrt{2[\psi(\beta_1) - \psi(0)]}\}, \quad (79)$$

with the square root in the argument of the parabolic cylinder function defined as in Eq. (65). By considerations analogous to those carried out for Eq. (65), this formula may be reduced to the approximations in Eqs. (77) and (78), provided that  $\beta_1 \approx 0$ ,  $\sqrt{\psi(\beta_1) - \psi(0)} \gg 1$ , and the combined expressions therefore permit the calculation of  $H'$  along the entire positive  $z$  axis.

The  $E$ -mode reflected field in the plasma half-space may be evaluated in a similar manner, and exhibits a behavior analogous to that in the line-source problem if proper account is taken of the equivalence between  $v$  and  $\rho$ .

## P R O B L E M S

- From the  $E$ -mode dispersion equation (7.1.5), derive the refractive index  $n(\bar{\theta})$ , and therefore the ray refractive index  $N(\theta)$  in Eq. (7.3.3c), by use of the relations  $N(\theta) = n(\bar{\theta}) \cos(\theta - \bar{\theta})$ ,  $\tan(\theta - \bar{\theta}) = (1/n)(\partial n / \partial \bar{\theta})$  (see Fig. 7.1.1 and Problem 33 of Chapter 1).
- Apply the coordinate scaling transformation in Eq. (7.2.22) to the integral representation in Eq. (5.4.12c) for the isotropic free-space Green's function to deduce the Green's function for the unbounded uniaxially anisotropic medium. Compare the result with the integral formulation in Eq. (7.3.8) and show that the two expressions are equivalent when  $\epsilon > 0$ . Explain why the expression in Eq. (7.3.8) remains valid when  $0 < \arg \epsilon \leq \pi$  whereas the integral expression obtained by coordinate scaling does not.
- Show that the Green's function in Eq. (7.3.14) for an unbounded uniaxially anisotropic medium can be expressed in the invariant form of Eq. (1.7.56), which involves the geometrical properties of the dispersion surface shown in Fig. 7.1.1.
- A perfectly conducting cylinder with radius  $\rho = a$  is embedded in an infinite homogeneous, uniaxial plasma whose optic axis is parallel to that of the cylinder. Time-harmonic excitation is provided by an axial electric dipole located at a distance  $\rho > a$ .
  - Referring to results in Sec. 6.7 for the cylinder diffraction problem in an isotropic medium, and employing coordinate scaling [see Eq. (7.2.22)], derive expressions for the total electromagnetic fields in the uniaxial environment.
  - For  $\omega_p < \omega$  and  $\omega_p > \omega$ , derive approximate field solutions for very small

cylinder radius, and compare the results with those for the isotropic case. Discuss the physical properties of the scattered field, especially for  $\omega < \omega_p$  ( $\epsilon < 0$ ), utilizing the concept of an equivalent line source (cf. Sec. 7.3c) to represent the effect of the induced currents on the cylinder.

5. A line source of unit strength magnetic currents in a uniaxially anisotropic dielectric  $\epsilon$  is located at  $Q$  in the presence of a smoothly curved, perfectly conducting cylindrical surface as shown in Fig. P7.1. The optic axis extends along the

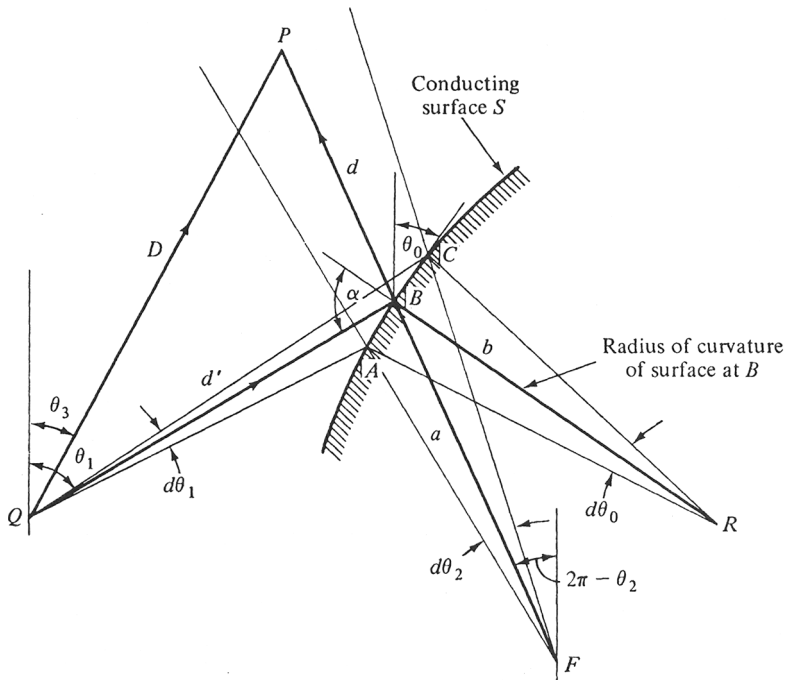


FIG. P7.1 Curved scatterer in anisotropic dielectric.

$y$  direction ( $\theta = 0$ ). Using the methods of geometrical optics (Sec. 1.7) and referring to Fig. P7.1 for definition of distance and angle variables, show that the magnetic field at the observation point  $P$  is given by:<sup>10</sup>

$$\mathbf{H} = \mathbf{H}_i + \mathbf{H}_r \quad (1)$$

$$\mathbf{H}_i = -\frac{\omega \epsilon_0 \sqrt{\epsilon}}{2\sqrt{2\pi k_0 D} N(\theta_3)} e^{ik_0 D N(\theta_3) - i\pi/4} \quad (1a)$$

$$\begin{aligned} \mathbf{H}_r = & \frac{-\omega \epsilon_0 \sqrt{\epsilon}}{2\sqrt{2\pi}} \sqrt{\frac{N(\theta_2) \sin(\theta_1 - \theta_0)}{N^2(\theta_1) \sin(\theta_2 - \theta_0)}} \\ & \times \frac{\exp\{ik_0 [d' N(\theta_1) + d N(\theta_2)] - (i\pi/4)\}}{\sqrt{k_0 [d' + (d m \sin(\theta_1 - \theta_0)/\sin(\theta_0 - \theta_2)) + (d' d n/b)(1/\sin(\theta_0 - \theta_2))]}}, \end{aligned} \quad (1b)$$

where  $\epsilon = y_0 z_0 \epsilon_0 + z_0 z_0 \epsilon_0 \epsilon$ ,  $N(\theta) = \sqrt{\cos^2 \theta + \epsilon \sin^2 \theta}$ ,  $m = (\partial \theta_2 / \partial \theta_1)$ , and  $n = (\partial \theta_2 / \partial \theta_0)$ ; the latter quantities may be evaluated from the ray reflection law in Eq. (7.5.9b) [with  $\varphi \rightarrow \theta + \alpha$ ,  $\theta_0 = (\pi/2) - \alpha$ ].

Show that this result reduces correctly to the one in Problem 30 of Chapter 1 for a cylindrical surface in an isotropic medium when  $\epsilon = 1$ , and to the infinite plane result in Sec. 7.4c when  $b \rightarrow \infty$ .

6. Utilizing the respective optical path lengths  $L_{12}$  and  $L_{23}$  from a source point 1 to an observation point 3 along incident and reflected trajectories, with point 2 lying on a plane boundary, show that the ray reflection law in Eq. (7.5.9b) can be derived by applying Fermat's principle

$$\delta(L_{12} + L_{23}) = 0, \quad L_{ab} = \int_a^b N ds, \quad (2)$$

requiring the optical length to be an extremum.  $\delta$  denotes the variational derivative and  $N$  the ray refractive index.

7. A uniform waveguide region is bounded transversely (if at all) by a perfectly conducting surface and is filled with an anisotropic dielectric having  $\epsilon_t = \text{constant}$ ,  $\epsilon_z(p, z) = \text{arbitrary}$ . The permeability  $\mu_t = \mu_z = \mu$  is constant and isotropic.  
 (a) Show that, in this region,  $H$  modes can exist and propagate as in an isotropic homogeneous medium with wavenumber  $k = \omega \sqrt{\mu \epsilon}$ .  
 (b) Show that  $E$  modes exist also and specify the corresponding field problem.
8. Consider the configuration shown in Fig. P7.2, where a line source of magnetic currents is located in the vacuum half-space  $z > 0$  and the field is observed in

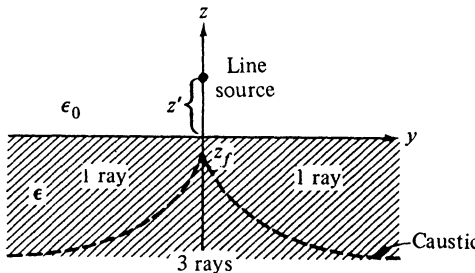


FIG. P7.2 Caustic for source exterior to plasma half-space ( $|z_f| = z' |\epsilon|$ ).

the uniaxially anisotropic plasma half-space  $z < 0$  described by the dielectric tensor  $\epsilon = y_0 z_0 \epsilon_0 + z_0 z_0 \epsilon_0 \epsilon$ .

- (a) Show that for  $\epsilon_z < 0$ , the refracted ray system forms a caustic given by the equation

$$\left| \frac{z \sqrt{|\epsilon|}}{z'} \right|^{2/3} - \left| \frac{y \sqrt{1 + |\epsilon|}}{z' |\epsilon|} \right|^{2/3} = |\epsilon|.$$

- (b) Determine the asymptotic field behavior (for large  $k_0$ ) everywhere in the plasma half-space.

## REFERENCES

1. BORN, M. and E. WOLF, *Principles of Optics*, Chapter XIV. New York: Pergamon Press, 1959.
2. LANDAU, L. D. and E. M. LIFSHITZ, *Electrodynamics of Continuous Media*, Chapter II. New York: Pergamon Press, 1960.
3. BUDDEN, K. G., *Radio Waves in the Ionosphere*. Cambridge, England: Cambridge University Press, 1961.
4. GINZBURG, V. L.; *The Propagation of Electromagnetic Waves in Plasmas*. New York: Pergamon Press, 1964.
5. LAX, B. and J. BUTTON, *Microwave Ferrites and Ferrimagnetics*. New York: McGraw-Hill, 1962.
6. FELSEN, L. B., "Propagation and diffraction in uniaxially anisotropic regions. I—Theory. II—Applications," *Proc. IEE (London)* 111 (1964), pp. 445-464.
7. CLEMMOW, P. C., *The Plane Wave Spectrum Representation of Electromagnetic Fields*, Chapter 8. New York: Pergamon Press, 1966.
8. ARBEL, E. and L. B. FELSEN, "Theory of radiation from sources in anisotropic media. Part I—General sources in stratified media. Part II—Point source in an infinite homogeneous medium," in *Electromagnetic Theory and Antennas* (E. C. Jordan, Ed.), pp. 391-459. New York: Pergamon Press, 1963.
9. STARAS, H., "The impedance of an electric dipole in a magneto-ionic medium" *IEEE Trans. on Antennas and Propagation AP-12* (1964), pp. 695-702.
10. RULF, B. and L. B. FELSEN, "Diffraction by objects in anisotropic media," *Proc. of Symposium on "Quasi-Optics," XIV*, pp. 107-147, Brooklyn, New York: Polytechnic Press, 1964.
11. FELSEN, L. B., "Radiation from a uniaxially anisotropic plasma half space," *IEEE Trans. on Antennas and Propagation AP-11* (1963), pp. 469-484.
12. BREKHOVSKIKH, L. M., *Waves in Layered Media*, Sec. 22. New York: Academic Press, 1960.
13. FELSEN, L. B., "Focusing by an anisotropic plasma interface," *IEEE Trans. on Antennas and Propagation AP-12* (1964), pp. 624-635.
14. BAÑOS, A., *Dipole Radiation in the Presence of a Conducting Half Space*, Chapter 3. New York: Pergamon Press, 1966.